Contents

Chapter 1

Introduction

Sulfur species exert a profound influence on the chemistry of the troposphere: their rates of emission, their chemical transformations, their transport and their removal processes have been the subject of numerous studies in the past decades. The most abundant sulfur trace gas produced mostly by man's activities is sulfur dioxide (SO_2) and accounts for nearly half the sulfur emitted into the atmosphere [Cul80]. This sulfur emission is concentrated in the continental regions of the northern hemisphere, it is quite interesting, therefore, to explore its contribution to atmospheric pollution. Its transport and oxidation pathways are also of great interest: its photochemical product is gaseous sulfuric acid (H_2SO_4), known to be a very efficient precursor of new aerosol particles [Sei98]. Due to its extremely low vapor pressure sulfuric acid rapidly condenses on surfaces or nucleates with the assistance of other atmospheric trace compounds particularly ions [Tur98] and ammonia [Mar97], to form new particles. These aerosol particles may contribute to radiative forcing. In the aqueous phase, sulfur dioxide will dissolve to form sulfates, thus altering the composition of fogs/clouds [Fin00]. Vertical profiles of sulfur dioxide with high spatial resolution are, therefore, useful in determining its fate and its role in new particle formation or acidification of fogs/clouds in the free troposphere.

The first part of this work is concerned with aircraft measurements of sulfur dioxide in the troposphere. The measurements have been performed on board of the research aircraft Falcon operated by the German Aerospace Center (DLR) in Oberpfaffenhofen, Germany, in the framework of the ScavEx project. During all flights air was sampled over continental Europe in altitudes ranging between 1-12 Km. Sulfur dioxide was

measured with an Ion Trap Mass Spectrometer, using the Chemical Ionization Mass Spectrometry (CIMS) technique. Several altitude profiles with high time resolution were obtained, signifying occasionally pollution episodes. One of the flights, served as a case study for a new particle formation event.

Sulfur emission from aircraft engines has been another topic of considerable interest due to the rapid long term growth of air traffic [Pen99]. Potential implications of sulfur emissions on climate concern formation of volatile aerosols, condensation trails and perhaps even clouds [Rei93]; [Rei94]; [Zha95]; [Yu97]; [Yu98b]; [Cur98]. Topics of discussion and research remain the partitioning of sulfur species in the exhaust of aircraft engines, their dependence on fuel sulfur content and combustor operating conditions [Schu02]. The most abundant sulfur species emitted by aircraft engines is sulfur dioxide (SO_2) in concentrations which are proportional to the fuel sulfur content. Sulfur dioxide formed during the combustion will convert rapidly to sulfur trioxide (SO_3) and sulfuric acid (H_2SO_4) already within the aircraft engine [Kat03]. This conversion seems to be induced mostly by OH radicals which react with sulfur dioxide leading to HSO_3 which in turn experiences rapid conversion to sulfur trioxide. Ultimately sulfur trioxide reacts with water vapor leading to gaseous sulfuric acid [Kol94]; [Lov96]. The conversion efficiency of total sulfur to SO_3 and H_2SO_4 (together termed as S(VI)) is defined as ϵ=S(VI)/S_T.

The rate limiting step is the reaction of SO_2 with OH, the rate coefficient of which is somewhat uncertain at the high temperatures prevailing in gas turbine engines [Tre99]. This uncertainty along with the poorly known OH concentrations represents a severe obstacle for theoretical model calculations of S(VI) formation in gas turbine engines. The numerous indirect attempts to quantify the amount of sulfuric acid emitted from aircraft engines are very susceptible to insufficient accuracy of the measurements or other perturbations [Schu02]. Previous measurements of sulfuric acid have been performed only in the exhaust of an aircraft engine [Cur02]. In the exhaust plume further oxidation of sulfur species is expected to occur (1-2 %) [Han99] leading to a slight increase of ϵ. So far, no direct measurements of S(VI) species have been attempted in the internal flow of an aircraft engine.

The second part of this work is concerned with ground based measurements of

S(VI) in the internal flow of an aircraft engine. This work has been part of the European funded project PartEmis, hosted by QinetiQ in Farnborough, UK where the necessary facilities were designed and produced. These facilities comprised a combustion system that in technology terms is compatible with the ICAO (International Civil Aviation Organization) emission standards and a Hot End Simulator (HES) attached to the combustor. The so-called HES is an expansion system that simulates the thermodynamic processes involved in the expansion of gases in the turbine and nozzle stages of an aircraft engine.

The principal aim of this work was to examine the effect of fuel sulfur content and the effect of combustor operating conditions on S(VI) emissions. For that reason measurements have been performed with three different fuel sulfur contents and additionally with a fuel doped with an additive recently introduced into civil aviation. The combustor was operated in two conditions representative of legacy and modern aircraft cruise. The differences between the old and modern cruise condition concern different combustor pressure, temperature and fuel flow. The results give insight into the sulfur oxidation in the successive pressure stages of an aircraft engine and also provide validation to modeling work reporting ϵ values with large uncertainties.

Chapter 2

Sulfur Dioxide in the atmosphere

Sulfur is one of the five life elements (C, O, N, S and P) which are essential to life on earth, present in the earth's crust at a mixing ratio of less than 500 ppm by mass - fourteenth most abundant - and in atmosphere at a total volume mixing ratio of less than 1 ppm [Tyn91]. Its biogeochemical cycle involves the transportation of sulfur among atmospheric, oceanic, biospheric and land compartments, the amounts contained in different reservoirs and the rate of exchange between them. In the biosphere and hydrosphere sulfur compounds are volatile and easily exchanged with the atmosphere.

Sulfur in the atmosphere exerts a profound influence on regional and global chemistry, climate and health of various living organisms. The most important natural source of atmospheric sulfur are the biogenic emissions, followed by sea spray and geothermal emissions (mostly volcanoes) while the main industrial sources remain the combustion of coal and petroleum. The atmospheric sulfur cycle is presented in Figure 2.1. Sulfur compounds are not accumulating in the atmosphere. A cycle operates whereby sulfur is continuously transported and converted between the different phases. The balance between the release of sulfur into the atmosphere and its return to the Earth's surface is delicate and over the past 100 y the increasing amounts of atmospheric sulfur generated by man may have shifted the balance point. This is shown by recent changes in the S-content of polar ice, which had previously remained constant over the centuries [Cul80].

Sulfur occurs either in the gas or aerosol phase and in five oxidation states (-2, -1, 0, 4, 6). Chemical reactivity of sulfur compounds is inversely related to their
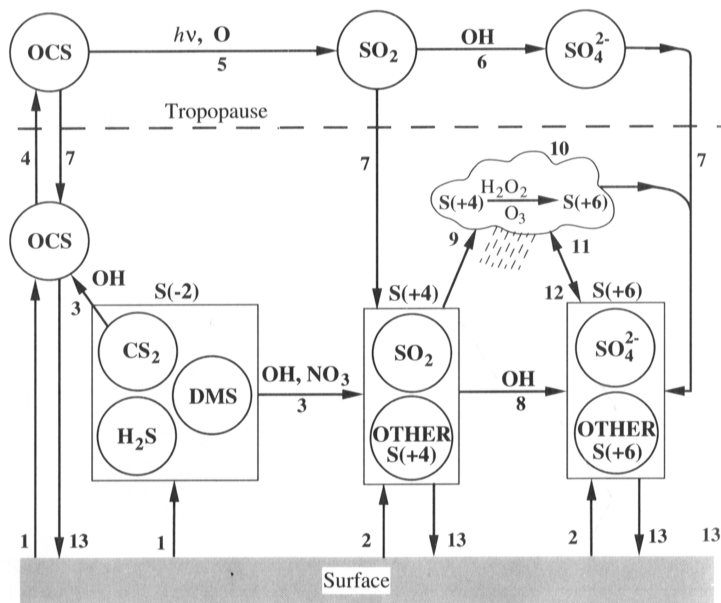
Figure 2.1: Exchanges of sulfur in the atmosphere. The paths are labeled according to the processes: (1) emissions of DMS, H$_2$S, CS$_2$ and OCS; (2) emissions of S(4) and S(6); (3) oxidation of CS$_2$, DMS and H$_2$S by OH and DMS by NO$_3$ in the troposphere; (4) transport of OCS into the stratosphere; (5) photolysis of OCS or reaction with O atoms to form SO$_2$ in the stratosphere; (6) oxidation of SO$_2$ in the stratosphere; (7) transport of stratospheric OCS, SO$_2$ and sulfate back in the troposphere; (8) oxidation of SO$_2$ and other S(4) products by OH in the troposphere; (9) absorption of S(IV) into hydrosols; (10) liquid phase oxidation of S(IV) by H$_2$O$_2$ in hydrosols; (11) absorption/growth of S(VI) aerosol into hydrosol; (12) evaporation of cloud water leaving residual S(VI) aerosol; (13) deposition of OCS, S(IV) and S(VI) [Sei98].

oxidation state. Reduced sulfur compounds (oxidation state -2 or -1) are usually found in the gas phase and once emitted tend to oxidise to the +4 oxidation state and ultimately to the +6 state. Oxidised sulfur compounds occur usually in the aerosol phase and their residence times are determined by wet and dry deposition. Usually the sulfur species in the +4 and +6 oxidation state are referred to as S(IV) and S(VI) compounds. Table 2 presents the atmospheric sulfur compounds.

Sulfur dioxide (SO_2) is the principal anthropogenic sulfur compound, which is predominantly emitted during fossil fuel burning. It has an important role in the atmospheric sulfur cycle through its contribution to acidic aerosol formation, aerosol and cloud droplet modification and acidic precipitation

Name	Formula	Oxidation State
Dimethyl sulfide(DMA)	CH_3SCH_3	-2
Carbon disulfide	CS_2	-2
Carbonyl disulfide	OCS	-2
Methyl mercaptan	CH_3SH	-2
Dimethyl disulfide	CH_3SSCH_3	-2
Dimethyl sulfoxide	CH_3SOCH_3	0
Sulfur dioxide	SO_2	4
Bisulfite ion	HSO_3^-	4
Sulfite ion	SO_3^{2-}	4
Sulfuric acid	H_2SO_4	6
Bisulfate ion	HSO_4^-	6
Sulfate ion	SO_4^{2-}	6
Methane sulfonic acid (MSA)	CH_3SO_3H	6
Dimethyl sulfone	$CH_3SO_2CH_3$	6
Hydroxymethane sulfonic acid	$HOCH_2SO_3$	6

Table 2.1: Atmospheric Sulfur Compounds and its state of oxidation [Sei98]

2.1 Precursors of Sulfur Dioxide

The naturally occurring sulfur compounds are in the reduced form and are distributed over the entire globe. These compounds, mostly due to biogenic activity, are oxidised upon their entry into the atmosphere to SO_2. The rate and the eventual products of their oxidation are important concerns. If they are oxidised to SO_2, they will lead to sulfuric acid. If they form other species such as methane sulfonic acid (MSA), they may be removed from the atmosphere without producing sulfuric acid. The homogeneous gas phase reactions with free radicals appears to be the major oxidation path [Fin00]. The initiation reactions in the oxidation to SO_2 are for all reduced sulfur compounds the rate limiting steps, thus determining the lifetime of these species.

For all of the reduced sulfur compounds presented in Table 2 except OCS the oxidation is initiated by reaction with OH and to a lesser extent by NO_3. The rate of reactions with other oxidants (O_3, NO_2, O_2 and RO_2) are too slow to compete with OH and NO_3 reactions [Tyn91]. In general if the oxidation takes place in a continental

troposphere NO_3 must also be taken into account. In a marine environment, where NO_3 is low, OH will be the dominant oxidant. Clorine atoms also react rapidly with reduced sulfur compounds and hence are potential oxidants in the early morning hours in coastal regions. There has been also a great deal of interest in the halogen oxides IO, BrO, ClO as potential oxidants for compounds as DMS [Tyn91]. Other removal processes such as rain out and uptake by the biosphere are not important, again with the exception of OCS. In general, H_2S, CS_2, CH_3SH, CH_3SCH_3 and CH_3SSCH_3 have their sources at the ground or at the oceans and their removal in the troposphere is so rapid that they do not reach stratosphere. Direct injection of these species into the stratosphere by volcanic eruptions is the only way to get in. $O(^3P)$ reactions and ultraviolet photolysis may play a major role in the oxidation of some of these species in the stratosphere.

The concentrations of the reduced sulfur compounds varies with location. Highest mixing ratios for H_2S occur in the wetlands 450-840 ppt, for DMS in marine surface layer 80-110 ppt and for CS_2 in the continental surface layer 35-120 ppt [Sei98]. In the calculations of the lifetimes of reduced sulfur species it is assumed that the basic removal mechanism is the reaction with OH radical. If τ is the residence time of the compound, Q the total quantity in the troposphere and R=k[OH]Q its rate of removal, the residence time under steady state conditions is defined as

$$t = \frac{Q}{k[OH]Q} = \frac{1}{k[OH]} \tag{2.1}$$

[OH] is an appropriate averaged tropospheric concentration of OH radicals taken to be 1×10^6 radicals cm^{-3}. The rate constant k for each reaction of these reduced sulfur compounds with the OH radical is known. With the help of equation 2.1 the estimated tropospheric lifetimes yield 2 days for DMS, 1.2 h for CH_3SSCH_3, 8 h for CH_3SH, 2.4 days for H_2S and 2.5 days for CS_2.

Carbonyl sulfide is the most abundant sulfur gas in the global background atmosphere ($\tilde{5}00$ ppt) due to its low reactivity and thus, relatively longer residence time (global atmospheric lifetime 7 years, lifetime with respect to reaction with OH radical 16 years). OCS is the only reduced sulfur compound that can be transported into the stratosphere and there converted to SO_2 and ultimately to fine H_2SO_4 aerosols. This process was first postulated by Crutzen (1976) to explain the the existence of the

background aerosol sulfate layer known as the Junge layer.

2.2   Sulfur dioxide

Anthropogenic emissions of sulfur dioxide, primarily from fossil fuel combustion, represent the largest contribution to the global sulfur budget. Coal and oil combustion constitute approximately 53 % and 28 % of the SO_2 source [Bra99]. Estimates of the global SO_2 emission flux ranges from 50 to 100 Tg(S) yr^{-1} increasing as the fossil fuel combustion increases [Ker00]. Mixing ratios of SO_2 in continental background air range from 20 ppt to 50 ppt. Urban SO_2 mixing ratios can attain values of several hundred ppb [Sei98]. Once emitted, the gaseous SO_2 is oxidised to form sulfates and sulfuric acid. The oxidation rate depends on a number of parameters including the presence of aqueous phase in the form of clouds and fogs, the concentration of oxidants and sunlight intensity. In the following the major oxidation pathways of sulfur dioxide will be presented, both in the gaseous and in the liquid phase.

2.3   Oxidation of Sulfur Dioxide in the gas phase

The reaction of sulfur dioxide with the OH radical is the major controlling step of gas phase oxidation of SO_2 in the atmosphere [Sto83].

$$SO_2 + OH + M \quad \rightarrow \quad OHSO_2 + M \tag{2.2}$$
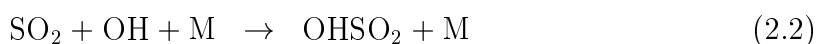
This is a termolecular reaction which can be treated, as a first approximation, as if it consists of two elementary elementary steps:

$$SO_2 + OH \quad \rightleftarrows \quad OHSO_2^\star \tag{2.3}$$

$$OHSO_2^\star \quad \leftrightarrows \quad OHSO_2 + M \tag{2.4}$$
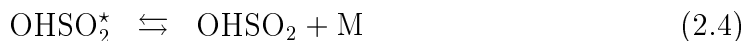
$HOSO_2^\star$ is the excited adduct that contains the excess internal energy from bond formation in 2.3 and $OHSO_2$ is the stabilized adduct resulting when some of its internal energy is removed by a collision with M. If the system is treated as if the energized adduct remains constant with time, then the rates of formation and loss are equal and thus:

$$k_3[OH][SO_2] = k_{-3}[HOSO_2^\star] + k_4[HOSO_2^\star][M] \tag{2.5}$$

This is an example of the steady state approximation. Rearranging, an expression for $HOSO_2^\star$ is obtained:

$$[HOSO_2^\star] = \frac{k_3[OH][SO_2]}{k_{-3} + k_4[M]} \tag{2.6}$$

The rate of the reaction in terms of product formation is given by

$$\frac{d[HOSO_2]}{dt} = \frac{k_3 k_4[M]}{k_{-3} + k_4[M]}[OH][SO_2] = k^{bi}[OH][SO_2] \tag{2.7}$$

where k^{bi} is the effective bimolecular rate constant $k^{bi} = k^{III}[M]$ which alternatively can be given as

$$\frac{1}{k^{bi}} = \frac{k_{-3}}{k_3 k_4[M]} + \frac{1}{k_3} \tag{2.8}$$

At infinite pressures $[M] \to \infty$ the rate constant k^{bi} has its high pressure limiting value $k^\infty = k_3$ in which all the energized adducts formed in 2.3 will be stabilized in 2.4 and none will have a chance to decompose back to reactants via -2.3.

As [M] approaches zero, k^{bi} approaches $k_3 k_4[M]/k_{-3}$, so that k^{III} is given

$$k^{III} = \frac{k_3 k_4}{k_{-3}} \tag{2.9}$$

With this approximate treatment of termolecular reactions is examined how the third order low pressure relates to the rates constants k_3, k_{-3} and k_4 for the elementary reactions assumed to be involved. The reaction of SO_2 with OH is in the fall off region between second and third order in the range of the total pressures encountered from the troposphere through the stratosphere. The adduct free radical formed in reaction 2.2 has a lifetime of 0.5 μs at 1 atm in air and reacts with O_2 [Sto83]

$$HOSO_2 + O_2 + M \quad \to \quad HO_2 + SO_3 + M \tag{2.10}$$
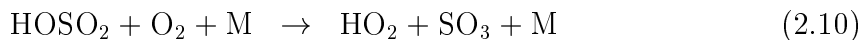
While OH is the major gas phase oxidant for SO_2 Grigee biradicals may also contribute. These biradicals are produced when the C-C and the two peroxy O-O bonds of a primary ozonide formed via reaction of O_3 with alkenes cleave simultaneously to give an aldehyde or ketone and an intermediate which is called the Crigee intermediate (CI). Oxidation of SO_2 by CI takes place particularly at night when OH concentrations are small but significant concentrations of O_3 and alkenes may exist, generating the CI. While one may expect that other tropospheric free radicals such as O_3, HO_2 and RO_2 could react with SO_2 in the gas phase, such reactions are not significant.

2.4 Oxidation of Sulfur Dioxide in the aqueous phase

In the atmosphere, suspended aqueous solutions are present in the form of aerosols, clouds, fogs and rain. However, they have different water contents. Clouds, fogs and rain have high liquid water contents (LWC) and thus have the potential for contributing significantly to atmospheric aqueous-phase oxidations [Fin00]. Clouds typically have LWC of the order of ~ 1 gm^{-3} with droplet diameters of the order of 5-50 μm; the number concentration and size distribution depend on the type of cloud. Fogs, have about 10 times smaller LWC and smaller droplet diameters 0.5-10 μm [Pru98]. Raindrops are much larger than cloud and fog droplets with diameters of 0.2-3 mm and corresponding large LWC. However, because of their size they remain suspended in the atmosphere for only minutes en route to the earth's surface and hence the potential for oxidation processes to occur in raindrops is minimized. Fine particles (diameter ≤ 2 μm) emitted directly or formed by chemical reactions can remain suspended for long periods of time. Many of these particles contain water either in the form of dilute aqueous solutions or as thin films covering an insoluble core. While the volume of liquid water present is much larger in clouds and fogs than in fine particles, the solute concentrations in the latter may be much higher and this may serve to increase the rate of aqueous phase oxidation.

Dissolved gaseous sulfur dioxide into water includes three chemical species:

$$\mathrm{SO_{2(g)} + H_2O} \quad \leftrightarrow \quad \mathrm{SO_2.H_2O} \tag{2.11}$$

$$\mathrm{SO_2.H_2O} \quad \leftrightarrow \quad \mathrm{HSO_3^- + H^+} \tag{2.12}$$

$$\mathrm{HSO_3^-} \quad \leftrightarrow \quad \mathrm{SO_3^{-2} + H^+} \tag{2.13}$$
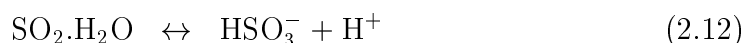
hydrated SO_2 ($SO_2 \cdot H_2$), the bisulfite ion (HSO_3^- or $HOSO_2^-$) which is the most common and the sulfite ion (SO_3^{2-}), all of them together termed as S(IV). Which of the above forms predominates in a solution depends on the acidity of the solution. The establishment of equilibria is very fast but in the atmosphere can be complicated by such factors as the size of the droplet, the efficiency with which gaseous SO_2 striking a droplet surface is absorbed, the chemical nature of the aerosol surface etc. According to Le Chatelier's pronciple [1] the more acidic the droplet, the more the

---

[1]Any change in one of the variables that determines the state of a system in equilibrium causes a
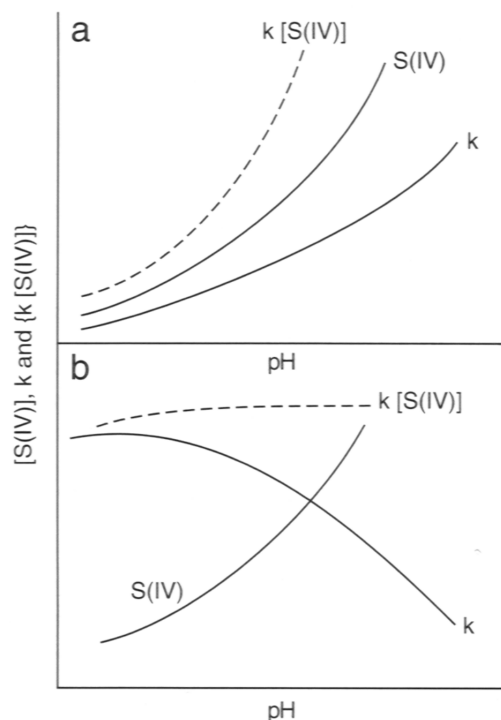
Figure 2.2: Effect of pH on the rate constant k and on the concentration of dissolved S(IV) and its total rate of oxidation k[S(IV)] [Fin00].

equilibria will shift to the less dissolved SO_2, in other words, as pH falls the S(IV) concentration falls.

The dependence of the S(IV) concentrations on the pH of the droplet plays a critical role in determining which oxidant dominates the S(IV) oxidation. *The rates of the various aqueous phase reactions show different dependencies on pH.* Some have rate coefficients that increase with increasing pH whereas some show the opposite trend. If the rate constant and the solubility of S(IV) vary with pH with the same manner, the overall rate of production of S(VI) (kS(IV)) will show a strong pH dependence. On the other hand, if the rate constant decreases with pH, then the rate constant and solubility works in the opposite directions and the net result in terms of S(VI) production may be a relatively small dependence on pH (see Figure 2.2).

Besides the effect of pH dependence that some mechanisms exhibit, there is an *effect of droplet size on S(IV) oxidation.* This is due to the fact that the chemical composition of fogs, clouds and particles varies as a function of particle size:

---

shift in the position of equilibrium in a direction that tends to counteract the change in the variable under consideration
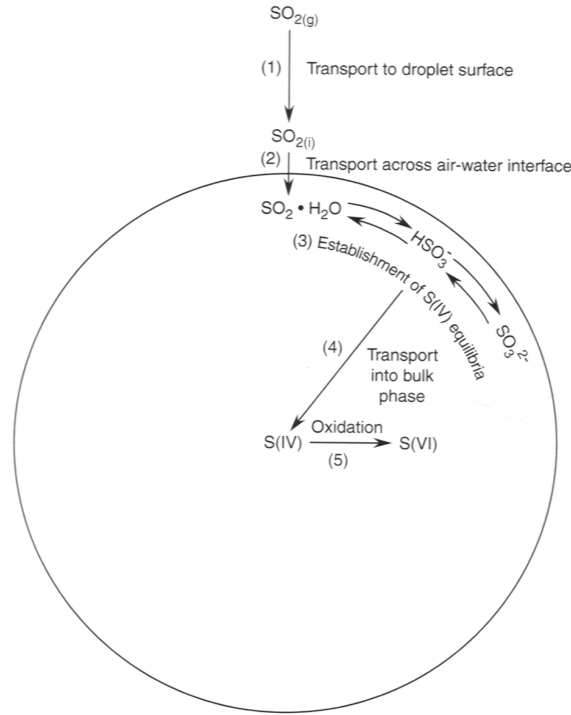
Figure 2.3: Schematic of steps involved in the transfer of SO_2 from the gas phase to the aqueous phase of an atmospheric water droplet and its oxidation in the liquid phase [Fin00].

larger fog and cloud droplets are formed on larger, coarse particles which contain largely elements associated with mechanical processes such as erosion and sea spray $(Mg^{+2}, Ca^{+2}, Na^+, Cl^-)$. The smaller fog and cloud droplets arise from the smaller, accumulation mode particles which contain species as sulfate and ammonium ions. As a result, for the oxidation mechanisms that depend significantly on pH and other solute concentrations the variation in composition with particle size can be important.

The sequence of processes that leads from gas phase SO_2 to aqueous phase sulfate as depicted in Figure 2.3

(1) *Transport of gas to the surface.* Assuming mixing occurs by molecular diffusion, the characteristic times for gas phase diffusion to the surface area range $10^{-10} - 10^{-4}$ s for droplets with radii from $10^{-5} - 10^{-2}$ cm respectively.

(2) *Transfer of the gas across the the air-liquid interface.* The time for the phase equilibrium to be established across the interface, if no reaction occurs, depends on Henry's law constant for the gas dissolving in the solution. This characteristic time also depends on the mass accommodation coefficient, i.e. the fraction of collisions with the surface that result in absorption of the molecule (a_{SO_2}=0.11 at -13 − 20°C).

Assuming a=1 the time to establish such equilibria is in the order of $<10^{-8} - 10^{-1}$ s over a droplet with a pH range of 2-6. If the molecule is absorbed into the droplet on only a small fraction of the collisions, this time will be much longer.

(3) *Formation of the S(IV)-H_2O equilibria.* This occurs in a time scale of a few milliseconds.

(4) *Transport of the dissolved species within the aqueous phase.* Diffusion in liquids is much slower than in gases, thus the characteristic for diffusion within the droplet itself ranges between $\sim 10^{-6} - 1$ s for droplets with radii from $10^{-5} - 10^{-2}$ cm respectively.

The rate of oxidation of SO_2 in % h^{-1} which occurs in aqueous solution in the atmosphere is given by [Fin00]:

$$\% h^{-1} = 3600 \times \frac{100k[X][S(IV)]V}{1000P_{SO_2}/RT + \eta H_{SO_2}P_{SO_2}V} \tag{2.14}$$

where k is the solution-phase rate constant ($Lmol^{-1}s^{-1}$), [X] and [S(IV)] are the aqueous-phase concentrations of the oxidant and [S(IV)] respectively (moles lt^{-1}), V the volume of liquid water per cubic meter of air, H_{SO_2}=1.2 $molL^{-1}atm^{-1}$ at 20-25 °C the Henry's low constant based on physical solubility, P_{SO_2} the gas phase pressure of SO_2 and η the ratio of the total dissolved S(IV) to that of dissolved SO_2 (i.e. $SO_2 \cdot H_2O$). As it can be seen from this expression, the LWC of an air mass plays a role in determining the oxidation rate of SO_2 in aqueous atmospheric droplets. The individual potential atmospheric oxidants of S(IV) in solution are summarized below.

- *Oxidation by O_2.*

  The uncatalyzed oxidation of S(IV) (i.e. in pure water without traces of catalysts) occurring in aqueous solution is very slow and therefore irrelevant to atmospheric solutions. Much more relevant to the aqueous phase in clouds and fogs in the atmosphere is the catalyzed oxidation of S(IV) by Fe^{+3} and Mn^{+2}, which are complex in both kinetics and mechanism. Both elements are common constituents of tropospheric aerosols due to their generation from erosion of the earth's crust. This oxidation pathway is likely to contribute in solution only at pH values near neutral (pH=6-7). As the oxidation occurs and acid forms, the pH falls and this results in a rapid quenching of this path (see upper panel in Figure 2.2).

- *Oxidation by O_3.*

  Although the physical solubility of ozon is fairly small, there is sufficient present in the troposphere to dissolve in clouds and fogs, presenting therefore a potential S(IV) oxidant. Each of the S(IV) forms ($SO_2 \cdot H_2O$, HSO_3^- and SO_3^{2-}) react with O_3 by unique mechanisms and rate constants. The overall rate of the S(IV) oxidation can be given by:

$$-d[S(IV)]/dt = (k_o a_o + k_1 a_1 + k_2 a_2)[S(IV)][O_3] \qquad (2.15)$$

  where a_i are the fractions of the total S(IV) and k_i the rate constants for the reactions with O_3 (k_o=$(2.4\pm1.1)\times10^4$, k_1=$(3.7\pm0.7)\times10^5$, k_o2=$(1.5\pm0.6)\times10^9$ in $Lmol^{-1}s^{-1}$ at room temperature [Hof86]. The three different terms in this equation predominate in different pH regimes: reaction with SO_3^{2-} predominates at high pH values, whereas that with $SO_2 \cdot H_2O$ and HSO_3^- at lower pH values. Overall, the oxidation falls sharply as the pH drops. As S(IV) is oxidised to sulfuric acid and pH falls the reactions become self-quenching. Since the ozon oxidation is important for higher pH values, this reaction is particularly important in sea salt particles, which have a pH of around 8.

- *Oxidation by H_2O_2*

  Hydrogen peroxide is a highly soluble compound (H_2O_2=$10^5 M\,atm^{-1}$): even gas phase concentrations in the low ppb range, quite common in the troposphere, lead to significant concentration in the liquid phase. It has been shown that H_2O_2 oxidizes rapidly S(IV) in solution. The oxidation reaction has a negative dependence on pH (see bottom panel of Figure 2.2) and the result is that the overall rate of production of S(VI) from this reaction is relatively independent of pH over a wide range of pH range of interest in the atmosphere. The ubiquitous occurrence of H_2O_2, its large Henry's law constant, its high reactivity and the pH dependence of the rate constant combine to make H_2O_2 the most important oxidant for S(IV) in the troposphere.

- *Oxidation by Oxides of Nitrogen*

  Some of the oxides of nitrogen (NO, NO_2, NO_3, HONO, HNO_3) are possible

oxidizing agents for dissolved S(IV). The reactions of NO and HNO_3 at atmospheric concentrations are too slow to be significant. Nitrous acid (HONO) reacts at a reasonable rate, however, the levels of gaseous HONO observed even in polluted ambient air (1-8 ppb) yield aqueous concentrations too low to contribute substantially to the aqueous phase oxidation unless other oxiants such as H_2O_2 and O_3 are absent. Dissolved NO_2 is relatively insoluble, the rate constant of its reaction with HSO_3^- and SO_3^{-2} however may be sufficiently large that the NO_2-S(IV) reaction could be significant ([Fin00] and references therein). There is also a variety of additional oxidations in atmospheric aqueous solutions that can be carried out by NO_3. The initiation reactions would be [Exn92]:

$$\mathrm{NO_{3(aq)} + HSO_{3(aq)}^-} \quad \longrightarrow \quad \mathrm{NO_{3(aq)}^- + H_{(aq)}^+ + SO_{3(aq)}^-} \qquad (2.16)$$

$$\mathrm{NO_{3(aq)} + SO_{3(aq)}^{-2}} \quad \longrightarrow \quad \mathrm{NO_{3(aq)}^- + SO_{3(aq)}^-} \qquad (2.17)$$
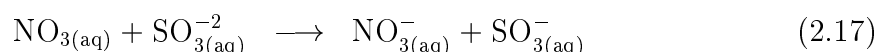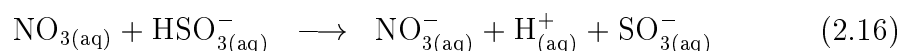
with $k_{HSO_3} = 1.7 \times 10^9$ and $k_{SO_3^{-2}} = 3 \times 10^8 \; Lmol^{-1}s^{-1}$. The SO_3^- radical anion is then oxidized to sulfate (i.e. S(VI)) in a series of subsequent steps.

Apart from the above mentioned oxidizing species there is a variety of radicals in atmospheric aqueous systems which can participate in S(IV) oxidation in clouds and fogs. These free radicals arise either form absorption from the gas phase or from in situ production, largely from photochemical processes. The oxidizing mechanisms are relatively complex and are terminated in many steps. A compilation of these reactions, their rate constants and their relative importance is given in [Fin00] and the references therein.

The relative importance of the oxidation of S(IV) in clouds by O_3, H_2O_2, NO_2 and Fe-, Mn-catalyzed O_2 oxidation is showed in Figure 2.4. It was assumed that SO_2=5 ppb, NO_2=1 ppb, H_2O_2 =1 ppb, Fe(III)=0.3 μM and Mn(II)=0.03 μM [Sei98]. Only the oxidation by H_2O_2 is relatively independent of pH and as shown, it is expected to be the most important oxidant for cloud and fogs at pH <4.5. At higher pH values oxidation both O_3 and catalyzed O_2 oxidation can compete. The S(IV) oxidation in aqueous phase predominates at night. Gas phase oxidation becomes significant during the day when OH concentrations are high.
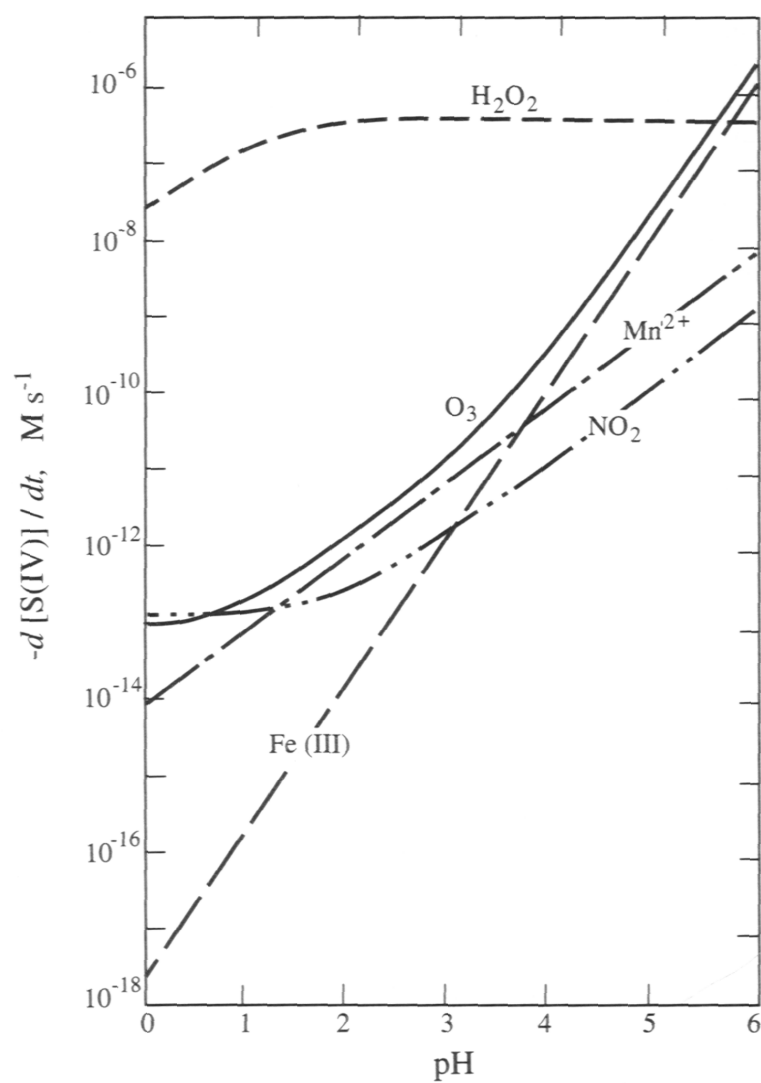
Figure 2.4: Comparison of aqueous phase oxidation paths. The rate of conversion of S(IV) to S(VI) as a function of pH [Sei98].

Chapter 3

Aircraft Sulfur (VI) emissions

Aircraft emissions are expected to have an impact on climate as a result of emitting radiatively active gases, chemical species which modify the atmospheric chemistry and substances which trigger the generation of contrails and at a later stage perhaps clouds. Among the exhaust species special attention gained the S-bearing compounds because of their high aerosol formation potential. Sulfuric acid formed in aircraft gas turbine exhaust plays potentially important roles in the formation of volatile aerosols, condensation trails and perhaps even clouds [Zha95], [Yu98a], [Yu98b], [Pen99], [Schu01]. In an aircraft engine gaseous sulfuric acid is formed via conversion of fuel sulfur. This conversion seems to be induced mostly by OH radicals which react with SO_2 leading to HSO_3 which in turn experiences rapid conversion to SO_3. Ultimately SO_3 reacts with water vapor leading to gaseous sulfuric acid [Rei93], [Rei94], [Kol94], [Lov96]. The rate limiting step is the reaction of SO_2 with OH whose rate coefficient is somewhat uncertain at the high temperatures prevailing in a gas turbine engine. This uncertainty along with the poorly known OH concentrations represents a severe obstacle for theoretical model calculations of S(VI) formation in gas turbine engines.

Gaseous sulfuric acid was originally detected in aircraft gas turbine exhaust at ground level [Fre94] using passive chemical ionization mass spectrometry relying on chemiions produced by the engine and in the wake of a jet aircraft in flight [Cur98] using CIMS. First quantitative measurements of total S(VI) (including gaseous and condensed species) were made by MPI-K, Heidelberg [Cur02]. From these measurements ϵ =3.3±1.8 % was obtained. Furthermore attempts have been made to infer ϵ

from SO_2 measurements building on the difference of measured and expected S(IV) (calculated from the FSC). This indirect method yielded e between 6 and 31 %. Aerosol impactor measurements of sulfate report ϵ values up to 37 %. The conversion efficiency ϵ has also been inferred indirectly from volatile aerosol number and size measurements, building on the assumption that these aerosols are composed only of an H_2SO_4/H_2O solution which is in equilibrium with ambient water vapor present in the exhaust plume. The resulting e range between 0.4 and 80 %. Particularly for small FSC these ϵ are probably overestimated at low FSC as the aerosols seem to be composed mostly of organics and not of H_2SO_4/H_2O. Previously reported modeling studies of aircraft plume chemistry predict abundance ratios ϵ=S(VI)/S_T ranging up to 55 %. A more recent theoretical model interpretation of volatile aerosol measurement suggests that the experimental data would be consistent with epsilon ranging between 0.5 and 5 % [Kae00]. The previous ϵ (see review paper [Schu02]) scatter over a wide range which may to some parts reflect real variations depending on engine type, operational engine conditions and perhaps fuel sulfur content. However, it seems likely that a major part of this scatter is due to problems of the measurements and models. Therefore additional direct measurements of e are needed in order to resolve this problem.

3.1   Sulfur chemistry in aircraft engines

Sulfur is contained in hydrocarbon fuels as substituent of elements in functional groups of aromatic and polyaromatic hydrocarbons. Despite certain differences in formation of compounds of the SO_x group for different combustor operating conditions, some generic reactions have been identified by the use of kinetic models analyzing combustion of hydrocarbon sulfur bearing fuels mixed with air [Sav02]. At first stage, H_2S is oxidised to SO_2:

$$H_2S + O \quad \rightarrow \quad HS + OH \qquad\qquad (3.1)$$

$$HS + O_2 \quad \rightarrow \quad SO + OH \qquad\qquad (3.2)$$

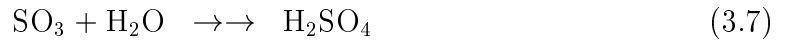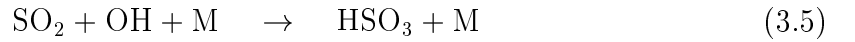$$SO + O_2 \quad \rightarrow \quad SO_2 + O \qquad\qquad (3.3)$$
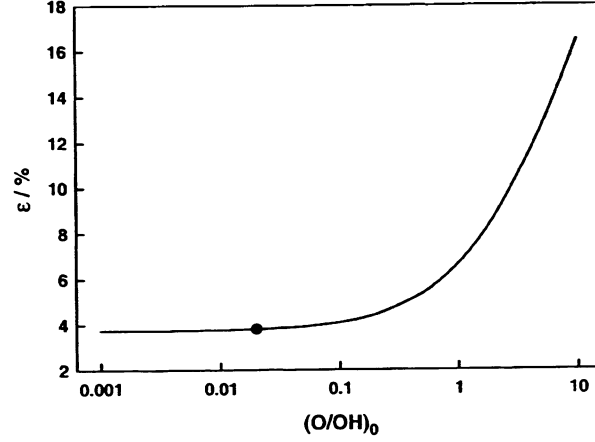
Figure 3.1: Dependence of ϵ on the initial O/OH ratio [Tre99].

The process of SO_3 formation proceeds significantly slower. It is a two stage process including oxidation of SO_2 by the OH radicals with participation of HSO_3. Formation of SO_3 directly from SO_2 proceeds even more slowly: $SO_2 + O_2 = SO_3 + O$. Concentrations of compounds other than SO, SO_2 and SO_3 in the combustor chamber are significantly lower.

Successive oxidative processes in the post-combustor flow occur in the high, intermediate and low pressure turbines of the engine as exhaust gases are cooled from the high combustor temperatures and pressures, (1200-2400 K and 8-45 atm) to the relative low temperatures and pressures at the nozzle exit (200-600 K and 0.2-1 atm) [Luk98].

$$SO_2 + O + M \quad \rightarrow \quad SO_3 + M \tag{3.4}$$

$$SO_2 + OH + M \quad \rightarrow \quad HSO_3 + M \tag{3.5}$$

$$HSO_3 + O_2 \quad \rightarrow \quad SO_3 + HO_2 \tag{3.6}$$

$$SO_3 + H_2O \quad \rightarrow\rightarrow \quad H_2SO_4 \tag{3.7}$$
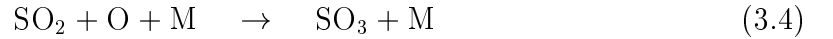
The oxidation mechanism of SO_2 via reaction with OH in the gas phase, proposed by Stockwell and Calvert [Sto83], is competing with the oxidation via O radicals, also present in the post combustor gas flow. Numerical simulations imply that the oxidation of SO_2 to SO_3 with O is of minor importance compared to reactions with OH, since the amount of O leaving the combustor is only 6% of the amount of OH radicals [Sta02]. In agreement with this study is the Tremmel and Schumann model

reporting that the oxidation of sulfur species occurs mainly via the $SO_2 + OH$ reaction. According to their calculations $SO_2 + O$ reaction does not have a noticeable impact on ϵ unless initial O exceeds more than 10% of the initial OH (see Figure 3.1). Still, a reaction flux analysis attempted for the Concorde turbine indicated that the reaction of SO_2 with atomic oxygen was the dominant mechanism for the formation of SO_3, although both O and OH decrease along the flow; the drop in OH was found to be primarily due to NO_y reaction with little contribution from SO_2 [Bro96b].

Indeed, reactants like NO, NO_2, NO_3, $HONO$, HNO_3, CO as well as the conversions within the HO_x family seem to compete with SO_2 for the O and OH oxidants. Lukachko et al reported a significant influence of NO_x and CO specifications on SO_x oxidation, presumably through competitions for O and OH [Luk98]. Calculations using similar initial conditions for SO_x at the combustor exit and variable initial NO_x and CO resulted in significantly different ϵ; higher initial NO_x and CO concentrations resulted in lower S(VI) concentrations at the nozzle exit (for the detailed gas phase chemical reaction mechanisms of post combustor exhaust plume and the corresponding rate constants see [Tre99] and [Luk98], Tables 1 and 2 respectively).

The reaction of SO_3 with water (Reaction 3.7) has been studied extensively. A direct reaction of SO_3 with one water molecule to produce sulfuric acid is rather unlikely; the gas-phase reaction was studied in the laboratory and exhibited a second-order dependence on water vapor and a strong negative temperature dependence. This suggests the formation of bound intermediates and a complex mechanism involving a water dimer and/or an $SO_3 \cdot H_2O$ adduct [Kol94], [Lov96], [Jay97]:

$$SO_3 + H_2O.H_2O \quad \rightarrow \quad H_2SO_4 + H_2O \tag{3.8}$$

$$\rightarrow \quad SO_3.H_2O + H_2O \tag{3.9}$$

$$H_2O + SO_3.H_2O \quad \rightarrow \quad H_2SO_4 + H_2O \tag{3.10}$$

$$\rightarrow \quad H_2O.SO_3 + H_2O \tag{3.11}$$
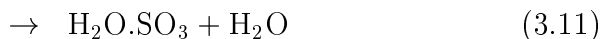
3.2   Sulfur conversion efficiency ϵ

As discussed above, the combustion of fossil fuels containing sulfur primarily leads to the formation and emission of sulfur dioxide which subsequently oxidizes to sulfur

trioxide and sulfuric acid (both termed as S(VI)). The efficiency of sulfur conversion efficiency ϵ to SO_3 and H_2SO_4 is defined as:

$$\epsilon = \frac{S(VI)}{S_T} = \frac{SO_3 + H_2SO_4}{S_T} \tag{3.12}$$

The magnitude of ϵ has been subject of several studies because of the relative important role that plays in the tropospheric chemistry and perhaps also climate. In the following will be discussed the dependence of epsilon on different combustion parameters and a short overview of the model results on aircraft engine internal oxidation will be given.

3.2.1   Dependence of ϵ on combustion parameters

The degree to which sulfur is oxidised within the engine depends significantly on the engine and its state of operation. According to model calculations, combustor exit temperature is one parameter that impacts markedly on exit speciation, so that higher temperatures result in higher sulfur conversion efficiencies. The reason for the decline in sulfur oxidation through the post combustor flow path with decreasing combustor temperatures may be lower O and OH content at the combustor exit and/or increase competition with NO_y for O and OH. The SO_3 and H_2SO_4 mixing ratios at the exit plane reported by Lukachko et al for different combustor exit temperatures is given in Figure 3.2. Interestingly, H_2SO_4 at the exit plane exhibits monotonic increase with decreasing combustor exit temperature while SO_3 showes a dependency peaking at combustor exit temperature 1675 K. The ϵ values range between 6.8 and 8.3 %. The Tremmel and Schumann model predicts the same dependence of ϵ on temperatures behind the combustor although the model supports lower ϵ values. Simulations for the ATTAS and the B737 engines yield ϵ=3.4-3.7 % and 5.6-5.9 % respectively for the for the same FSC; the calculated conversion efficiencies are higher for the B737 than for the ATTAS because of the higher combustor temperature and pressure.

The model calculations of Savelev et al demonstrate a different dependence of ϵ on initial combustor temperature [Sav02]. As seen in Figure 3.3 higher initial temperatures T_o result in lower sulfur conversion efficiencies. On the other hand, higher initial combustor pressures result in higher ϵ values. The same model investigates the dependency of air-to-fuel ratio (AFR) on the degree of sulfur oxidation in an aircraft
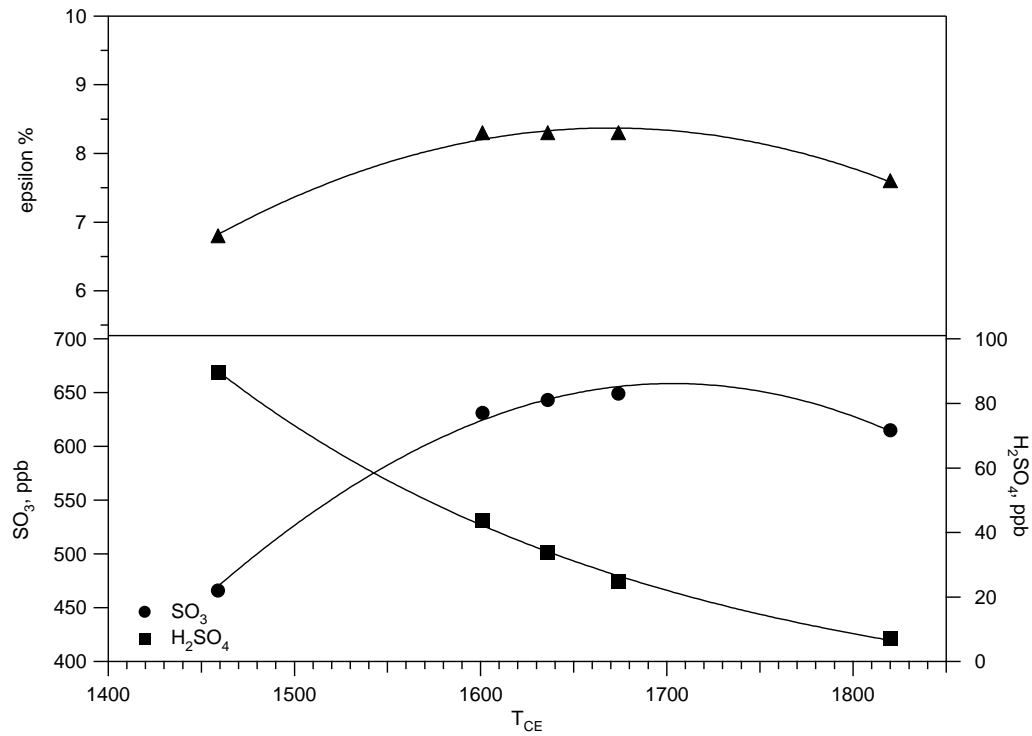
Figure 3.2: Model nozzle exit SO_3 and H_2SO_4 mixing ratios for different combustor exit temperatures T_{CE}. Data taken from [Luk98].

engine. It seems that higher AFR result in higher ϵ (see Figure 3.3). For the latter model the ϵ values are ranging from $<0.3\%$ to 2.5% by assuming typical residence time of the gas in the combustor chamber $10\,$msec and FSC$=0.3\,\%$. Heterogeneous reactions on combustion soot particles and post-combustor internal turbine surfaces were found to have negligible effect on exhaust sulfur levels [Bro02] and were not taken into account for none of the above mentioned work.

3.2.2   Dependence of ϵ on Fuel Sulfur Content

Theoretically investigated has also been the dependency of ϵ on FSC. Engine chemistry models imply decrease of ϵ with FSC because of the finite amount of oxidizing radicals available at combustor exit. The model of Brown et al [Bro96b] yielded ϵ values from $1\,\%$ for FSC$=2$ ppm up to $6\,\%$ for FSC$=5400\,$ppm in the aircraft engine. Other models imply a weaker dependence of ϵ on FSC. The ϵ values of Tremmel and Schumann [Tre99] lie in the range of $3.8\,\%$ to $3.5\,\%$ (see Figure 3.4). A minor reduction of epsilon with FSC is also predicted by the model of Starik et al, for which ϵ
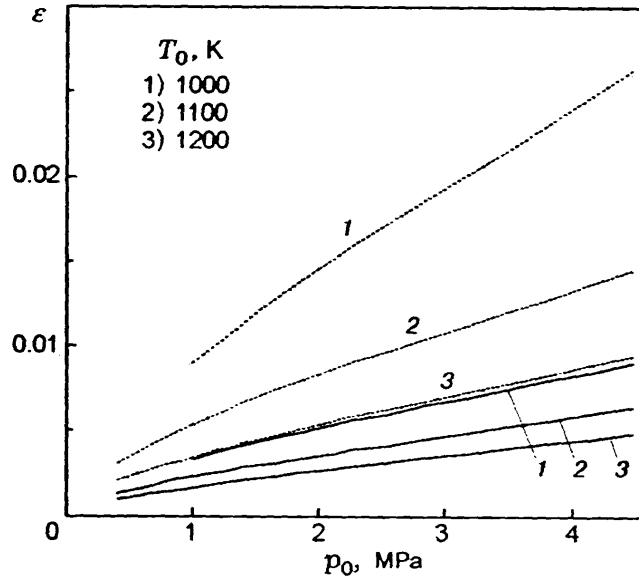
Figure 3.3: Combustor conversion efficiency ϵ as a function of the initial combustor pressure and temperature and of the mixture for AFR=3 (solid curve) and 4 (dotted curve) [Sav02].

in an RB211 engine was computed to be 9 % and 8.4 % for FSC of 0.04 and 0.3 % respectively [Sta02]. A tenfold increase of SO_2 at the combustor exit in the model of Lukachko et al resulted in a slight decrease in percent SO_x oxidation to SO_3 and H_2SO_4 of 0.6 % a and 0.1 % respectively [Luk98].

Most volatile aerosol measurements in the exhaust of aircraft plumes suggest a strong increase of ϵ with decreasing FSC but this may be misleading. The sulfuric acid concentration inferred form these studies is indirectly estimated from the measured aerosol particle size spectra, assuming that it is the only condensable gas contributing to volatile particle formation in the young exhaust plume. If it is so, then conversion efficiencies as high as 60 % should be assumed in order to account for the numerous volatile particles [Fah95]. An effort performed by Konopka et al to deduce the sulfuric acid content in volatile particles indicated that even 100 % conversion would not suffice to explain measured volume of volatile material in exhaust aerosol in some cases [Kon97] (oversampling of ice particles containing volatile particles could not be excluded). On the other hand, a more recent theoretical model interpretation of volatile aerosol measurement suggests that the experimental data would be consistent with epsilon ranging between 0.5 and 5 % [Kae00]. Since measurements of OH in the aircraft exhaust plumes exclude major sulfur oxidation in the aging plume $\epsilon < 2$ %
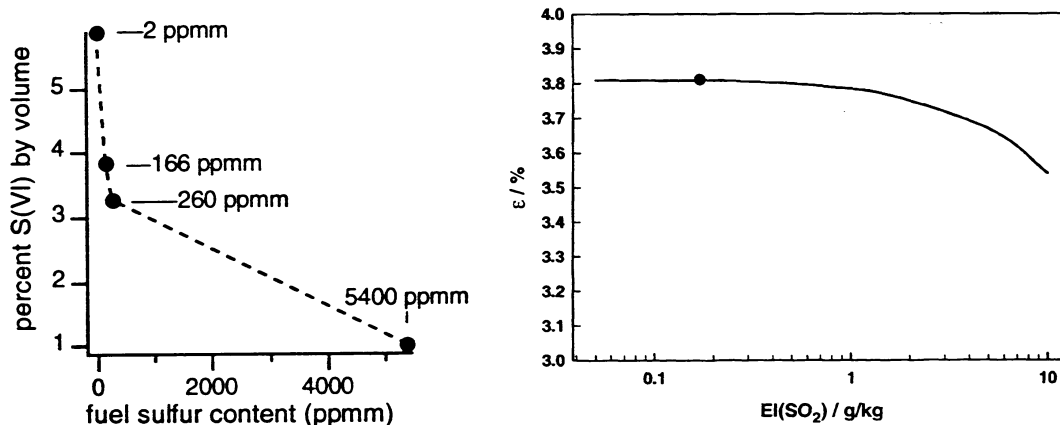
Figure 3.4: Percent conversion of fuel sulfur to S(VI) with FSC a) Strong predicted dependency of ϵ on FSC [Bro96b] b) Weaker dependency of ϵ on FSC [Tre99]

[Han97] and in-flight sulfuric acid measurements suggested ϵ values in the range of few percent [Cur98], [Cur02], these extremely high fuel sulfur conversions at lower FSC should be rather considered as overestimations. Alternative mechanisms of new volatile particle formation suggested that species other than H_2SO_4 may contribute to or control initial particle growth with low FSC, most probably exhaust hydrocarbons [Kae98], [Yu99], [Brock00].

The study of Miake-Lye et al. suggesting an increase of epsilon with increasing FSC may be subject to inaccuracies or errors in measurements [Mia98]. The results reported are based on measurements of volatile aerosol in the wake of a B737 airliner in flight burning fuels with two different sulfur contents, namely 72 and 676 ppm. The dramatic increase of the volatile component of the aerosol emissions with increasing FSC was interpreted as a result of an enhanced sulfur conversion efficiency, since the composition of the volatile component of the aerosol was attributed to the condensed sulfur. The sulfur fraction which has been condensed was determined by the measurements of SO_2 and CO_2 in the wake and the known FSC. Problems in measuring the total FSC (see discussion in [Hun00]) may have affected the results.

In Figure 3.5 is presented a compilation of previously reported ϵ for different FSC, including mostly indirectly inferred ϵ. Different colors are used for different techniques. Most data were taken from the review by Schumann et al. [Schu02] (see table 8 of this paper). The red symbols are direct measurements building on S(VI)
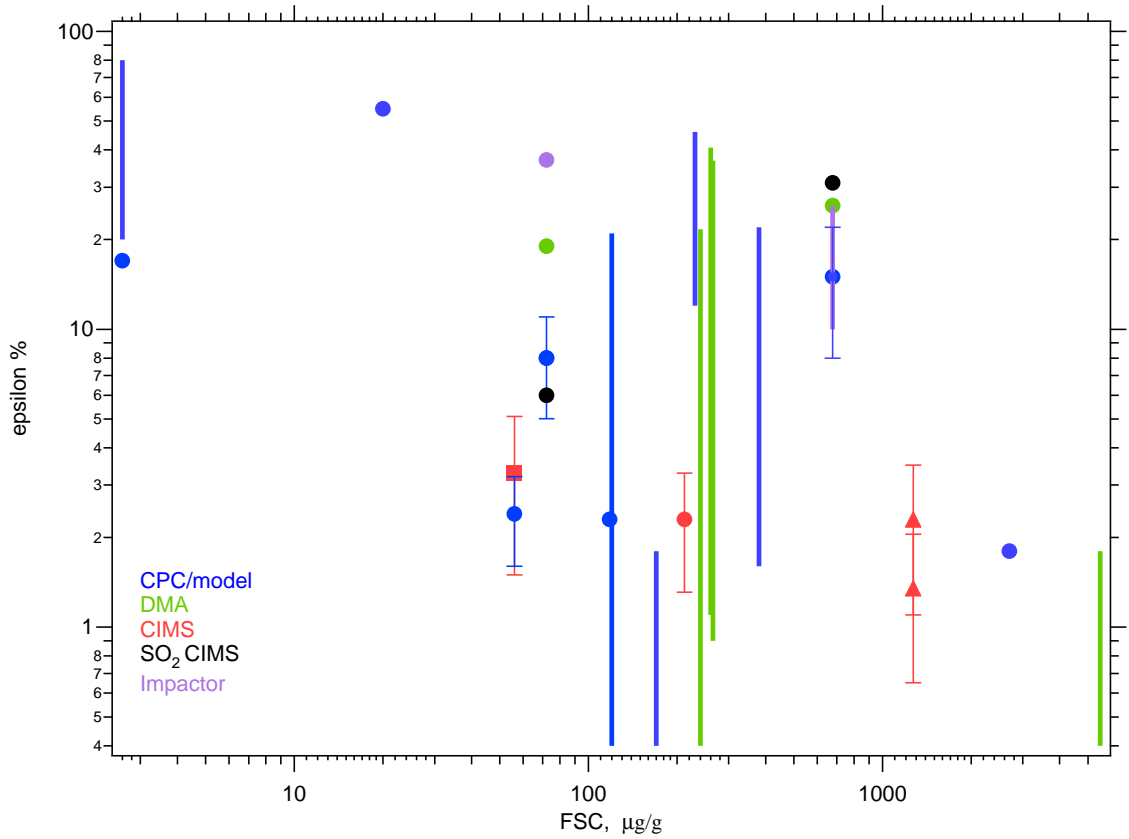
Figure 3.5: Overview of reported conversion efficiencies [Kat03]. For details see text.

data made by the MPIK-Heidelberg group; the red square refers to measurements in the wake of an aircraft in flight [Cur02]; the red circle refers to modeled results combined with experiments taking place in the exhaust of an aircraft engine [Sor03]; the red triangles refer to measurements performed in the internal flow of an aircraft engine [Kat03]. Epsilon values derived from DMA, CPC and impactor instruments were calculated from particulate volume presuming that the particles are exclusively composed of sulfuric acid and water. Although a first look at the figure suggests that the results scatter over a wide range, one may notice that the direct measurements of S(VI) species conducted in the exhaust of an aircraft engine (symbols with red color) are in favor of lower conversion efficiencies in the range of some percent.

3.3 Transformations of Sulfur emissions in the atmosphere

Aircraft emissions may cause changes in the background distributions of sulfuric acid and soot aerosols at regional and global scales. Although they are small compared with other global emissions from anthropogenic and natural sources, they occur in the upper troposphere and lower stratosphere, where background values are lower and removal processes are much less effective than near the Earth's surface. Moreover, aircraft aerosol particles tend to be smaller than background particles, so small emission masses may still cause large changes in aerosol number and surface area densities. In addition, aerosol particles from aircraft can participate in the formation of contrails and clouds in the upper troposphere, hence potentially alter the radiative balance of the atmosphere [Pen99].

3.3.1 Formation and growth of S-bearing aerosols

As already discussed in the previous chapters, fuel sulfur is emitted from aircraft engines mainly as SO_2 and to a lesser extend as SO_3 and H_2SO_4. Further oxidation of SO_2 occurs in the nascent plume via oxidation with OH radicals, which however is relative inefficient $\epsilon{<}2\,\%$ due to rapid depletion of OH [Han97]. The sulfur oxidation efficiency in the plume increases if the amount of directly emitted SO_3 increases: the fast SO_3 hydrolysis reaction produces H_2SO_4 directly, bypassing the slower SO_2+OH reaction and eliminating the dependence on OH. At this early stage of the plume atmospheric mixing processes causing gradients in relative humidity and temperature may lead to enhancements of particle formation rates. It is generally recognized that H_2SO_4 is an efficient aerosol precursor due mainly to its extremely lower vapor pressure. Sulfuric acid may promote nucleation of new aerosol particles in the a jet plume via different pathways. Binary homogeneous nucleation involves condensation of gaseous H_2SO_4/H_2O particles in the absence of surfaces that could assist the phase transition. The molecularized, hydrated H_2SO_4 clusters are formed at plume ages below 0.1 s and have a mean diameter d $<$ 1 nm. Their concentration is controlled by the FSC and the direct emissions of SO_3 [Kae99].

Formation of H_2SO_4/H_2O particles is accelatrated by Chemi-Ions (CI) which are
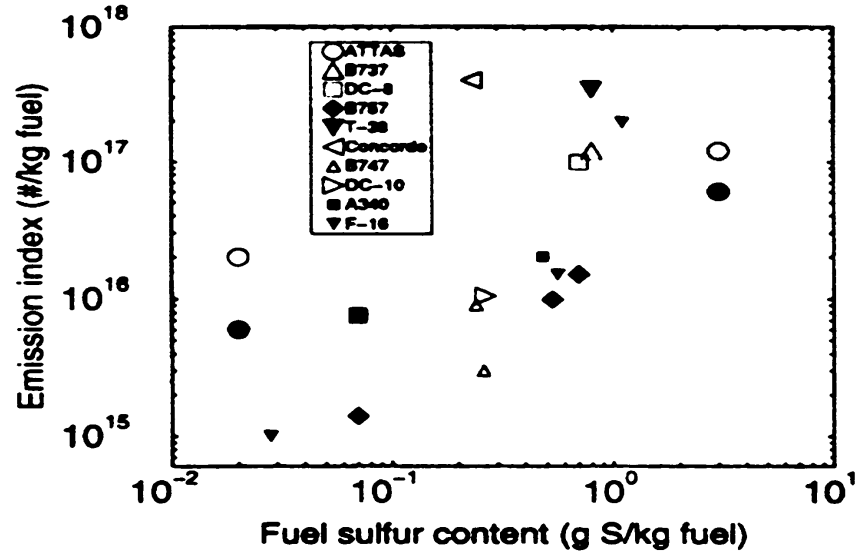
Figure 3.6: Emission indices of volatile particles measured in plumes of various aircraft. Particles were measured with diameters D>4-6 nm at plume ages less than 20 s, with D>9 nm at ages 0.25-1 min and with D>12 nm at ages 1-2 min [Kae99].

emitted from jet engines [Fre94]; [Arn98]; [Yu97]; [Yu98a]; [Yu98b]. These ions are generated by chemiionization processes within the engine combustors and provide centers around which molecular clusters rapidly coalesce, thus promoting the formation of electrically charged H_2SO_4/H_2O aerosols [Yu97]. Since nucleation and growth preferably occurs among the charged particle fraction due to low energy barriers, charged particles are generally predicted to rapidly occupy larger $D > 1$ nm sizes.

If soot, also emitted from aircraft engines, does participate in the gas-to-particle conversion process, the nucleation is referred to as heterogeneous. Sulfur trioxide and sulfuric acid might easily adsorb on soot. Direct emissions of S(VI) gases can lead to S(VI) mass fractions in the range of 0.7-14 % via adsorption from the gas phase depending on soot surface parameters [Kae98]. In the presence of H_2O, adsorbed molecules can lead to a liquid coating around the particles. Therefore heterogeneous nucleation can potentially alter the chemical surface reactivity of the soot particles. The primary soot mode is typically characterized by number-averaged sizes in the range 10-30 nm.

Coagulation, self-coagulation and condensation are the basic mechanisms controlling aerosol evolution in the early plume [Yu98a]. Particles from the ion mode grow beyond the smallest detectable size (3 nm with CN counters) due to enhanced growth

rates, whereby scavenging of the neutral mode clusters is the key growth path in the decaying wake. The impact of S emissions on the growth of these particles is shown in Figure 3.6, where emission indices (EI) of volatile particles in the plumes of various aircrafts are plotted against FSC. Decreasing sulfur emissions cause a reduction to EIs.

3.3.2   Formation of contrails and cirrus clouds

The increase of relative humidity that occurs in the engine plume as a result of mixing warm and moist exhaust gases with colder and less humid ambient air may lead to formation of contrails. Sulfur bearing aerosols formed in the aircraft plume can possibly contribute to their formation. Under favourable temperatures and pressures, volatile and soot particles may undergo freezing (homogeneous and heterogeneous respectively) via water uptake and form contrail ice particles. In a contrail, particles have to grow to sizes $>0.1\,\mu$m by H_2O uptake to form water ice. The threshold activation size and hence, freezing probability depends on the maximum super-cooling reached in the expanding plume. Decreasing ambient temperature and increasing ambient humidity both lower the threshold size and increase the homogeneous freezing rates. There seems to be a correlation between aircraft fuel consumption and contrail frequency [1] as shown in Figure 3.7. The correlation implies that contrail coverage is limited mainly by the number of aircraft flights not by atmospheric conditions at cruise altitudes.

Aircraft contrail may perturb natural cirrus or trigger formation of cirrus clouds which are much more extensive in scale than the initial contrails [Pen99]. Aged contrails often cannot be distinguished from cirrus, which poses an observational problem in determining the frequency and area of coverage by contrails. Still, observations from space [Min98] and from in situ measurements [Schr00] clearly show that persistent contrails may develop into cirrus clouds. Attempts have been made to calculate the average change in cirrus cloud occurrence as a function of aviation fuel use at the observation locations. The results indicate a statistically significant increase in cirrus occurrence in the North Atlantic flight corridor compared with the rest of the North

---

[1]Contrail frequency refers to the probability that a contrail will be observed somewhere within the scene being viewed
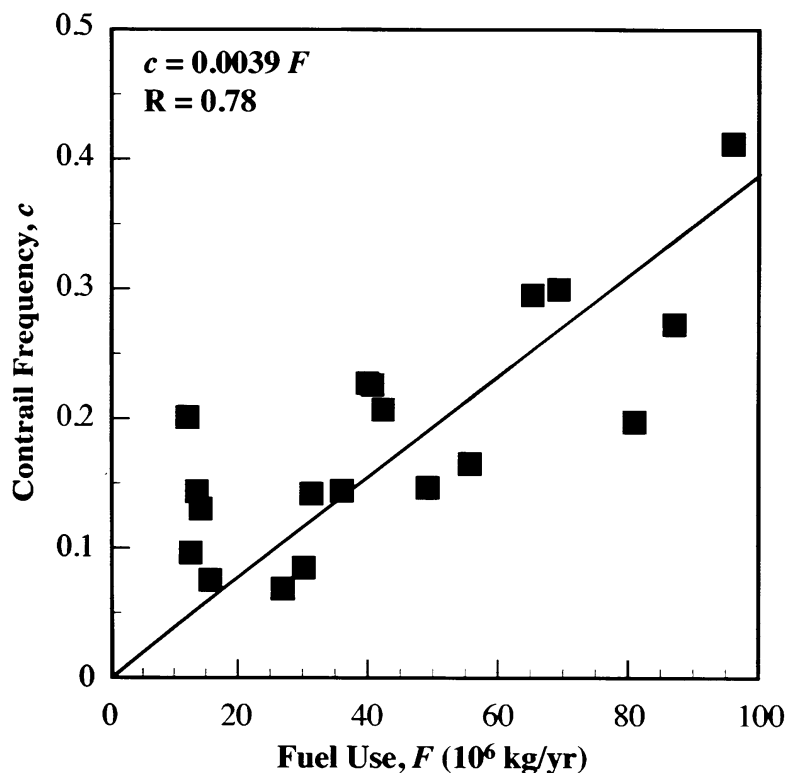
Figure 3.7: Correlation of mean annual contrail frequency based on observations vs aircraft fuel usage [Pen99].

Atlantic ocean.

3.4   Impacts of Sulfur aircraft emissions on climate

Aircraft emissions are expected to modify the earth's radiative forcing as a result of several processes: the emissions of radiatively active gases, like CO_2 and H_2O; the emissions of chemical species which affects radiatively active substances, like NO_x which modifies the O_3 concentration; the emission of substances which trigger the generation of contrails and at a later stage perhaps clouds, like soot and sulfuric acid. From the total amount of aircraft emissions which is small relatively to many other emissions, one might anticipate that the change in radiative forcing and consequently in climate will be small relative to natural variability for the present air-traffic. However, most aircraft emissions are taking place close to the tropopause where radiative

effects are large. The climate response depends on several internal quantified processes which are still poorly quantified [Bra98].

Sulfur aircraft emissions contribute 0.16 % to the total atmospheric burden of sulfate. The ratio between the global emissions of aircraft sulfur and total sulfur is 0.06 % [Kje99]. Because of the long turn-over time for aircraft sulfur the contribution to the atmospheric sulfur content is larger than would be expected judging only from the emissions. Compared to other sulfur sources contribution of aircraft sulfate has a high efficiency, similar to volcanic emissions. Nevertheless, on a global scale the additional amount of sulfate from aircraft is a very small contribution to the total burden of sulfate.

Sulfate aerosols related to aviation may have a direct radiative effect which has been estimated to be in the range of -0.12 to -0.40 Wm^{-2} for the North Atlantic flight corridor, depending on season and relative change in background conditions [For95]. A further impact of aircraft sulfur and soot emissions is indirect: the aircraft-induced aerosols provide surfaces for heterogeneous chemical reactions, which in turn may modify the evolution of the chemical composition of the gaseous aircraft emissions and of the background atmosphere. However, currently not much is known about the large scale impact of these processes.

Chapter 4

Ion Trap and Chemical Ionization Mass Spectrometry

The Paul Ion Trap, named after Wolfgang Paul the Nobel Prize winner in 1989 for the development of the Ion Trap technique, is a device which functions both as an ion store in which gaseous ions can be confined for a period of time and as a mass spectrometer of considerable mass range and variable mass resolution. Coupled with the chemical ionization technique which uses selected reactant ions to ionize the sample yielding mass spectra which are relatively easy interpreted, appears to be a powerful scientific tool for atmospheric research. In the following it will be given a description of the Paul Ion Trap Mass Spectrometer theory and the Chemical Ionization technique used for accomplishment of the measurements presented in this work. For a more detailed description see [Mar97].

4.1   The Ion Trap

The quadrupole ion trap consists essentially of three electrodes which are shown in Fig 4.1. Two of the three electrodes are virtually identical and have a hyperboloidal geometry. They are called end-cap electrodes. The third electrode is also of hyperboloidal geometry and is called the ring electrode. The ring electrode is positioned symmetrically between two end-cap electrodes. The radius of the ring electrode in the central horizontal plane is r_o and the separation of the two end-cap electrodes measured along the axis of the ion trap is $2z_o$. The electrodes in theory extend to
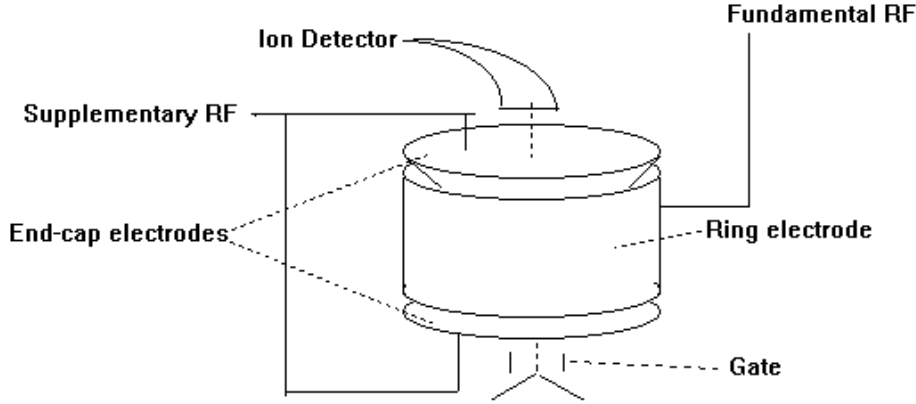
Figure 4.1: Schematic presentation of an ion trap and applied potentials.

infinity but for practical purposes are truncated. The geometries of the electrodes are defined so as to produce an ideal quadrupole field which, in turn, will produce a parabolic potential well for the confinement of ions.

In the trapping potential well created within the electrode assembly of the ion trap are confined the ion species. This well is created from the field which exists when a Radio Frequency (RF) potential is applied to the ring electrode and the two end-cap electrodes are grounded. For an ideal quadrupole field, the following identity is given:

$$r_o^2 = 2z_o^2 \tag{4.1}$$

so that once the magnitude of r_o is given the sizes of all three electrodes and the electrode spacings are fixed. However, the ratio of z_o^2 to r_o^2 is not necessarily restricted to 2.

4.1.1   The quadrupole field

The quadrupole ion trap is a dynamic instrument since ion trajectories are influenced by a set of time-dependent forces. An ion in a quadrupole field experiences strong focusing in the sense that the restoring force, which drives the ion back towards the centre of the device, increases as the ion deviates from the centre of the device. It

has been found that the motion of ions in a quadrupole field can be described mathematically by the solutions to the second-order linear differential equation described originally by Mathieu. This equation is known as the Mathieu equation and its solutions and the ideas of stability and instability to describe the trajectories of ions confined in quadrupole devices and to define the limits to trajectory stability can be applied for the ion trap quadrupole field.

In order to adopt the solutions to the Mathieu equation, it is assumed that the equation of motion of an ion confined in a quadrupole device can be described by the Mathieu equation. An expression for a force is thus obtained and it is compared to the expression for the force on an ion in a quadrupole field. This comparison, allows one to express the magnitudes and frequencies of the potentials applied to ion trap electrodes, the size of the ion trap and the mass/charge ratio of ions confined therein in terms of Mathieu's dimensionless parameters, a_u and q_u.

The commonly accepted form of Mathieu eqquation is:

$$\frac{d^2u}{d\xi^2} + (a_u - 2q_u cos2\xi)u = 0 \tag{4.2}$$

where u represents the coordinate axes x, y and z, m is a dimensionless parameter equal to Ω t/2 such that Ω must be a frequency as t is time, and a_u and q_u are additional dimensionless parameters known as trapping parameters. Ω will reappear as the radial frequency (in rad s^{-1}) of the RF potential applied to the ring electrode. By substituting $\xi = \Omega$ t/2:

$$\frac{d^2u}{dt^2} = \frac{\Omega^2}{4}\frac{d^2u}{d\xi^2} \tag{4.3}$$

Combining these equations and multiplying by m yields:

$$m\frac{d^2u}{dt^2} = \frac{-m\Omega^2}{4}(a_u - 2q_u cos\Omega t)u \tag{4.4}$$

The left side of this equation represents the force on an ion i.e. mass times accelaration.

The field in quadrupole devices is uncoupled so that the forces in the three coordinate directions may be determined separately. We consider the force in the x-direction F_x, experienced by an ion of mass m, and charge e at any point within a quadrupole field :

$$F_x = ma = m\frac{d^2x}{dt^2} = -e\frac{\partial\varphi}{\partial\chi} \tag{4.5}$$

where a is the acceleration of the ion, e is the electronic charge and φ is the potential at any point (x, y, z) within the field. Similar expressions for F_y and F_z can be obtained. The latter equation relates the force on an ion to the field within the ion trap. The quadrupole potential φ can be expressed as:

$$\varphi = \frac{\varphi_o}{r_o^2}(\lambda x^2 + \sigma y^2 + \gamma z^2) \tag{4.6}$$

where φ_o is the applied electric potential (which is an RF potential either alone or in combination with a direct current (DC) potential, λ, σ and γ are weighting constants for the x, y and z coordinates, respectively, and r_o is a constant which is defined separately depending on whether the quadrupole device is an ion trap or mass filter.

It can be seen that the potential increases quadratically with x, y and z. In any electric field, it is essential that the Laplace condition, which requires that the second differential of the potential at a point be equal to zero, be satisfied; the Laplace condition ensures that the field in the x, y and z directions is linear. When that is done, it is found that:

$$\lambda + \sigma + \gamma = 0 \tag{4.7}$$

For the ion trap $\lambda = \sigma = 1$ and $\gamma = -2$. Equation 4.6 can be transformed in cylindrical coordinates by employing the standard transformations x=rcos θ, y=rsin θ and z=z thus it can be also written as:

$$\varphi_{r,z} = \frac{\varphi_o}{r_o^2}(r^2 - 2z^2) \tag{4.8}$$

The applied electric potential φ_o (applied to the ring electrode), is either an RF potential VcosΩt or a combination of a DC potential, U, of the form

$$\varphi_o = U + Vcos\Omega t \tag{4.9}$$

where Ω is the angular frequency (in rad s^{-1}) of the RF field. Note that Ω is equal to 2πf, where f is the frequency in hertz. When the expression for φ and λ=1 are substituted into 4.6 and φ is differentiated with respect to x, one obtains the following expression for the potential gradient:

$$\frac{\partial \varphi}{\partial \chi} = \frac{2x}{r_o^2}(U + Vcos\Omega t) \tag{4.10}$$

Substitution into equation 4.5 yields an expression for the force on an ion:

$$m\frac{d^2x}{dt^2} = \frac{-2e}{r_o^2}(U + Vcos\Omega t)x \tag{4.11}$$

Comparison of the right terms of the last equation with 4.4 (u represents x) gives:

$$a_x = \frac{8eU}{mr_o^2\Omega^2} \quad q_x = \frac{-4eV}{mr_o^2\Omega^2} \tag{4.12}$$

When this derivation is repeated to obtain the force on an ion in the y-direction in a the quadrupole ion trap, it is found that $q_x=q_y$ since $\lambda=\sigma=1$. And also:

$$a_z = -\frac{8eU}{mr_o^2\Omega^2} \quad q_z = \frac{4eV}{mr_o^2\Omega^2} \tag{4.13}$$

As already mentioned the electrodes of the ion trap are truncated in order to obtain a practical working instrument but this truncation introduces higher-order multipole components to the potential :

$$\varphi_{r,z} = C_0^0 + C_1^0 z + C_2^2(\frac{1}{2}r^2 - z^2) + C_3^0(\frac{3}{2}r^2 - z^2) + ... \tag{4.14}$$

The C_n^0 coefficients correspond to monopole, dipole, quadrupole, hexapole and octopole components, respectively, of the potential $\varphi_{r,z}$. For the pure quadrupole ion trap, only the coefficients corresponding to n=0 and n=2 are non-zero.

In order to compensate for these higher order multi-pole components, the electrodes of most commercial devices are assembled in such a way that the distance between the end-cap electrodes has been increased; the value of has been z_0 is increased by 10.6%. However, there was no corresponding modification of the shapes of the electrodes, which would be required in order to maintain a purely quadrupolar geometry.

The immediate consequences are that the asymptotes to the end-cap electrodes no longer coincide with those for the ring electrode. Furthermore $r_o^2 \neq 2z_o^2$. In order to compensate, in part, for the stretching of the ion trap, the trapping parameters are now calculated using the actual values of z_o and r_o as follows:

$$a_r = \frac{8eU}{m(r_o^2 + 2z_o^2)\Omega^2} \quad q_r = \frac{-4eV}{m(r_o^2 + 2z_o^2)\Omega^2} \tag{4.15}$$

and

$$a_z = \frac{-16eU}{m(r_o^2 + 2z_o^2)\Omega^2} \quad q_z = \frac{8eV}{m(r_o^2 + 2z_o^2)\Omega^2} \tag{4.16}$$

4.1.2   The potentials on the electrodes

In order to verify the potentials on the ring and end-cap electrodes in the commercial ion trap, an alternative electrode equation to equation 4.8 must be used:

$$\varphi_{r,z} = \frac{\varphi_o(r^2 - 2z^2)}{2r_o^2} + c \qquad (4.17)$$

where c is a constant. The ring electrode potential is given by equation 4.17 for z=0 and r=r_o:

$$\varphi_{r_o,0} = \frac{\varphi_o r^2}{2r_o^2} + c = \varphi_o \qquad (4.18)$$

from which c=$\varphi_o/2$ is obtained. The potential in the end-cap electrode (r=0, z=z_o) is given by:

$$\varphi_{0,z_o} = \frac{-2\varphi_o z_o^2}{2r_o^2} + \frac{\varphi_o}{2} = 0 \qquad (4.19)$$

Hence equation 4.17 reduces to:

$$\varphi_{r,z} = \frac{\varphi_o(r^2 - 2z^2)}{2r_o^2} + \frac{\varphi_o}{2} \qquad (4.20)$$

The constant term does not change the equations of motion derived from the partial differentials, but the potential along the asymptotes of the hyperbolas is changed. It should be noted that an ion at the centre of a commercial ion trap experiences a potential of $\varphi_o/2$ but no net field and "sees" a potential of -$\varphi_o/2$ on the end-cap electrodes and a potential of $\varphi_o/2$ on the ring electrode.

4.1.3   Regions of trajectory stability

Quadrupole ion trap operation is concerned with the criteria that govern the stability (and instability) of the trajectory of an ion within the field, that is, the experimental conditions that determine whether an ion is stored within the device or is ejected from the device and either lost or detected externally. The solutions to Mathieu's equation are of two types: i) periodic but unstable and ii) periodic and stable. Solutions of type i) are called Mathieu functions of integral order and form the boundaries of unstable regions on the stability diagram. The boundaries, which are referred to as characteristic curves or characteristic values, correspond to those values of a new trapping parameter β_z, which is a complex function of a_z and q_z. The boundaries
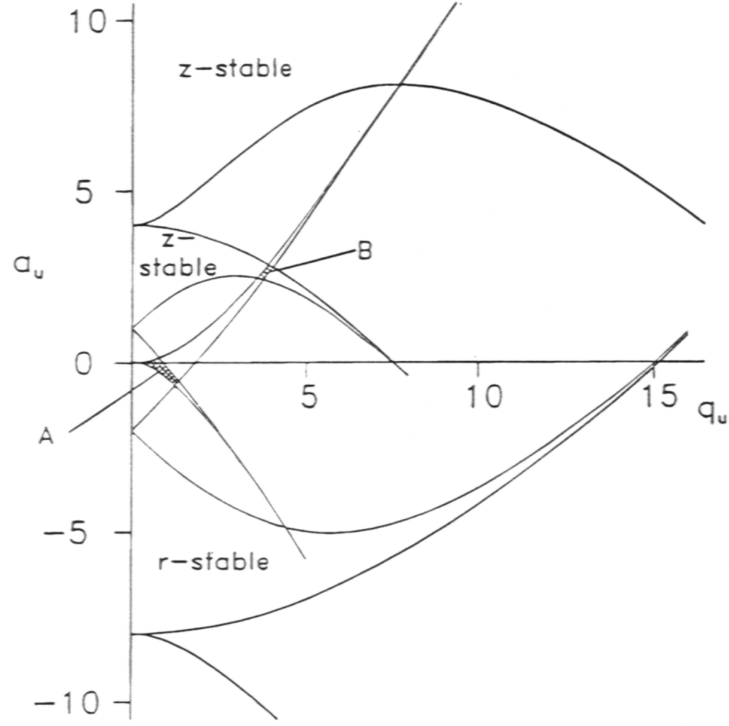
Figure 4.2: Mathieu stability diagram in (a_z, q_z) space for the quadrupole ion trap both the r and z directions. Regions of simultaneous overlap are labeled A and B. Taken from [Mar97].

represent, in practical terms, the point at which the trajectory of an ion becomes unbounded.

Solutions of type ii) determine the motion of ions in the ion trap. The stability regions corresponding to stable solutions of the Mathieu equation in the r-direction are shaded and labeled r-stable in Fig. 4.2. Ions can be stored in the ion trap provided that their trajectories are stable in the r- and z-directions simultaneously; such trajectory stability is obtained in the region closest to the origin, that is, region A in Fig. 4.2, which is plotted in a_u, q_u space. Regions A and B are referred to as stability regions; region A is of the greatest importance at this time (region B remains to be explored) and is shown in greater detail in Fig. 4.3. The coordinates of the stability region in Fig. 4.3 are the Mathieu parameters a_z and q_z. Here, it is plotted a_z versus q_z rather than a_u versus q_u, which is unnecessarily confusing because u=r, z. The β_z=1 stability boundary intersects with the q_z axis at q_z=0.908; this working point is that of the ion of lowest mass/charge ratio (that is, low-mass cut-off) which
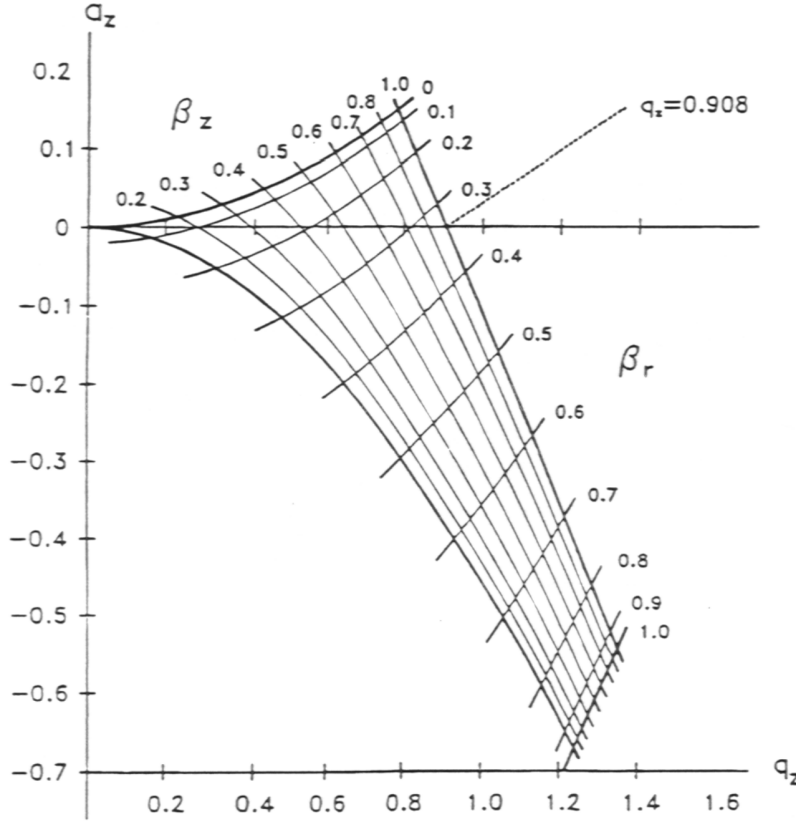
Figure 4.3: Stability diagram in (a_z,q_z) sapce in th region of simultaneous stability in both the r and z directions near the origin for the three dimensional quadrupole ion trap; the iso-β_t and iso-β_z are shown in the diagram. The q_z axis intersects the $\beta_z{=}1$ boundary at $q_z{=}0.908$, which corresponds to q_{max} in the mass-selective instability mode. Taken from [Mar97].

can be stored in the ion trap.

4.1.4   Operation of the ion trap as a mass spectrometer

As a storage device, the ion trap acts as an electric field test-tube for the confinement of gaseous ions, either positively or negatively charged. The confining capacity of the electric field test-tube arises from the formation of a trapping potential well when appropriate potentials are applied to the electrodes of the ion trap. The pressure of helium in the ion trap is set at about 10^{-3} Torr in order to cool the ions and herd them to the center of the trap under the action of momentum dissipating collisions.

The ring electrode is driven at an initial RF voltage V_o and a fixed frequency so that all ions in a given range of mass/charge ratio are trapped within the imposed

quadrupole field. The value of the initial RF voltage imposes a low-mass cut-off (LMCO) usually in the range m/z 20-50, so that ions of lower mass/charge ratio are not stored. No DC potential is applied between the ring and end-cap electrodes (U=0) so that the confining field is purely oscillatory. Ions follow Lissajous-type trajectories and are subjected simultaneously to about 20,000 collisions per second with helium; those ions which are not lost from the ion trap become focused near the trap centre. The principal method for measuring the mass/charge ratios of confined ions is to tip the potential well, or basin of the ion trap in a particular direction so that ions tumble out of the potential well and leave the ion trap in order of ascending mass/charge ratio. As the RF amplitude is ramped over the period 30-85 ms, the mass-selective ion ejection and mass analysis occur.

Once the ion cloud within the ion trap has been focused collisionally to the centre of the trap over a period of some 1-30 ms, the amplitude of the RF potential is ramped. The ramping of the RF potential amplitude, which is described as an analytical scan, causes the q_z values of all ion species to increase throughout the ramp. As the value for each q_z ion species reaches a value of 0.908, the ions are ejected axially through the end-cap electrodes.

4.2   Chemical Ionization Mass Spectrometry

Chemical ionization uses ion-molecule reactions in the gas phase to produce ions from the sample molecule. The advantage of these reactions is that they are relatively fast ($k \sim 10^{-9}$) and very selective: the reactions can only occur for trace gases having a large large proton affinity (chemical ionization mass spectrometry of negative ions) or large gas phase basicity. That reduces significantly the perturbation of interference with other trace gases. The most simple reaction system is a bimolecular reaction transforming $E^{\pm}$ into $P^{\pm}$ and a neutral product B by reaction with a trace gas A. The ratio of the product $P^{\pm}$ to educt ions $E^{\pm}$ ions after reaction time τ is a measure of the absolute number density of the trace gas A with which the educt ions have reacted.

Generally the assumption $[A] \gg E^{\pm}$ is valid and the reaction can be treated as

pseudo-first order ([A]=const.):

$$E^{\pm} + A \xrightarrow{k_v} P^{\pm} + B \tag{4.21}$$

$$d_t[E^{\pm}] = -k_v[A][E^{\pm}] \tag{4.22}$$

$$d_t[P^{\pm}] = +k_v[A][E^{\pm}] \tag{4.23}$$

where k_v is the rate coefficient (units: cm^3/s). $E^{\pm}$ is exponentially decreasing with a lifetime $\tau = (k_v[A])^{-1}$:

$$[E^{\pm}] = [E^{\pm}]_0 \cdot e^{-t\tau^{-1}} \qquad (\tau^{-1} = k_v[A]) \tag{4.24}$$

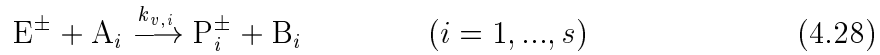$$[P^{\pm}] = [E^{\pm}]_0 \cdot \left(1 - e^{-t\tau^{-1}}\right) \tag{4.25}$$

Since

$$[E^{\pm}]_0 = [E^{\pm}]_t + [P^{\pm}]_t \tag{4.26}$$

at a given time t_M the concentration of A is related with the ratio $V = [E^{\pm}]_{t_M}/[P^{\pm}]_{t_M}$ (ACIMS-formula):

$$[A] = \frac{1}{t_M k_v} \ln(1 + V) \qquad V = \frac{[P^{\pm}]_{t_M}}{[E^{\pm}]_{t_M}} \tag{4.27}$$

The generalization of formula 4.27 for the case of several trace gases reacting with one educt ion species to (distinguishable) products is straightforward and yields [Kno89]:

$$E^{\pm} + A_i \xrightarrow{k_{v,i}} P_i^{\pm} + B_i \qquad (i = 1, ..., s) \tag{4.28}$$

$$d_t[E^{\pm}] = -\sum_{i=1}^{s} k_{v,i}[A_i][E^{\pm}] \tag{4.29}$$

$$d_t[P_i^{\pm}] = k_{v,i}[A_i][E^{\pm}] \tag{4.30}$$

$$[E^{\pm}] = [E^{\pm}]_0 \cdot e^{-t\tau^{-1}} \qquad \left(\tau^{-1} = \sum_{i=1}^{s} k_{v,i}[A_i]\right) \tag{4.31}$$

$$[P^{\pm}] = [E^{\pm}]_0 \cdot \left(1 - e^{-t\tau^{-1}}\right) \qquad \left([P^{\pm}] = \sum_{i=1}^{s}[P_i^{\pm}]\right) \tag{4.32}$$

$$[P_i^{\pm}] = \frac{\tau}{\tau_i}[E^{\pm}]_0 \cdot \left(1 - e^{-t\tau^{-1}}\right) \qquad \left(\tau_i^{-1} = k_{v,i}[A_i]\right) \tag{4.33}$$

$$[A_i]_{t_M} = \frac{1}{t k_{v,i}} \frac{[P_i^{\pm}]_{t_M}}{[P^{\pm}]_{t_M}} \ln\left(1 + \frac{[P^{\pm}]_{t_M}}{[E^{\pm}]_{t_M}}\right) \qquad \left([P_{t_M}^{\pm}] = \sum_{j=1}^{s}[P_j^{\pm}]_{t_M}\right) \qquad (4.34)$$

Equation 4.34 is termed as *Parallel-ACIMS formula* and allows the calculation of the concentration of one specific trace gas A_i if only the fractions $[P_i^{\pm}]/[P^{\pm}]$ and $[P^{\pm}]/[E^{\pm}]$ are known. Equation 4.34 is usually used to infer trace gas concentrations via CIMS. It can be seen that the relative distribution among the product species $[P_i^{\pm}]/[P^{\pm}]$ reflects the lifetime of $E^{\pm}$ against the respective reaction if the destruction of the educt ions involves several trace gases. Hence it must be known to determine the trace gas concentrations $[A_i]$.

The uncertainty in determination of the number density of a trace gas using the ACIMS formula depends mostly on the uncertainties in the rate coefficient k and the determination of the reaction time τ. The uncertainty of the reaction coefficients is available in literature, while the uncertainty of the reaction time has to be defined in the laboratory. The appropriate gas velocity to convert reaction distance to reaction time is not the bulk velocity given by the total volumetric flow and the geometric cross section of the reactor. The reaction time is determined by the the core gas velocity, which can be slightly greater than the bulk gas velocity, since ions are ejected close to the z-axis of the flow tube. In case of an ideal laminar flow the core gas velocity would be two times larger than the bulk gas velocity.

4.2.1   Detection of Sulfuric Acid

The detection of sulfuric acid employs the gas phase ion-molecule reaction of H_2SO_4 with gaseous $NO_3^-(HNO_3)_n$ ions (n=0,1,2):

$$NO_3^-(HNO_3)_n + H_2SO_4 \longrightarrow HSO_4^-(HNO_3)_n + HNO_3 \qquad (4.35)$$
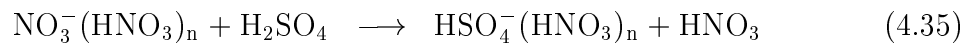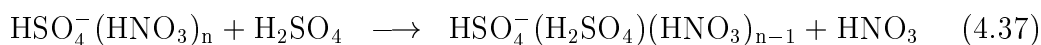
which was originally proposed by Arnold and Fabian [Arn80] and subsequently investigated in the laboratory by Viggiano et al [Vig82]. The rate coefficients are k_1=2.32, k_2=1.86 and k_3=1.72·$10^9 cm^3 s^{-1}$ for n=0,1,2 respectively at 300 K [Vig97]. These rate constants are precise to within 10-15%.

The family of product ions $P^{\pm}$ in the ACIMS formula includes the $HSO_4^-(HNO_3)_n$ ions and the family of educts $E^{\pm}$ the $NO_3^-(HNO_3)_n$ ions with n=0-2. Since there are three different reaction coefficients k_1, k_2 and k_3 for reactions with n=0-2, in the

ACIMS formula a weighted rate coefficient k=$a_1k_1 + a_2k_2 + a_3k_3$ has been used . The weigh factors a_n are defined for n=0,1,2 as:
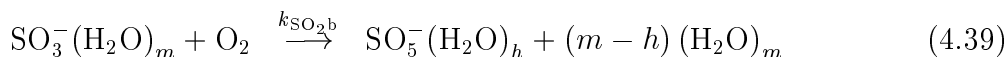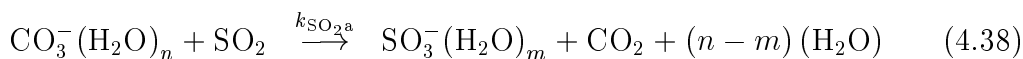
$$a_n = \frac{P_n^{\pm}}{\sum P^{\pm}} \tag{4.36}$$

The primary product ions of these reactions are $HSO_4^-(HNO_3)_n$ with n=0, 1, 2 but for high concentrations of H_2SO_4 in the flow reactor appear also secondary and tertiary products like $HSO_4^-(H_2SO_4)$ and $HSO_4^-(H_2SO_4)_2$ respectively. These form by reaction of $HSO_4^-(HNO_3)$ with H_2SO_4 in a ligand exchange reaction:

$$\text{HSO}_4^-(\text{HNO}_3)_n + \text{H}_2\text{SO}_4 \quad \longrightarrow \quad \text{HSO}_4^-(\text{H}_2\text{SO}_4)(\text{HNO}_3)_{n-1} + \text{HNO}_3 \tag{4.37}$$

When $HSO_4^-(H_2SO_4)_m(HNO_3)_l$ are produced to a measurable extend they have to be included in the sum of the production ion abundance ratio R.

4.2.2   Detection of Sulfur Dioxide

For the detection of sulfur dioxide, CO_3^- ions react with SO_2-molecules to form SO_3^- which reacts with O_2 in a consecutive reaction to SO_5^-:

$$\text{CO}_3^-(\text{H}_2\text{O})_n + \text{SO}_2 \quad \overset{k_{\text{SO}_2\text{a}}}{\longrightarrow} \quad \text{SO}_3^-(\text{H}_2\text{O})_m + \text{CO}_2 + (n-m)\,(\text{H}_2\text{O}) \tag{4.38}$$

$$\text{SO}_3^-(\text{H}_2\text{O})_m + \text{O}_2 \quad \overset{k_{\text{SO}_2\text{b}}}{\longrightarrow} \quad \text{SO}_5^-(\text{H}_2\text{O})_h + (m-h)\,(\text{H}_2\text{O})_m \tag{4.39}$$

The rate coefficients of these reactions are: $k_{\text{SO}_2\text{a}} = 5 \cdot 10^{-10}\,\text{cm}^3\text{s}^{-1}$ ($n = 0$) and $k_{\text{SO}_2\text{a}} = 1.4 \cdot 10^{-9}\,\text{cm}^3\text{s}^{-1}$ ($n \geq 1$); $k_{\text{SO}_2\text{b}} = 2.0 \cdot 10^{-12}\,\text{cm}^3\text{s}^{-1}$ [Moe92]. The accuracy of this rate coefficient is 30 %.

The same rate coefficients of the $CO_3^-(H_2O)_n+SO_2$ reaction were also measured by Seeley et al., with an uncertainty of $\pm$30 % [See97]. The values obtained at 158 K were 0.88·10^{-9} for n=0 and 1.65·10^{-9} for n=1, with a temperature dependence of k_n=A×$(300/T)^m$, where A=0.37 and 1.6·10^{-9}; m=1.27 and 0 for n=0 and n=1, respectively. At room temperature this result was 20 % lower than the result of Moehler et al. All of the results, though, are within the combined error limits of the measurements. The n=0 reaction is an exothermic reaction but unlike many exothermic ion molecule reactions which proceed at collision rate, the n=0 reaction proceeds at a fraction of the collision rate (40 %). However, this behaviour is common wit CO_3^- reactions involving O^- transfer [Arn95a].

4.3   Experimental set up

The apparatus used for the measurements of the trace gases consists of a stainless steel flow reactor (inner diameter 4cm), a high frequency discharge ion source and an Ion Trap. The ions $P^\pm$ used as probes for trace gas detection are generated in the **ion source**, in an atmosphere containing oxygen (O_2) and another trace gas (e.g. CO_2 or NO_2 for production of CO_3^- or NO_3^- ions, respectively). Subsequently, they are introduced into the flow reactor which contained the sample gas to be analyzed and react with the trace gas. The educt ions have time τ to react with the trace gas until they reach the inlet of the mass spectrometer. At that point only a fraction of the gas flow enters the mass spectrometer through a critical orifice (diameter 0.2 mm).

The ions are transmitted to the ion trap through the **ion optics**. These ion optics consist of two octapoles and an itneroctapol lens. Each octapole is an octagonal array of cylindrical rods that acts as an ion transmission device. An RF voltage (2.45 MHz, 400 V) and dc offset voltage (-10 to +10 V) that are applied to the rods give rise to an electric field that guides the ions along the axis of the octapole. During ion transmission, is positive for negative ions. The octapole RF is turned off during mass analysis. The two octapoles are separated by the interoctapole lens, which assists in the focusing of ions. It also serves as a baffle between the first octapole region and the analyzer region. A tune procedure can optimizes optimize the potentials applied to the lenses to maximize the ion current to the mass analyzer.

The **mass analyzer** is mounted on the analyzer mount opposite to the second octapole (Figure 4.4). As already mentioned includes three stainless steel electrodes: the entrance endcap electrode, the exit endcap electrode and the ring electrode. Together they form a cavity in which the mass analysis occurs. After being analyzed, ions are ejected through the exit endcap electrode towards the ion detection system.

The **ion detection** system includes a 15 kV conversion dynode and a channel electron multiplier (Figure 4.5). The **conversion dynode** is a concave metal surface to which a potential of +15 kV is applied for negative ion detection. When an ion strikes the surface of the conversion dynode, one or more secondary particles are produced. The secondary particles are focused by the curve surface of the conversion dynode and are accelerated by a voltage gradient into the electron multiplier. The **electron multiplier** includes a cathode and an anode. Secondary particles from

the conversion dynode strike the inner walls of the electron multiplier cathode with sufficient energy to eject electrons. The ejected electrons are accelerated further into the cathode, drawn by the increasingly positively potential gradient. Due to the funnel shape of the cathode, the ejected electrons do not travel far before they again strike the nner surface of the cathode, thereby causing the emission of more electrons. Thus, a cascade of electron is created that finally results in a measurable current at the end of the cathode where the electron are collected by the anode. The current collected is proportional to the number of secondary particles striking the cathode.

The whole system is enclosed into a vaccum manifold, a thick-walled, aluminum chamber with removable top cover plate devided into two two regions: the first octapole region,which is evacuated to 1 Torr and the analyzer region, which is evacuated to $2 \cdot 10^{-5}$ Tor. A Balzers-Pfeiffer TMH 260-130 split flow turbomolecular pump provides the vacuum for the first octapole and analyzer region of the vacuum manifold.
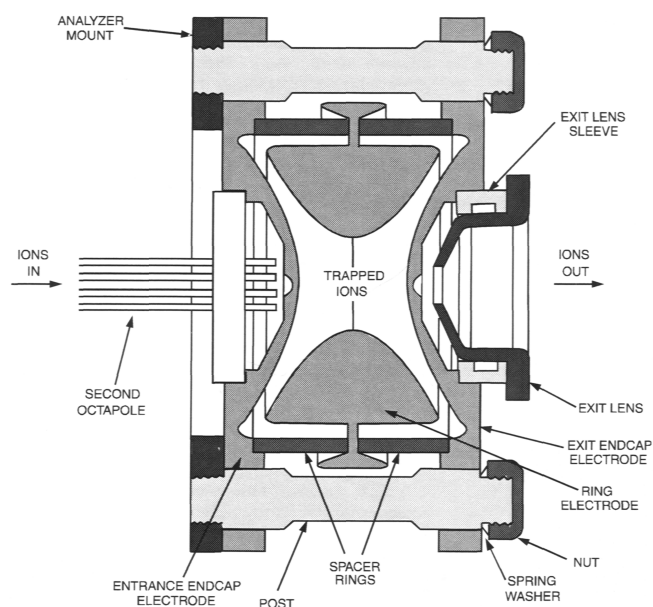
Figure 4.4: Cross sectional view of the mass analyzer [Fin96].
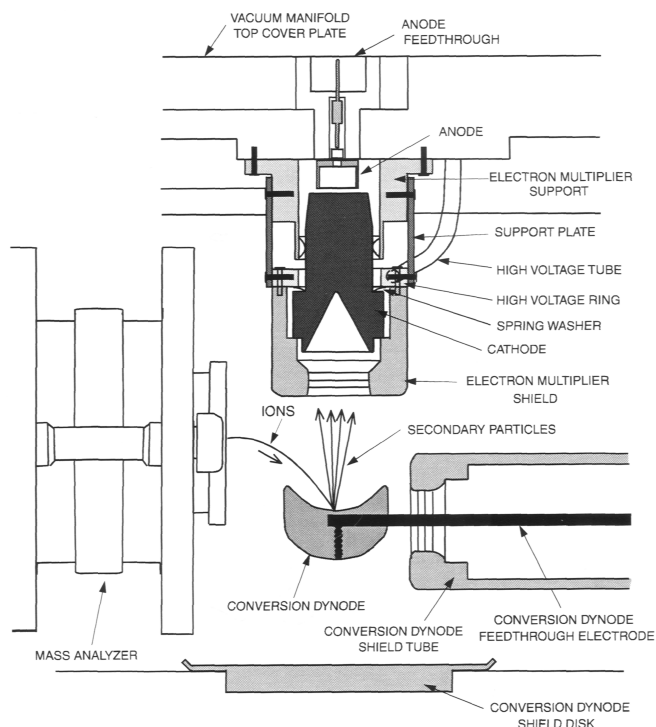
Figure 4.5: Cross sectional view of the ion detection system, showing the electron multiplier and the conversion dynode [Fin96].
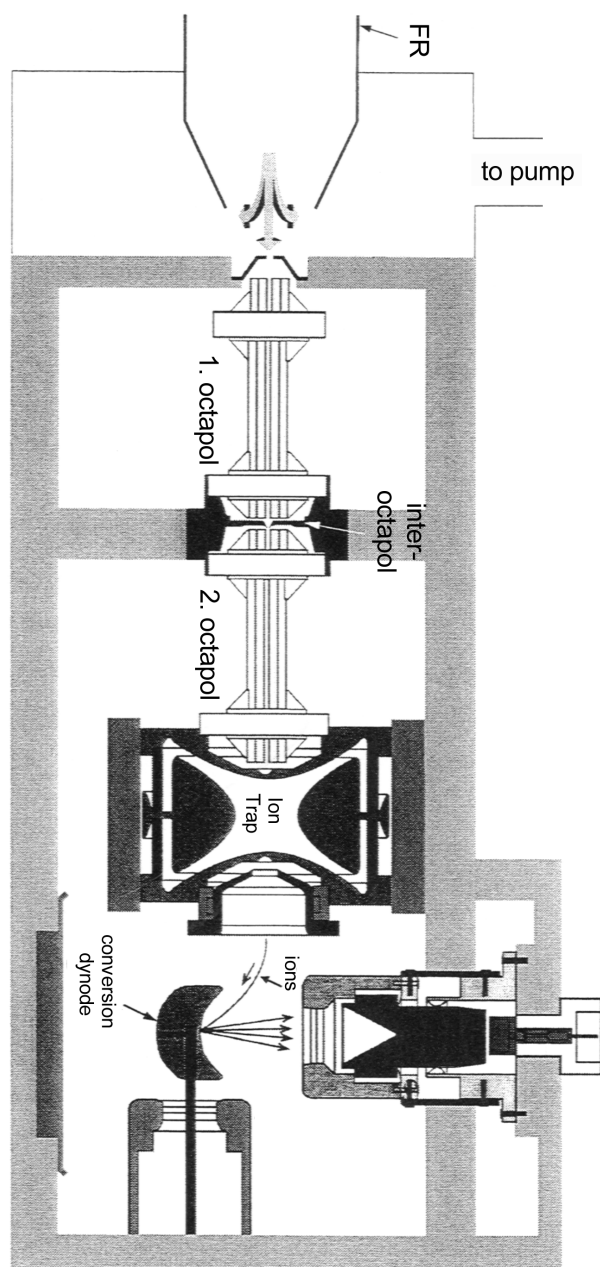
Figure 4.6: Schematic view of the Ion Trap Mass Spectrometer consisting of a flow reactor (FR), two octapole lenses and the ion trap.

Chapter 5

Aircraft based measurements of atmospheric Sulfur Dioxide

5.1 The ScavEx project

The aircraft based measurements of sulfur dioxide (SO_2) were made in the framework of the ScavEx epxeriment (Schneefernerhaus Aerosol and Reactive Nitrogen Experiment) which was designed for studies on the interactions of aerosols and reactive trace gases and their influence on atmospheric processes and the climate in the Alps. It consisted of continuous lab and modeling work and a series of measuring campaigns, which began in spring 2001 and lasted three years. During the ScavEx experiment airborne measurements for the study of transport phenomena and vertical structures were conducted, hosted by the German Aerospace Centre (DLR) in Oberpfaffenhofen (ca 25 km west of Munich). The aircraft used was the Falcon 20E, D-CMET operated by DLR. In the following there will be presented the data obtained during the aircraft ScavEx campaign in April 2001.

5.2 Experimental setup

For the sulfur dioxie aircraft measurements was used for the first time the Paul Ion Trap Spectrometer (PITMAS). The benefits for using this instrument in an aircraft campaign was its high sensitivity and time resolution and also its compact set up
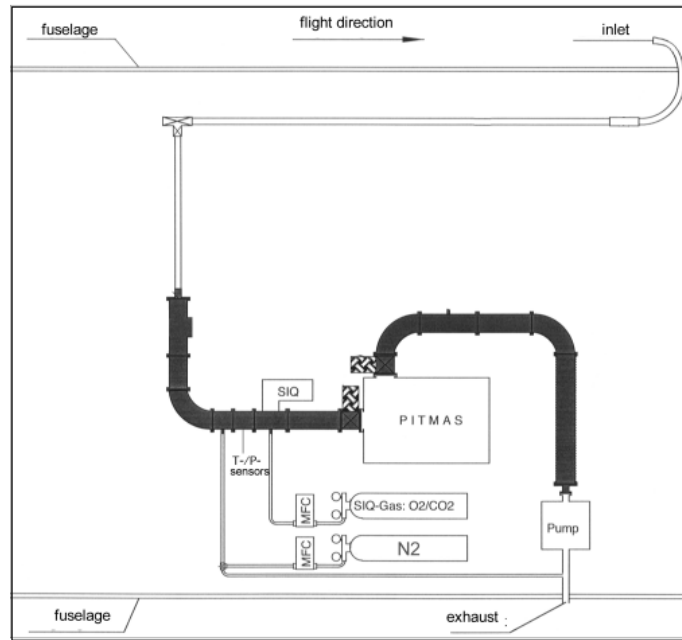
Figure 5.1: The research aircraft Falcon stationed in Oberpfaffenhofen, Germany

which occupied two aircraft racks. When compared to the linear quadrupole mass spectrometer also used by our group aircraft based CIMS, PITMAS offers three important advantages: i) dehydration of water cluster ions which makes the mass spectra more simple and reduces masking of mass peaks ii) the possibility of fragmentation studies of mass selected ions which allows unambiguous ion identification iii) a high mass resolution also at larger mass numbers.

The experimental set up is given in Figure 5.2. Ambient air was sampled with a backward facing aircraft inlet provided by DLR and introduced into the flow reactor (FR) through a teflon critical orifice (diameter 0.2 cm). The air sampled was directed through a 2 m long PTFE sampling line (diameter 1/2") into the stainless steel flow reactor (inner inner diameter 4 cm, length 35 cm). At a distance of 20 cm from the inlet of the PITMAS was mounted a high frequency glow discharge ion source for production of reagent ions CO_3^- (1.9 slm gas mixture of 1000 ppm CO_2 in O_2). The FR pressure and temperature were monitored during the flights and saved with the help of a Labview program. The pressure in the FR was kept constant at 45 mbar with help of a regulating valve between the FR and the pump. Measurement were taken every 1 s corresponding to a horizontal resolution of 200 m.

Figure 5.2: Set up for the measurements of Sulfur Dioxide on board of the research aircraft Falcon.

For the background measurements was used a 2 lt Nitrogen 5.0 gas bottle [Gri00]. The background signals ranged between 20 and 200 ppt in the different flights but mostly were around 100 ppt. Although these values were fairly high they did not pose problems to the detection of atmospheric SO_2, which was clearly above this limit. However, it was proved that this set up for background measurements was not very well fitted to the needs of the experiment: the properties of dry nitrogen are different from the properties of the ambient air masses encountered. Therefore, the background and the trace gas measurements are not really comparable. Secondly, the background measurements were carried out only twice, in the beginning and at the end of every flight but they apparently should be taken more regularly for two reasons: i) because the flight altitude changes continually and thus the properties of the air masses intercepted change and ii) the instrument has an unstable performance at least during the first 60 min of flight (see below). Thus the background should be checked more often in order to investigate how it responds with time. In the meantime this was achieved by our group [Ger03].
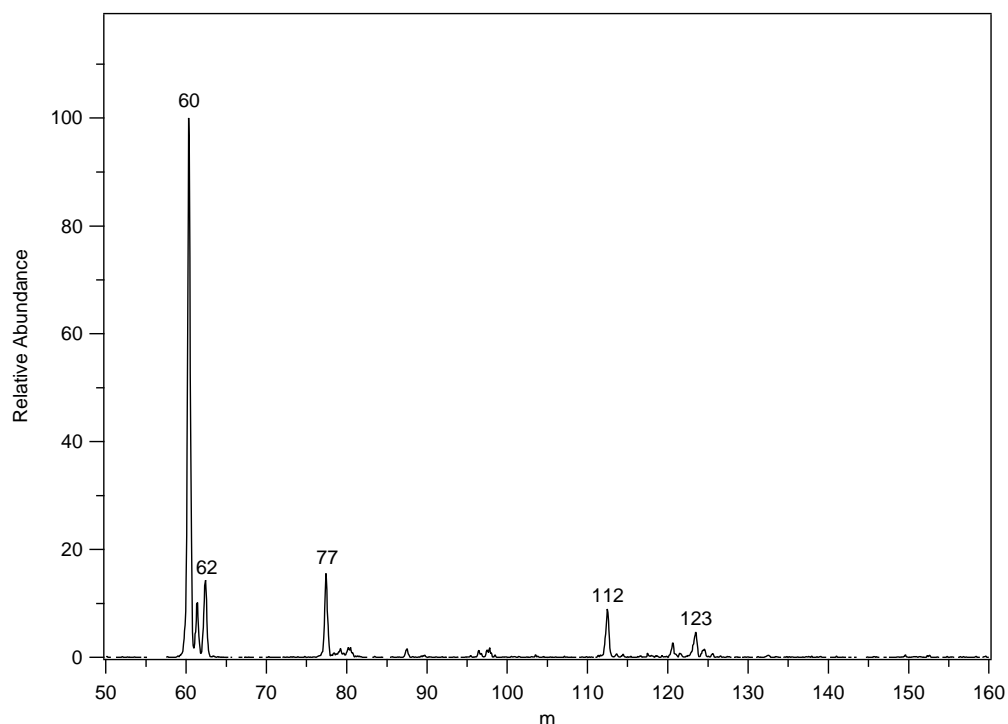
Figure 5.3: Negative ion mass spectrum obtained by the Ion Trap Mass Spectrometer during the flight of 18 April 2001.

5.3 Flight on 18 April 2001

5.3.1 Sulfur dioxide measurements

In the flight of 18 April 2001 Falcon flew from Oberpfaffenhofen to Hamburg and then southwards to Venice returning to Oberpfaffenhofen over Zugspitze. In Figure 5.3 is shown one spectrum obtained during the flight at the time when high SO_2 concentrations were observed. Mass 60 corresponds to the educt ion CO_3^- and mass peak 112 to the SO_5^- product ion. Also at lower relative abundances appear mass peak 62 (NO_3^-) the presence of which is discussed below, mass peak 77 ($HOCO_3^-$, see below) and mass peak 123 ($CO_3^- HNO_3$) which reveals the presence of small quantities of nitric acid (HNO_3) in the flow reactor. Since nitric acid also reacts with the educt ion CO_3^- it should be examined whether the use of the parallel ACIMS formula is necessary. This formula introduces a correction factor 112/(112+123), which during the flight remains >0.8, min other words the SO_2 concentrations calculated with the ACIMS formula without taking into account the parallel products can be <20 %

overestimated. This uncertainty is below the error of these measurements $\pm 40\,\%$.

Mass peak 77 is the ion $HOCO_3^-$ formed in the flow reactor when OH radicals produced in the ion source react with the CO_3^- educt ions. These ions may pose problems to the detection of sulfur dioxide since they react with the latter to form ions with mass peaks: 80 (SO_3^-), 81 (HSO_3^-), 96(SO_4^-), 97 (HSO_4^-). The rate coefficient of the reaction was measured and was found to be significantly below the calculated collision limit $\sim$60\,\% (k=$0.6\cdot10^{-9}\,cm^3s-1$ [Win95]). The difference may be the result of possible barrier to the reaction. Since the CO_3^- ions are more abundant than the $HOCO_3^-$ (ratio of CO_3^- to $HOCO_3^-$ variates between 4-7) and the rate coefficient of $HOCO_3^-$ with SO_2 is lower that the one of CO_3^- with SO_2, it is assumed that the presence of the ion $HOCO_3^-$ does not significantly disturb the measurements. Nevertheless, since the presence of $HOCO_3^-$ may lead to an underestimation of the sulfur dioxide concentrations, it would be preferable to suppress its formation. Some suggestions to achieve that are described in [Uma01].

In Figure 5.4 is shown the concentration of SO_2 measured together with the flight altitude. The error of SO_2 is $\pm$43 \% determined mostly by the error of k ($\pm$ 30%) and the error of τ ($\pm$ 30 \%). The highest altitude the Falcon reached was 10.5 km, remaining there for around 20 min and returned to 5 km altitude for the rest of the flight time. For the ascending part, the data retrieved from the spectra cannot be used for the SO_2 evaluation (for a more detailed description of this complication see below).

Between 11:20-11:25 Falcon intersected polluted air masses with SO_2 concentrations exceeding by far the local background-air values. Assuming an aircraft velocity of 200 m/s the horizontal distance over which this polluted plume extends is $\sim$ 60 km. During the first 2 min of interception there was encountered an air mass with SO_2 mixing ratios not higher than 1.9 ppb and then follows the highest SO_2 peak reaching 2.6 ppb (see the blow up panel in Figure 5.4). As the aircraft leaves behind the polluted air masses the concentrations fall rapidly down to 0.2 ppb and numerous smaller peaks follow ranging between 0.1 to 0.6 ppb which finally fade down to 0.1-0.2 ppb. The gap in the data between 12:02 and 12:35 was due to operation of the CIMS instrument in a different mode (atmospheric natural ions). When the instrument is again turned to the negative ion mode the concentrations of SO_2 are in the same
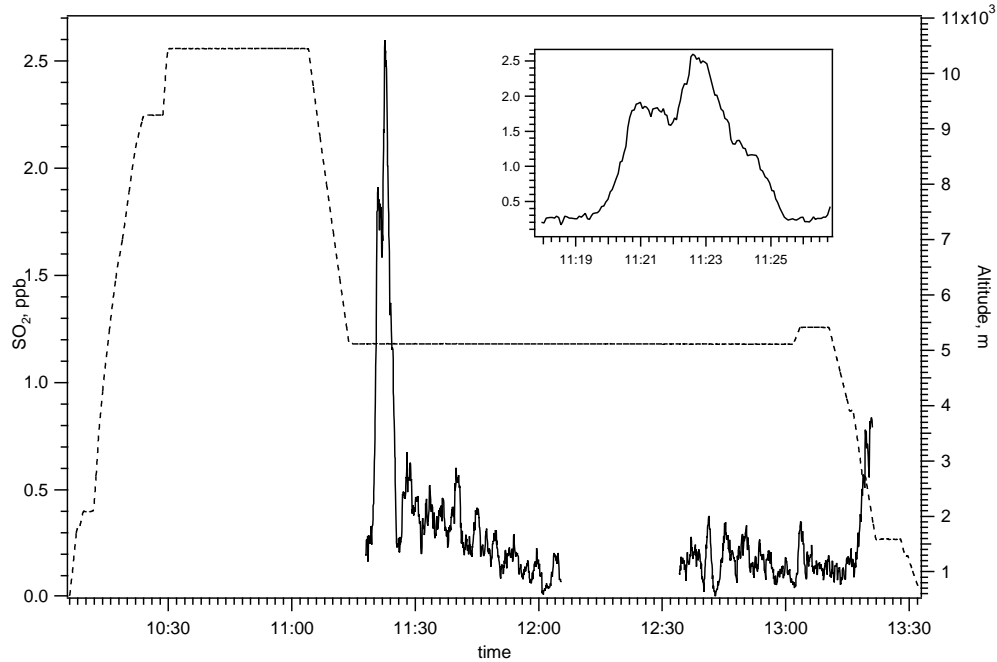
Figure 5.4: Measured SO_2 and altitude profile for the flight on 18 April 2001

range as the background values measured before and raise again to reach 0.8 ppb when the Falcon flies above Zugspitze in an altitude of 4 km.

Air mass back trajectory analysis performed at the Royal Netherlands Meteorological Institute indicated that the air masses encountered between 11:15-11:30 (air mass 1: AM1) above Hamburg experienced large-scale upward transport from the 2 km level 36 h prior to the measurements. Figure 5.5 shows that 1.5 days before the measurements air masses over Great Britain (top panel) ascent form the 800 hPa pressure level (2 km) to the 520 hPa pressure level which corresponds to a 5.2 km altitude (bottom panel). Hence it is likely that AM1 picked up SO_2 from the polluted PBL of the British Isles and/or continental Europe. It seems that a substantial fraction of the gaseous SO_2 initially contained in such PBL air masses survived the fast vertical transport and did not suffer from "wet removal" by cloud processes.

During the same flight were performed measurements of aerosol particles with diameters >4 nm by the German Aerospace Center (DLR). Figure 5.6 shows SO_2 mole fractions (log scale) together with ambient relative humidity, temperature and the measured n_4. AM1 is rich not only in SO_2 but also in n_4, the concentration of which reaches $25 \cdot 10^3$ cm^{-3} while the background values do not exceed $500 \, cm^{-3}$. It
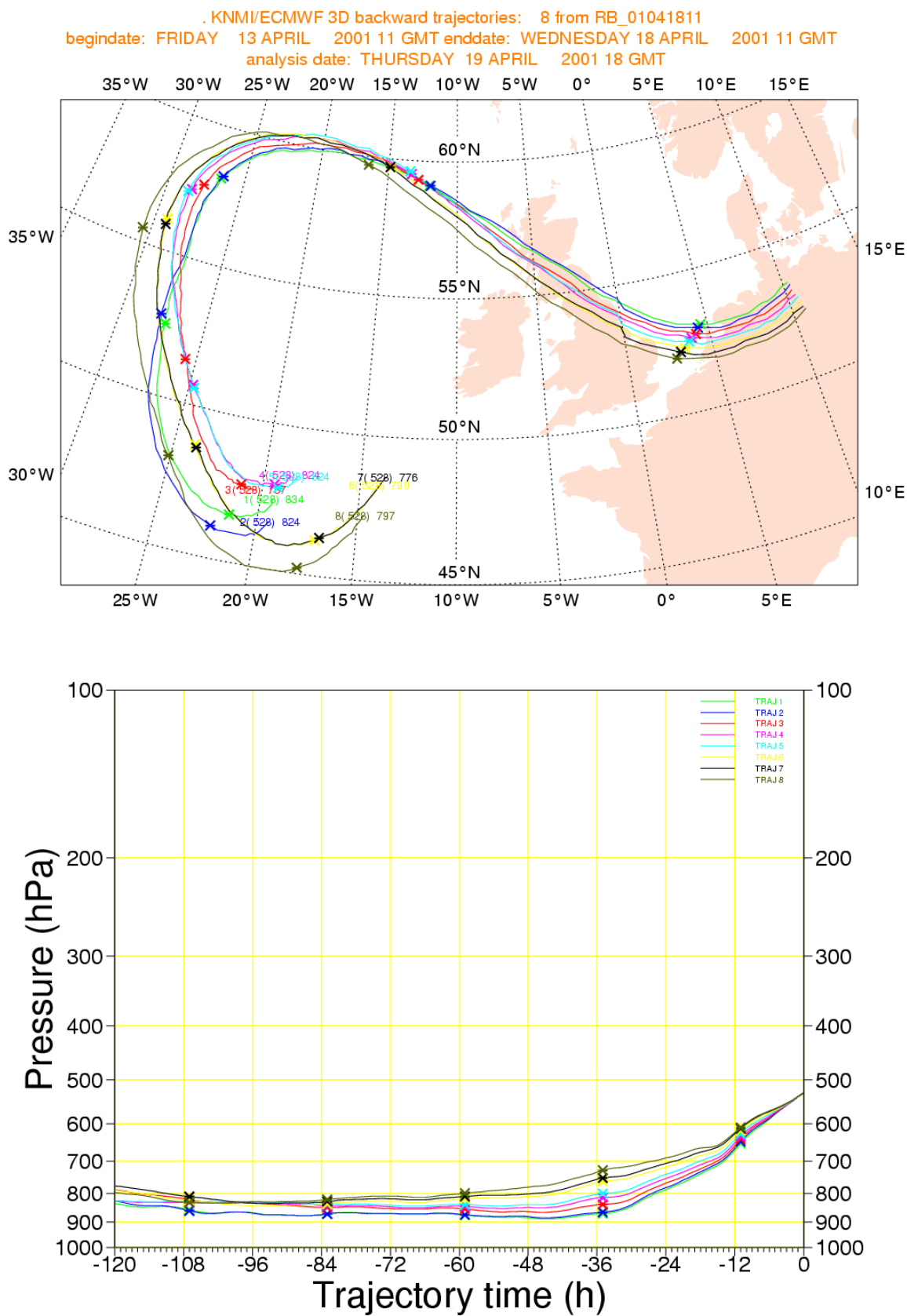
Figure 5.5: Trajectories of air masses five days prior to the measurements of 18 April 2003.
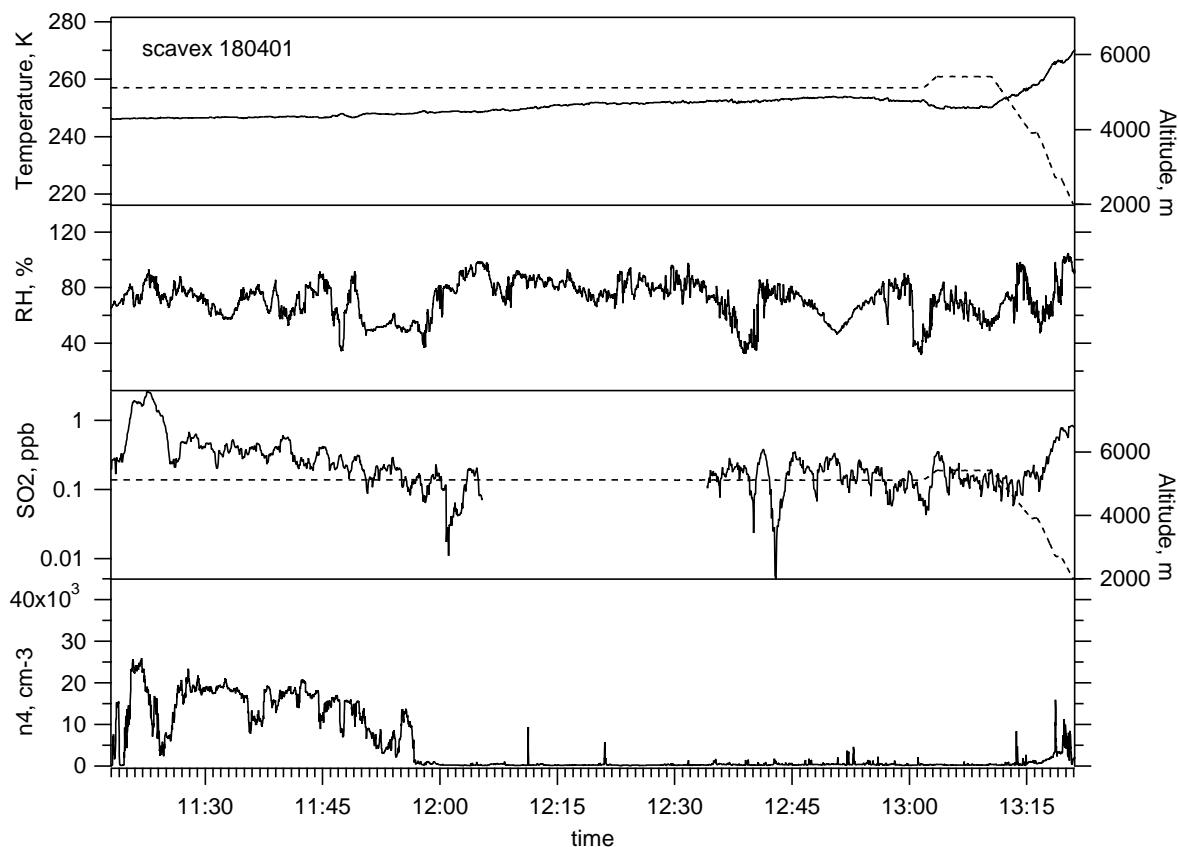
Figure 5.6: The sequence of SO_2 mole fraction measurements during the flight on 18 April 2001. Also shown are the flight altitude, atmospheric temperature, atmospheric relative humidity, number concentration of aerosol particles with diameters >4 nm measured by DLR.

seems that large SO_2 leads to a large production of gaseous sulfuric acid GSA, which in turn promotes aerosol formation via H_2SO_4/H_2O nucleation and aerosol growth via H_2SO_4/H_2O condensation. A scatter plot of the measured n_4 vs SO_2 shows they are linearly correlated and quite interestingly, two different regression lines may fit to the data, corresponding potentially to two air masses with different properties and ages (the age of the air mass corresponds to the time elapsed after contact with the planetary boundary layer) (Figure 5.7). Indeed, a closer look of the properties within AM1 shows that there are some variations not only in the SO_2 mixing ratios but also in the particle number densities: in Figure 5.8 is presented the time sequence of AM1 and the measured SO_2, n_4 and additionally n_{20} (particles with diameters >20 nm). The first part of AM1 (11:20-11:23) has higher number densities of n_4 and n_{20}, while in the second part of AM1 for which the SO_2 mixing ratios are higher, the

particle number densities reduce from 25 to 10-15 cm^{-3}. These particles may have been formed in the upper troposphere from the observed SO_2, although it cannot be entirely ruled out that they have already been formed in the polluted PBL.

5.3.2 Potential implications for aerosol formation

One of the possible particle formation routes is conversion of SO_2 into gaseous sulfuric acid (GSA), which may, depending on conditions, either condensate on pre-existing particles or nucleate to form new particles [Laa00]. Laboratory measurements have indicated that the product of this reaction is in fact GSA [Rei93], [Rei94]. Additional laboratory work confirmed [Kol94], [Lov96] this finding. The atmospheric nucleation mechanism of H_2SO_4 is not well understood: whether the smallest stable clusters are formed by binary homogeneous nucleation of sulfuric acid and water vapor or by a more complicated mechanism involving ions [Tur98], [Eic01] or other trace gases (as for example NH_3) is not known.

Aerosol formation and growth is promoted by enhanced SO_2 and OH. The reaction of SO_2 with OH ultimately leads to gaseous sulfuric acid (see § 1.3) which condenses and possibly may even undergo homogeneous nucleation leading to the formation of new aerosol particles. Both condensation and nucleation proceed via a bi-molecular (H_2SO_4-H_2O) mechanism. The condensational sink for gaseous sulfuric acid is dependent on the characteristics of the ambient aerosol population. If the ambient aerosol has diameters smaller than the mean free path of molecules in air (kinetic limit) diffusion effects become negligible and the lifetime of H_2SO_4 against condensation becomes:

$$\tau_c = \frac{4}{\gamma S u} \tag{5.1}$$

where γ the sticking probability, u the mean thermal velocity and S the surface area density of aerosols. Another limiting case is that no ambient particles exist and hence the lifetime of H_2SO_4 becomes limited by collisions with itself:

$$\tau_n = \frac{1}{k_c[H_2SO_4]} \tag{5.2}$$

where k_c the collision rate coefficient with another gaseous sulfuric acid molecule.

Considering the maximum measured SO_2 molecular number density $4 \cdot 10^{10} \, cm^{-3}$, a typical daytime summer OH-concentration of $2 \cdot 10^6 \, cm^{-3}$ [Sei98] and an effective
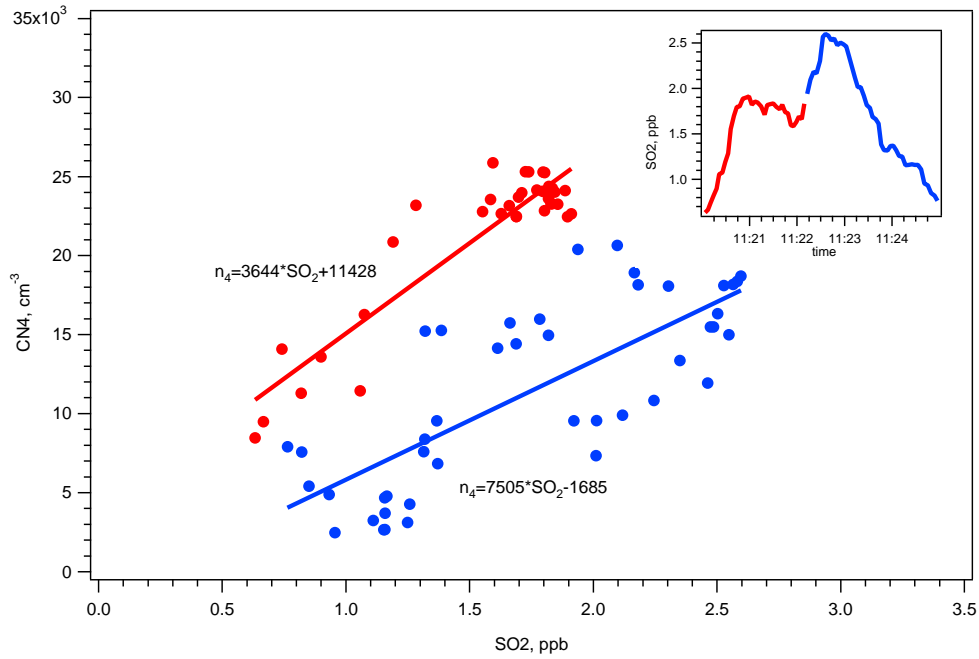
Figure 5.7: Scatter plot of n_4 and the SO_2 mole fraction for the air mass 1 encountered during the flight of 18 April 2001.
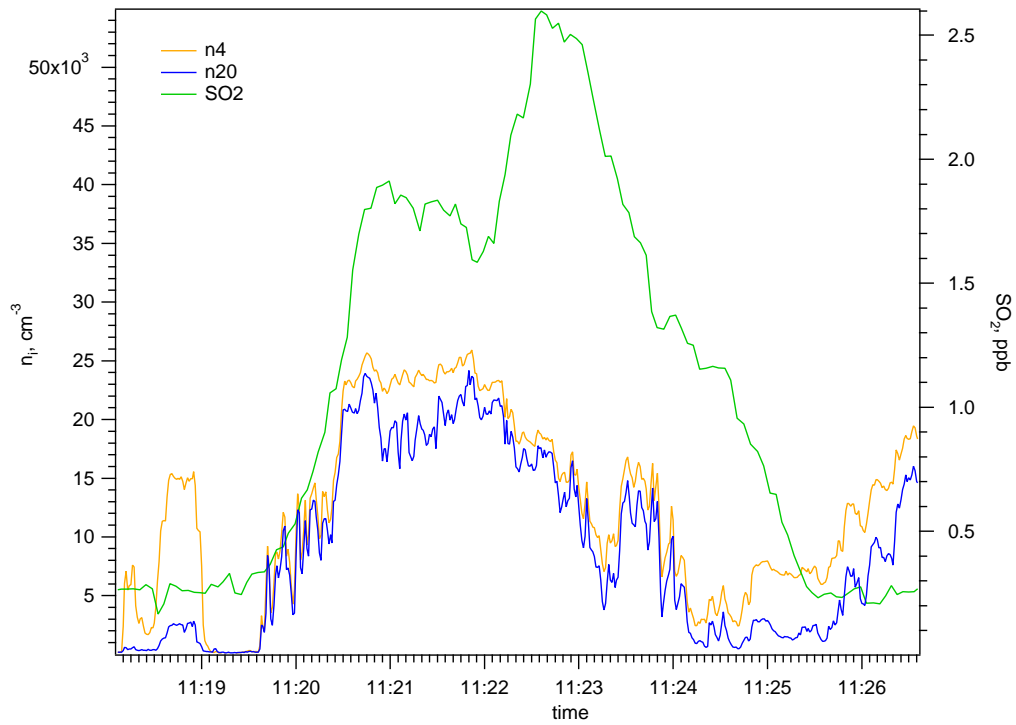
Figure 5.8: SO_2 mixing ratios measured by MPI-K and number densities n_4, n_{20} number densities measured by DLR for air mass 1 in the flight on 18 April 2001.

rate coefficient k for the $SO_2 + OH$ reaction of $1 \cdot 10^{-12}$ cm$^{-3}s^{-1}$ [Woh99] one obtains:

$$P = k[SO_2][OH] \sim 1 \cdot 10^5 cm^{-3} s^{-1} \tag{5.3}$$

which would be the daytime rate of gaseous sulfuric acid production by oxidation of SO_2. The maximum number density of aerosols with diameter d=20 nm measured was n_{20}=15·10^3 cm^{-3} which would contain about 6.6·10^8 H_2SO_4-molecules per cm^3 if they were composed of H_2SO_4. Hence the H_2SO_4 molecules contained in these aerosols may be formed from the observed SO_2 within only around 1.8 h.

New aerosol formation by homogeneous nucleation requires a large supersaturation and concentration of gaseous sulfuric acid and a low total surface area density S of pre-existing aerosol. The measured aerosols have a surface area density of S=2·10^{-7} cm^2 per cm^3 (S=$4\pi r^2 n_{20}$). This would imply a GSA-lifetime with respect to collision with aerosols of about $\tau_c \leq 911$ s (15 min), using equation 5.1, where u the mean thermal velocity [Sei98]:

$$u = \sqrt{\frac{8kT}{\pi m}} \tag{5.4}$$

For the estimated production rate of sulfuric acid P $\leq 1 \cdot 10^5$ $cm^{-3}s^{-1}$ the steady-state GSA concentration would be GSA=P·τ_c=9·10^7 cm^{-3}. This implies a GSA lifetime τ_n with respect to collision with another GSA-molecule ≥ 2 min, assuming a collision rate coefficient k_c of $1 \cdot 10^{-10}$ $cm^3 s^{-1}$. Since $\tau_n < \tau_c$, removal of GSA could occur via homogeneous nucleation, provided that the rate of the forward nucleation rate coefficient (gain of molecules in a cluster) is larger than the reverse rate coefficient (loss of molecules from a cluster): since, from the principle of reversibility, at equilibrium every forward processes has to be matched by its corresponding reverse process, it follows that if a cluster grow by the addition of single molecules, evaporation also occurs, one molecule at a time. If so, nucleation can occur only when the gain of molecules (monomers) in a cluster of size i (i-imer) is more efficient than the loss of molecules. The rate at which a cluster loses monomers should depend only on the cluster size and temperature.

Parameterizations for sulfuric acid/water nucleation rates in the atmosphere at temperatures between -40 °C and +25 °C and relative humidities between 10 and 100 % yield a formula that gives, at given temperature T and RH, the sulfuric acid vapor concentration needed to produce a binary homogeneous nucleation rate of

J=1 $cm^{-3}s^{-1}$ [Kul98]:

$$N_{a,c} = exp(-14.5125 + 0.1335T - 10.5462RH + 1958.4RH/T) \qquad (5.5)$$

For T=247 K and RH=90 % measured in AM1 (11:22-11:23) the critical sulfuric acid vapor concentration would be $N_{a,c}$ =1.1 · 10^7 cm^{-3}, which is lower than the estimated sulfuric acid vapor GSA $\sim$ 1.8 ·10^8 cm^{-3}. Therefore, it is conceivable that for the SO_2 mixing ratios measured within air mass 1, binary homogeneous nucleation may have taken place leading to formation of new particles. The critical sulfuric acid vapor concentration $N_{a,c}$ predicted by the binary homogeneous nucleation theory is usually an upper limit, as the nucleation processes in the atmosphere may be assisted by other trace gases, such ammonia, or ions. If this is the case, then the critical H_2SO_4 vapor pressure can be two or three orders of magnitude lower [Fin00].

Heterogeneous condensation may be considered as a competitive mechanism of GSA depletion: sulfuric acid vapor may scavenge onto preexisting particles, if available, leading to its growth. If the concentration of particles is sufficiently high, this may dominate over the formation of new nuclei via homogeneous nucleation. However, a third path which involves combination of nucleation and condensation growth events can not be excluded. In fact, such mechanisms have been observed in smog chamber studies [Fla91]: heterogeneous condensation may initially promote growth of preexisting particles, but at a too slow rate, the condensation material would accumulate and would lead to a burst of new particle formation. Based only on the current measurements of SO_2 mixing ratios and particle number densities it is not possible to draw any safe conclusions on the pathway of the sulfuric acid depletion. Detailed model calculations would considerably help in providing some plausible answers.

5.4   Two Flights on 25 April 2001

In the first flight on the 25th of April the Falcon flew from Oberpfaffenhofen southward to Parma and returned to Oberpfaffenhofen flying over Zugspitze. At the first ascending part of the flight Falcon reached the 6.5 km flight altitude and then in the stacked descending part reached down to 1.2 km. The first 60 min of the flight (7:00-8:00) are excluded from the data analysis. As shown in Figure 5.9 the count rate of

the core ion CO_3^- (m=60) is in the beginning very low and during the first flight hour increases very markedly. Interestingly, mass number 62 which could be identified as NO_3^- exhibits the inverse profile, starting with high count rates which decrease exponentially to remain 4-5 times lower than the final count rates of mass 60 (CO_3^-). Due to the observed instability of the main core ion CO_3^- and the interference with the ion NO_3^-, which seems that acts as a rival, it is not possible to draw any inferences from the data. The reason causing this instability is not quite clear. It may be a start-up effect (see below) which was also observed in the second PITMAS instrument of our group used for ground based measurements (Uecker, personal communication) or a sampling line effect: if some NO_2 were adsorbed on the walls during earlier measurements, then its desorption could convert CO_3^- to NO_3^- ions in the beginning of the flight.

Also shown in Figure 5.10 two negative spectra obtained during the first flight on 25 April 2001. In the bottom panel is presented an averaged spectrum corresponding to the beginning of the flight, when the mass peak 62 (NO_3^-) is still high. In this spectrum the mass peak 125 ($NO_3^-HNO_3$) is also very pronounced, indicating the presence of nitric acid in the flow reactor. After the first 60 min the NO_3^- ion is markedly lower, spectral line 125 ($NO_3^-HNO_3$) practically disappears as expected.

Alternatively, there was checked whether temperature could be affecting the CR of the core ion CO_3^-. An investigation of a correlation between temperature in the flow reactor and mass 60 revealed that both have a similar trend (see Figure 5.11). In the beginning of the flight the gas temperature in the flow reactor was 23 °C and at the end of the flight reached 34 °C: the sample gas temperatures simply follow cabin air temperatures, which increase significantly during the flight as a result of the simultaneous instrument operation and the absence of ventilation. By the time temperature reaches a plateau CO_3^- seems to stabilize. If so, then obviously higher temperatures favor higher CR of the CO_3^- ion. Similar trends for temperature and m60 are observed in the second flight of the same day: as temperature increases from 29.5 to 33 °C the count rate of m60 increases 6 times (Figure 5.12).

The sulfur dioxide measurement with time is given in Figure 5.13 together with the flight altitude. There is no significant variation observed for the different altitudes from 2.5 up to 6 km, the mixing ratios range between 0.15 ppm to 0.25 ppb. In the
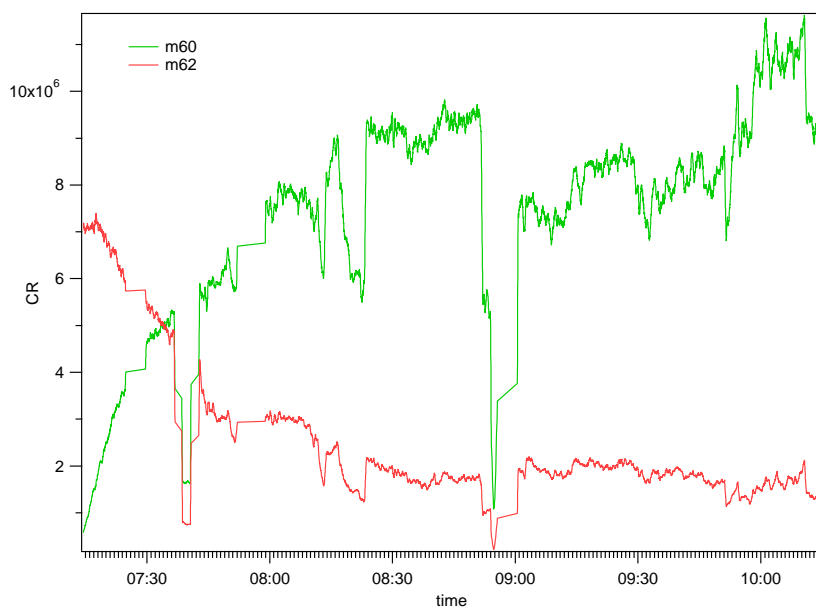
Figure 5.9: Count rates of CO_3^- and NO_3^- during the first flight on 25 April 2001.
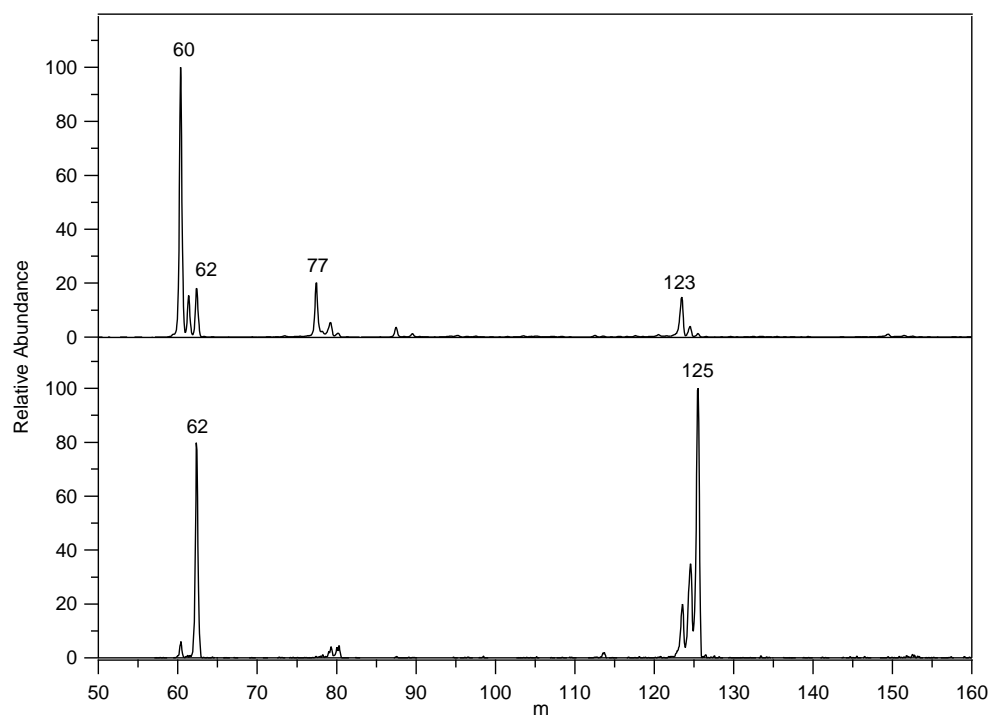
Figure 5.10: Negative ion spectra obtained during the first flight of 25 April 2001. The bottom spectrum was obtained in the beginning and the top spectrum was obtained at the end of the flight.
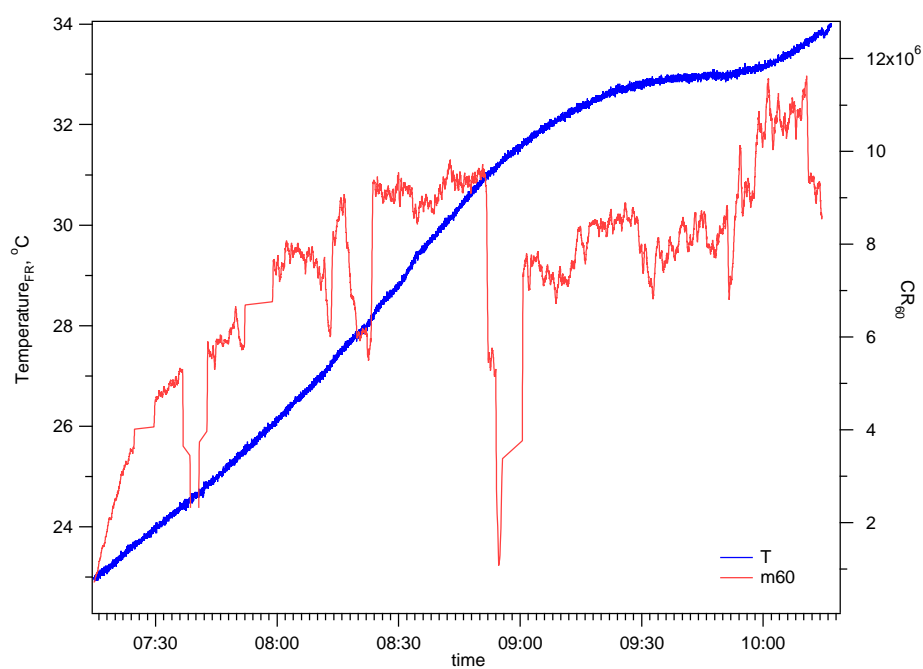
Figure 5.11: Temperature in the flow reactor and CO_3^- during the first flight on 25.04.01
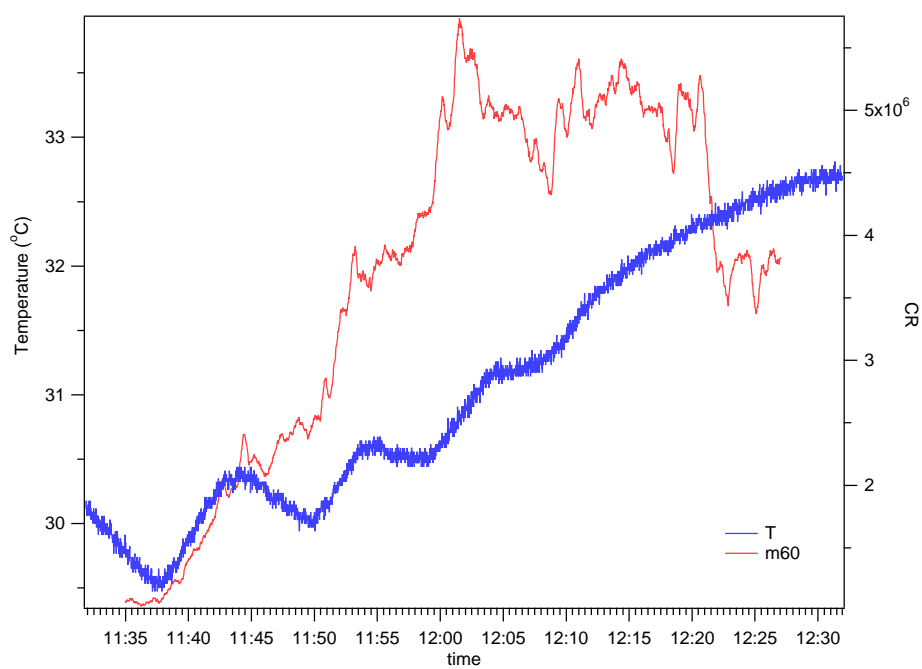
Figure 5.12: Temperature in the flow reactor and CO_3^- during the second flight on 25.04.01
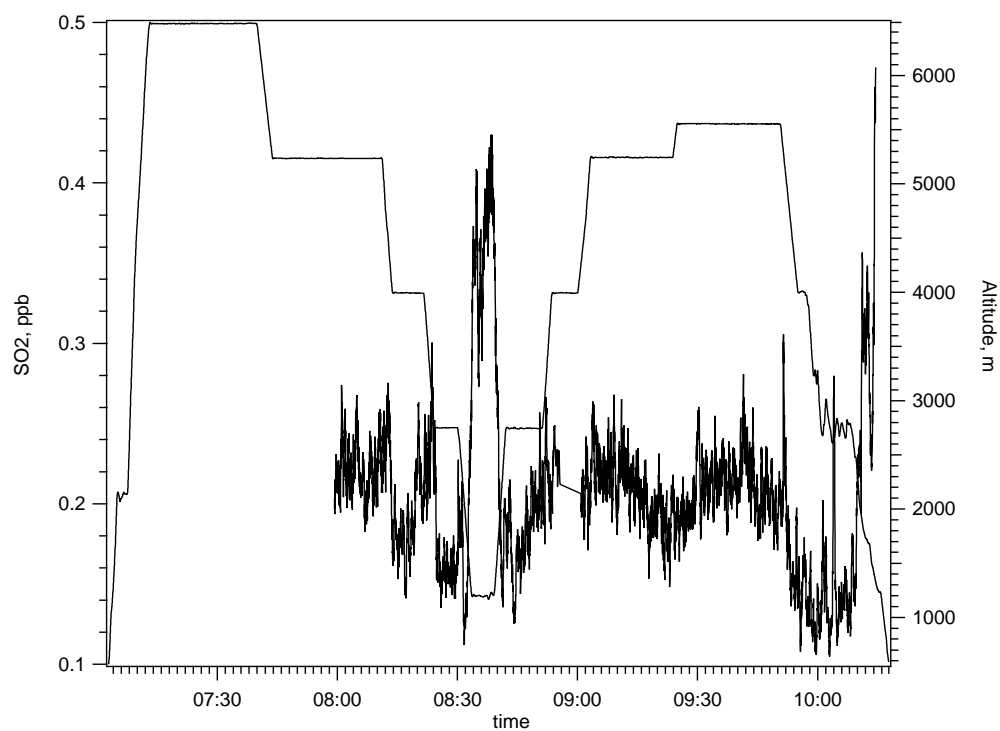
Figure 5.13: Sulfur dioxide measured during the first flight on 25th of April

Figure 5.14: Sulfur dioxide measured during the second flight on 25th of April

lowest flight level (1.2 km) there seems to be intercepted an air mass with somewhat higher SO_2 mixing ratios, which, however, do not exceed 0.4 ppb. As Falcon flies over Zugspitze on the return back to Oberpfaffenhofen in 2.5 km flight altitude the mixing ratios tend to increase again, indicating more polluted atmospheric air masses in the planetary boundary layer.

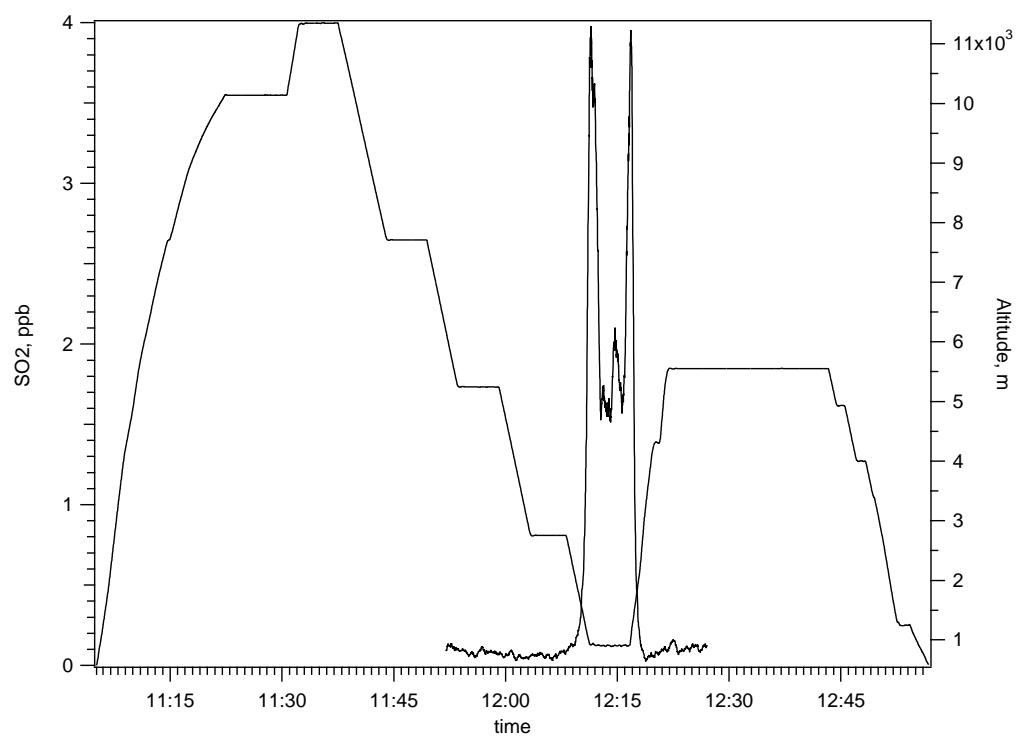In the second flight on the 25th of April Falcon flew eastwards over Linz and Vienna and returned in Oberpfaffenhofen. The highest flight altitude was 11 km and the lowest 1 km. The concentrations during the flight remained low (around 200 ppt) for flight altitudes h >1.5 km and increased rapidly when Falcon reached down to 1000 m. At this time, Falcon was over Linz, an industrial area where fossil fuel burning is intense and thus high S emissions are expected. Falcon intercepted polluted air masses for around 10 min, extending in a 100 km distance. The mixing ratios fluctuated between 2 and 4 ppb. As Falcon left behind Linz and ascended at the 5.5 km altitude the mixing ratios dropped down to the initial values (see Figure 5.14).

5.5   Future directions

Summarizing, PITMAS has been successfully adapted for the in-flight SO_2 measurements. Its high time resolution and low demands on space and operating costs are the most important benefits for using it in aircraft campaigns. The first attempt of measuring sulfur dioxide was successful, providing altitude profiles in the background and polluted troposphere (Figure 5.15 and challenging for further improvements in the measuring technique. These improvements involve:

- *Background measurements.*

  Lowering of the background limit improves significantly the quality of in-flight SO_2 measurements. The background signal should be lower than the typical SO_2 mixing ratios in the lower troposphere (20-60 ppt). The use of filter materials, which trap SO_2 while keeping the rest of other sample air properties unchanged, seems quite promising: preliminary results of laboratory studies showed that these filters may produce almost SO_2-free air. The material used
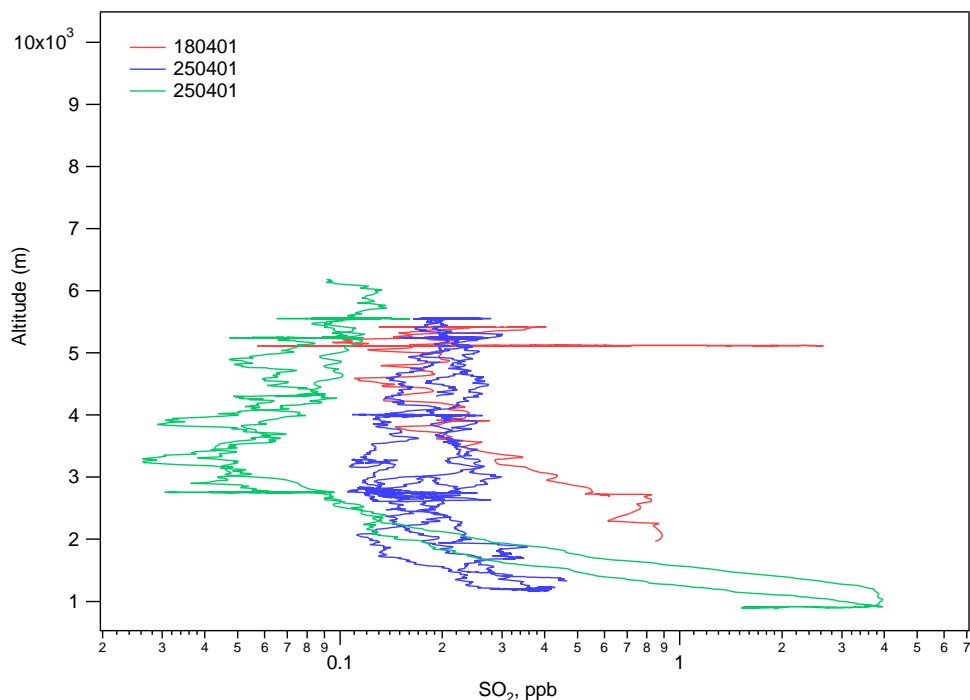
Figure 5.15: Altitude profiles obtained during the ScavEx campaign with the Ion Trap Mass Spectrometer.

for the measurements was an aluminum substrate with an impregnation of sodiumcarbonate and potassium permanganate (Purafil, Umwelttechnik MCZ). The use of the filter was recently tested in aircraft measurement and proved to be very efficient (background suppressed down to 20-40 ppt [Ger03].

- *In flight calibration.*

Of great importance would also be an in-flight SO_2 calibration. Preliminary calibration measurements in the lab showed that there is a dependency of SO_2 calibration factors on the water vapor concentration (see Figure 5.16). The calibration factor is defined as the ratio of SO_{2exp}/SO_{2meas}. For these calibration measurements were use gas bottles of standard SO_2 concentration in N2 (1ppm SO_2 in N2 5.0) and the measured sulfur dioxide signals were compared with the expected. It seems that there is a tendency for slightly smaller calibration factors (slope of the regression lines) for higher water vapor content. The quantity of water vapor in the flow reactor was controlled qualitatively, with the use of different critical orifices, trough which humidified nitrogen flowed. Later
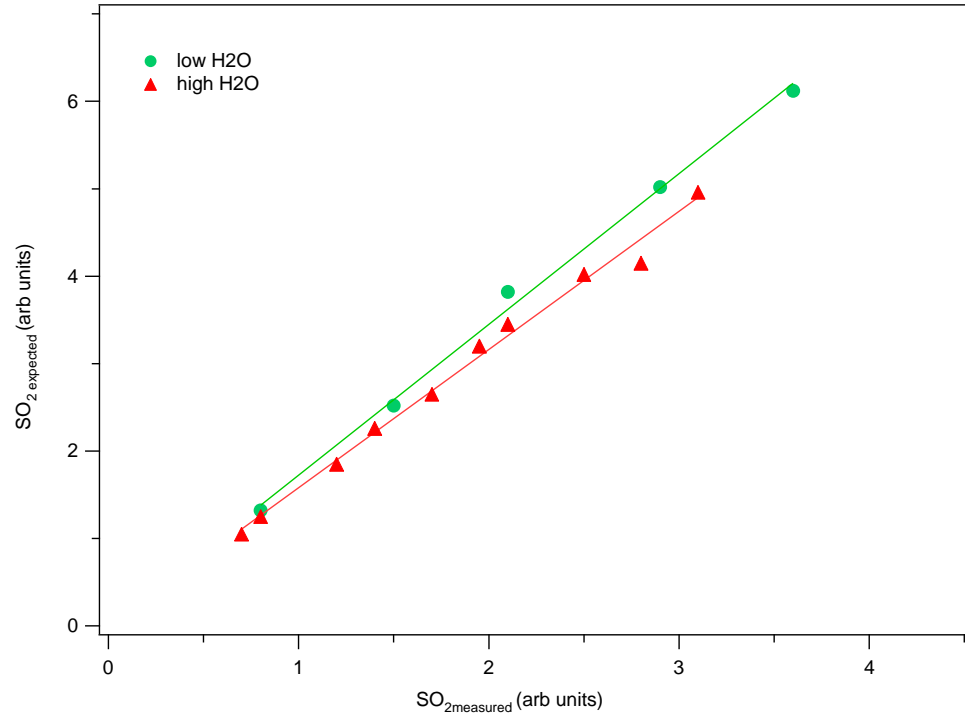
Figure 5.16: Dependency of calibration factors on water vapor content

aircraft measurements and subsequent more precise lab measurements with a use of a dew point meter, confirmed this dependency of the calibration factor on the concentration of the water vapor in the flow reactor [Ger03].

- *Improvement of the instrument stability.*

  As discussed previously, PITMAS did not have a stable performance throughout the flight: the count rate of the educt ion CO_3^- had a markedly increasing profile for the first 40-60 min thus not allowing evaluation of the data. Possible reason of this perturbation could be the initialization of the electronics which takes place only after take off. For the optimum performance of the instrument is suggested a continuous run of the instrument. Unfortunately, for the aircraft measurements this has not been up to now possible: according to the safety instructions there is no power supply during the fueling of the aircraft (i.e. before take off) and therefore the instrument can initialize only after the flight starts. This 'warming up' face, during which no useful data can be obtained, is almost one third of the flight time. With the help of an internal power supply
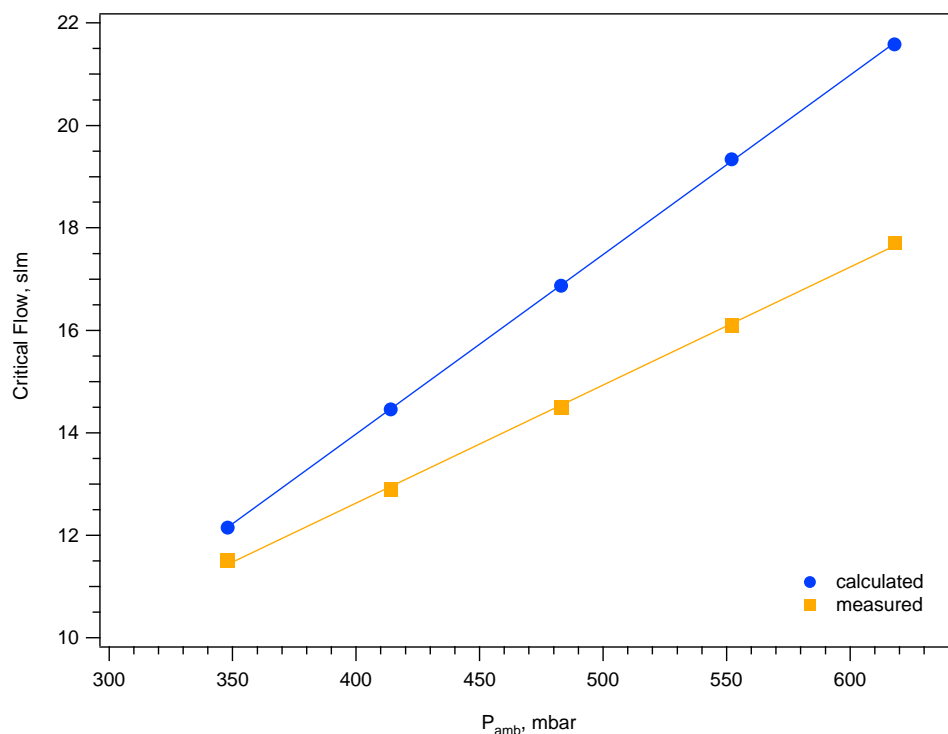
Figure 5.17: Measured and calculated gas flow through the 2 mm critical orifice

the instrument could run for a few hours before the begin of the measurements and therefore make use of the data during the whole flight.

Provision of power supply some time in advance could also keep the TMP running providing this way a 'cleaner' mass spectrometer chamber. During this campaign after the turning off of the pump air of the aircraft cabin full of impurities was entering the mass spectrometer chamber, which to some extend could have affected the quality of the measurements.

In case that the instability of the count rate of the educt ion CO_3^- is caused and/or enhanced by the changes of temperature in the cabin, the flow reactor should be kept in a constant temperature (e.g. in 35 °C which was always the final temperature of the gas sample) with a help of heating bands and insulating materials.

- *Critical orifice*

For the air sampling was used a 2 mm critical orifice made of Teflon. In the laboratory was investigated whether the critical flow F correlates linearly with

the pressure up-stream P (see Figure 5.17). For a number of pressures (corresponding to the atmospheric pressures in different flight altitudes) the flow remains proportional to P as expected. The regression line F=aP+b though, deviates from the one calculated with the help of the formula giving the critical flow F^* as a function of pressure P:

$$F^* = 18.96 \cdot 10^6 \cdot \frac{\pi R T_o}{M P_o} \cdot (\frac{2}{k+1})^{\frac{1}{k-1}} \sqrt{\frac{2k}{k+1} \cdot \frac{M}{RT}} \cdot r^2 P \qquad (5.6)$$

where r the radius of critical orifice in mm, R=0.0831 $mbar\, m^3\, mol^{-1}\, K^{-1}$, T_o=273.15 K, P_o=1013.25 mbar, k=1.4054, M=28.013, P and T ambient pressure and temperatures. As demonstrated in the graph the flows measured are lower than the flows predicted. It is therefore necessary not only to calibrate the teflon orifices but also to check whether their regression lines are reproducible with time. In order to avoid potential complications it is suggested the use of a stainless steel critical orifices which can not deform with time and the flows are reproducible, so it suffices if they are calibrated once.

Chapter 6

Measurements of S(VI) in the internal flow of an aircraft engine

Gaseous S(VI) has been measured in the simulated internal flow of an aircraft gas turbine at ground level during the European Commission funded project PartEmis (Measurement and prediction of emissions of aerosols and gaseous precursors from gas turbine engines). Objective of the project PartEmis was to go further than earlier studies, by gaining a detailed understanding of the composition and transformation of combustion gases and particles formed inside an aircraft engine.

6.1 The PartEmis project

Two campaigns were planned during the PartEmis project. Both were hosted by QinetiQ (former DERA) in Farnborough, UK where the necessary facilities were designed and produced. These facilities comprised a combustion system that in technology terms is compatible with the ICAO (International Civil Aviation Organization) emission standards and a Hot End Simulator (HES) attached to the combustor. The so-called HES is an expansion system that simulates the thermodynamic processes involved in the expansion of gases in the turbine and nozzle stages of an engine. The principal aim of the tests was to examine the effect of fuel sulfur content (FSC) on aerosol and aerosol precursor emissions. The base fuel, therefore, was chosen to be low sulfur kerosene (50 ppm), doped to modify the sulfur content up to a maximum of 1270 ppm. The combustor was operated in two conditions representative of legacy
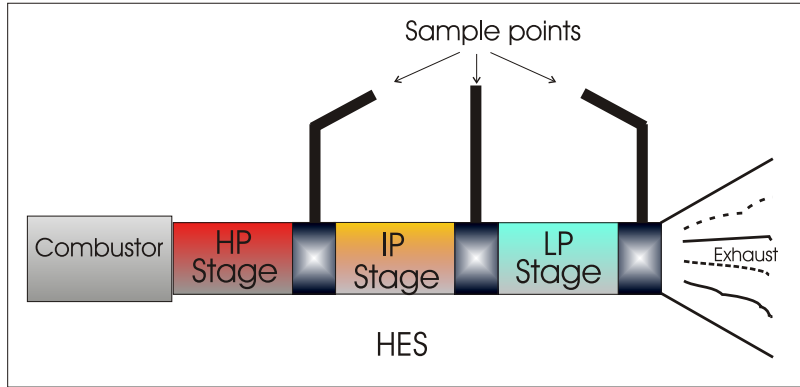
Figure 6.1: Schematic presentation of the combustor and the Hot End Simulator [Kat03].

and modern aircraft cruise. The differences between the old and modern cruise condition concern different combustor pressure and temperatures, fuel flows (FF) and air-to-fuel ratios.

The initial campaign took place during the period 25 January and February 1, 2001. Measurements were made in the exhaust of the combustor and gas was sampled at eleven probe positions across combustor's exit nozzle, a 36° smile shaped discharge nozzle. QinetiQ accommodated researchers from seven separate research groups to carry out the following measurements: DLR-IPA, black carbon and ultrafine particles; University of Vienna, cloud condensation nuclei; Technical university of Vienna, aerosol composition; Paul Scherrer Institute, hygroscopicity of aerosol particles; University of Wuppertal, hydrocarbon analysis; University of Leeds, OH radicals; MPI-K, S(VI) and ions. Modeling work has been also conducted by QinetiQ, University of Essen and University of Strasbourg. The major experimental and modeling results of the PartEmis I campaign are given in the overview paper [Wil03], while more descriptive work of each group is given in: [Gys03], [Pet03], [Hav03], [Arn03], [Kat03].

The second PartEmis campaign took place in March 2002. Measurements were made in the exhaust of the combustor and the attached HES (Figure 6.1). The difference between a real gas turbine engine and the HES is that the latter has no moving parts and therefore cannot simulate the dynamic effect that a rotating turbine can have on the particulates in the air path. The simulation of the inter-stage thermodynamic conditions in the HES were achieved by passing the hot combustion products through a series of heat exchangers, which extracted energy from the gas, lowering

	Old Cruise	Modern Cruise
T combustor inlet (K)	566	766
T combustor outlet (K)	1125	1360
P combustor (bar)	7.05	8.2
Air mass flow (kgs^{-1})	2.12	2.12
Fuel flow (kgs^{-1})	0.032	0.035
Air fuel ratio	66	60.4

Table 6.1: Combustor operating conditions during the PartEmis II campaign [Wil03]

its temperature and by cross sectional area changes which controlled the pressure. As in the first campaign, measurements were made for the old and modern cruise condition and different FSC. The HES was designed to have temperature ratios and residence times similar to those found in a modern aircraft engine at a cruise altitude of 35,000 ft.

The FSC levels covered the range from low sulphur fuel (50 ppm) to the contemporary average (410 ppm) and to a maximum of about three times this average (1270 ppm) defined here as Low, Mid and High (L, M, H) FSC, respectively. The sulphur content was varied by adding known quantities of benzenethiol (C_6H_5SH) to the low FSC fuel. In addition, a Shell additive known as APA101 (0, 256, 1280 $\mu g\,l^{-1}$; None, Standard, High or N, S, H) was used with low FSC fuel in order to study the effects on exhaust emissions. This additive was originally developed to extend the thermal stability of JP-8 jet fuel for use in military applications by at least 100° F (55° C). The use of APA101 Additive has been shown to: i) increase the thermal stability of JP-8, ii) reduce fuel manifold and nozzle coking deposits in gas turbine engines, and iii) clean-up carbon deposits in the hot engine sections from the combustor through to the afterburner. The direct benefits are reduced fuel-related maintenance costs and increased reliability of turbine engines. APA101 additive fuel has found widespread use in U.S. military aircraft and is currently being assessed by several commercial airlines. Details of the two combustor operational conditions are given in Table 6.1.

	Temperature (K)	Pressure (bar)	Residence Time (ms)
CE	1448	7.9	5
HP	1106	3.7	5.5
IP	923	2.6	6.3
LP	646	1.9	11

Table 6.2: HES operating conditions during the PartEmis II campaign
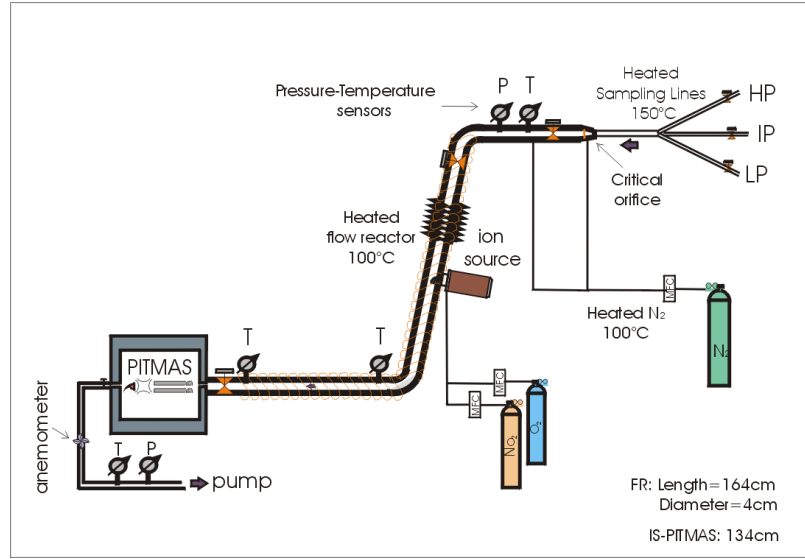
6.2 Experimental setup

The MPI-K instruments were installed in the combustor room, where no one could gain admittance during the test runs for safety reasons. For the accommodation of all the partners there was provided another room, the so-called control room, from which our instruments could be controlled and remotely operated. The remote operation of the instrumentation meant additional complication to the set up planning, offered on the other hand, the advantage of shorter sampling lines. For the instruments of the other participants installed in the control room a 20 m long unheated sampling line was used.

For the S(VI) measurement during the PartEmis campaign a CIMS instrument was used, equipped with a stainless steel flow reactor (FR inner diameter 4 cm, total length 164 cm), a high frequency glow discharge ion source for reagent ion production and the Quadrupole Ion Trap Mass Spectrometer (IT-MS) for ion detection. Heating bands were wrapped around the flow reactor in order to keep the gas temperature in the range of 100° C. The flow reactor was insulated with aluminum foil. The gas temperature of the sample flow was measured and controlled with Pt 100 sensors mounted at three positions inside the flow reactor. With two pressure sensors was the pressure in the flow reactor controlled and kept constant during each HES run. The flow was regulated with a remotely controlled valve placed between the flow reactor and the two parallel-connected pumps used.

The exhaust coming from HES was introduced in our flow reactor through a critical orifice. The critical orifice used initially (0.3 mm) was exchanged with a smaller one

Figure 6.2: Schematics of the experimental set up during the PartEmis II campaign

(0.2 mm) in the last day of the experiment, when the combustor was burning the fuel with the highest sulfur content. To avoid getting extremely high concentrations of sulfuric acid in the flow reactor during this last test, either a higher dilution should be applied or a smaller sample flow from HES should be allowed to enter the flow reactor. Since our pumps could not afford a higher flow, it was decided to use the smaller orifice. The flow trough these orifices were < 2 slm, depending on the pressure behind.

Exhaust gas was sampled at the three stages in the internal flow of the HES. These stages were representative of the high, intermediate and low pressure turbines of a real engine, were therefore named High, Intermediate and Low pressure stages (HP; IP; LP). The HES conditions and residence times of the exhaust gas in the HES are given in Table 6.2. Three stainless steel sampling lines (SL) heated up to 150 °C to avoid condensational losses were used to sample gas at the three stages in the internal flow of the HES. The length of the SL was 170 - 190 cm, the inner diameter between 0.457 cm - 0.75 cm and the gas flow velocities were ranging from 20 - 120 m/s resulting in gas residence times 15 - 95 ms. In comparison to the residence time of the exhaust gas in the HES ($<$5ms) these are markedly larger. This may have caused implications in our measurements concerning undesirable, post HES oxidation of the exhaust gas in the SL.
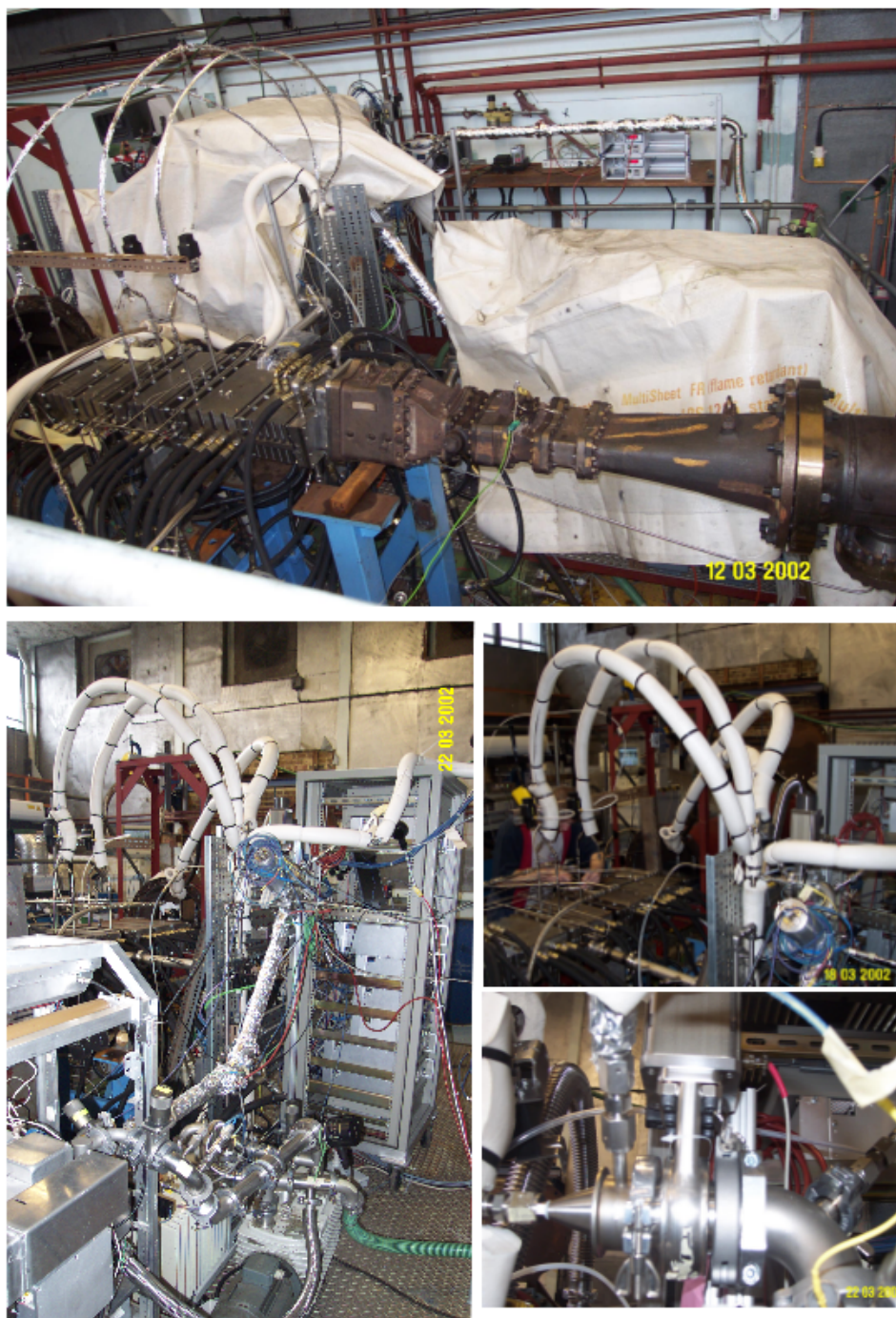
Figure 6.3: Combustor room - upper panel: combustor and HES; lower-left panel: set up for the S(VI) measurements; lower right panels: sampling lines for the HP-IP-LP stages and critical orifice.

In Figure 6.2 it shown a schematic of the sulfuric acid set up during the PartEmis 2002 campaign. The ion source was mounted 134 cm upstream of the mass spectrometer inlet orifice. The high frequency discharge burns in a buffer gas of O_2 (7.2slm) and NO_2 (2500 ppm in N_2, 0.8 slm). The dilution N_2 added to the flow reactor was heated up to 100 °C before introduced to the flow reactor. All of the valves and the flow controllers were remotely operated.

6.3   High Fuel Sulfur Content

Measurements for the highest FSC=1270 ppm were made for the two operating conditions of the combustor in the exhaust of the HES. Gas was sampled for 20 min at HP and the IP stage and for 40 min at the LP stage of the HES. Measurements of SO_2 by QinetiQ required the total sample flow and thus were conducted separately. There is no available time-series of SO_2 for comparing with the our obtained H_2SO_4 but only an average value for every pressure stage. During the two runs (old and modern cruise condition) the FR was heated and the temperature ranged between 67-69 °C. The pressure in the FR was kept constant at 47 mbar and the total flow was 56 slm resulting in a residence time of 73 ms.
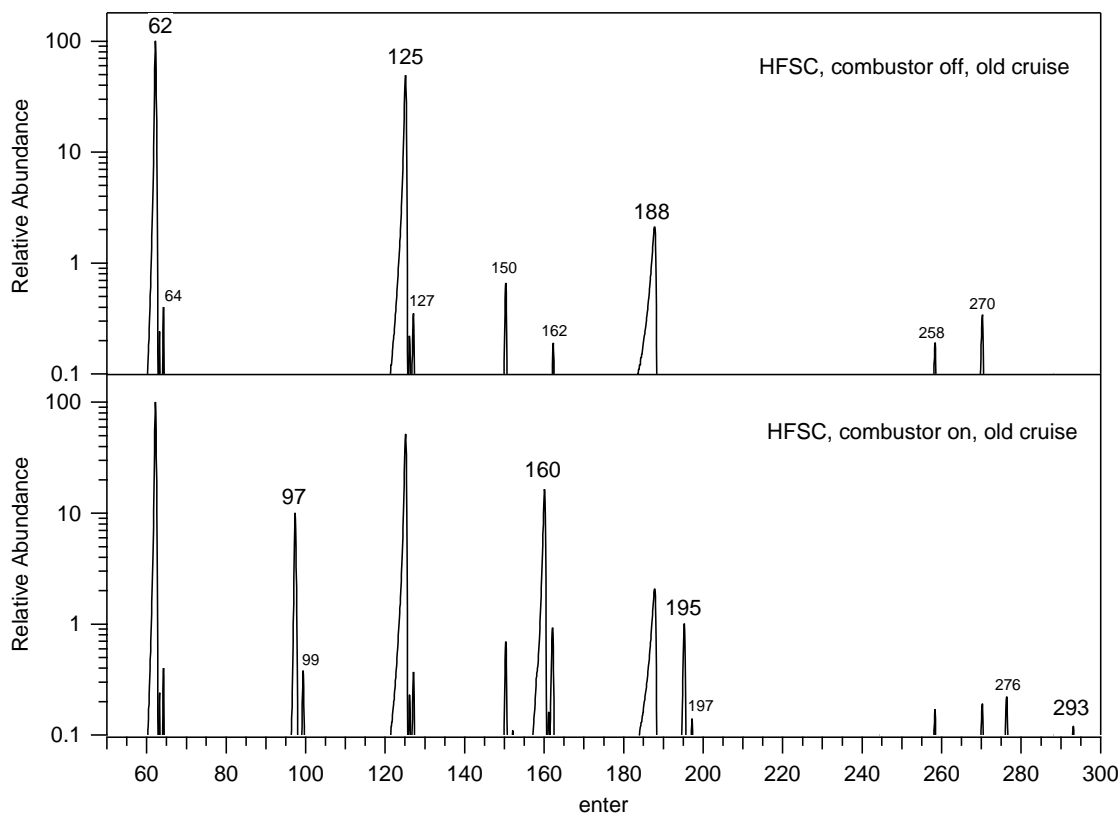
6.3.1   Old Cruise condition

Figure 6.4 shows two mass spectra obtained by the CIMS instrument: the top panel is the background spectrum and the bottom panel the average spectrum obtained during the 3rd test point (old cruise; LP stage). Both spectra contain the reagent ions NO_3^- (m=62), $NO_3^-(HNO_3)$ (m=125) and $NO_3^-(HNO_3)_2$ (m=188). The combustor-on spectrum contains additionally four product ion species HSO_4^- (m=97), $HSO_4^-(HNO_3)$ (m=160), $HSO_4^-(H_2SO_4)$ (m=195) and $HSO_4^-(H_2SO_4)_2$ (m=293) which are the product ions of the ion-molecule reactions used for the sulfuric acid detection. With relatively lower abundance ($<1\%$) appear as well lines which are not identified. These are: 64 and 127=64+63, which are present in combustor on and off spectra without any significant fluctuation in their peak height. Their mass difference is 63, probably identified as HNO_3; lines 150, 152, 258 and 270 which are present in both combustor on and off spectra without variation; lines 99

and 197=99+98 which have a mass difference of 98 and appear at the combustor-on spectrum, following the variations of lines 97 and 160; finally, line 162 appears in both spectra with higher peak in combustor on spectrum. According to MS^2 studies this ion has two daughter ions, one with mass 116 (neutral ion 46=NO_2) and another one with mass 99 (neutral ion 63=HNO_3).

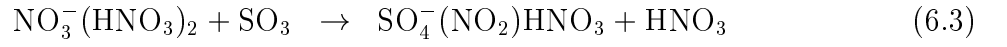## 6.3.2 Modern Cruise condition

Figure 6.5 shows two mass spectra obtained by the CIMS instrument: the bottom panel is the average spectrum obtained during the 6th test point (modern cruise; LP stage). The reagent and product ions are to be clearly seen. As in the old cruise condition appear additionally lines which are not identified with relatively lower abundance (<1 %). These are the same as in the old cruise and some new,

Figure 6.4: Mass spectra of negative ions measured by the CIMS instrument for combustor off (top panel) and combustor on (bottom panel) for the LP stage, old cruise condition and FSC=1270 ppm.

namely the pair 89,152=89+63; the triplet 99,197=99+98,295=197+98 and finally masses 204 and 276.

Interestingly, product ions of the SO_3 reactions with $NO_3^-(HNO_3)_n$ and HSO_4^- $(HNO_3)_n$ are virtually absent (m=96, 142, 205, 177, 240) [Rei93]; [Rei94]; [Arn95]; [Rei97]:

$$NO_3^- + SO_3 \quad \rightarrow \quad SO_4^- + NO_2 \tag{6.1}$$

$$NO_3^-(HNO_3) + SO_3 \quad \rightarrow \quad SO_4^-(NO_2) + HNO_3 \tag{6.2}$$

$$NO_3^-(HNO_3)_2 + SO_3 \quad \rightarrow \quad SO_4^-(NO_2)HNO_3 + HNO_3 \tag{6.3}$$

$$NO_3^-(HNO_3)_n + SO_3 \quad \rightarrow \quad HSO_4^-(HNO_3)_{n-1}SO_3 + HNO_3 \tag{6.4}$$
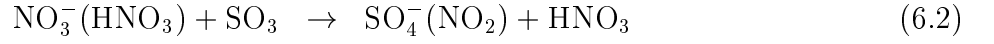
This strongly suggests that SO_3 is already converted in the 2 m long sampling line to gaseous H_2SO_4. Probably, gaseous SO_3 entering the SL undergoes rapid conversion
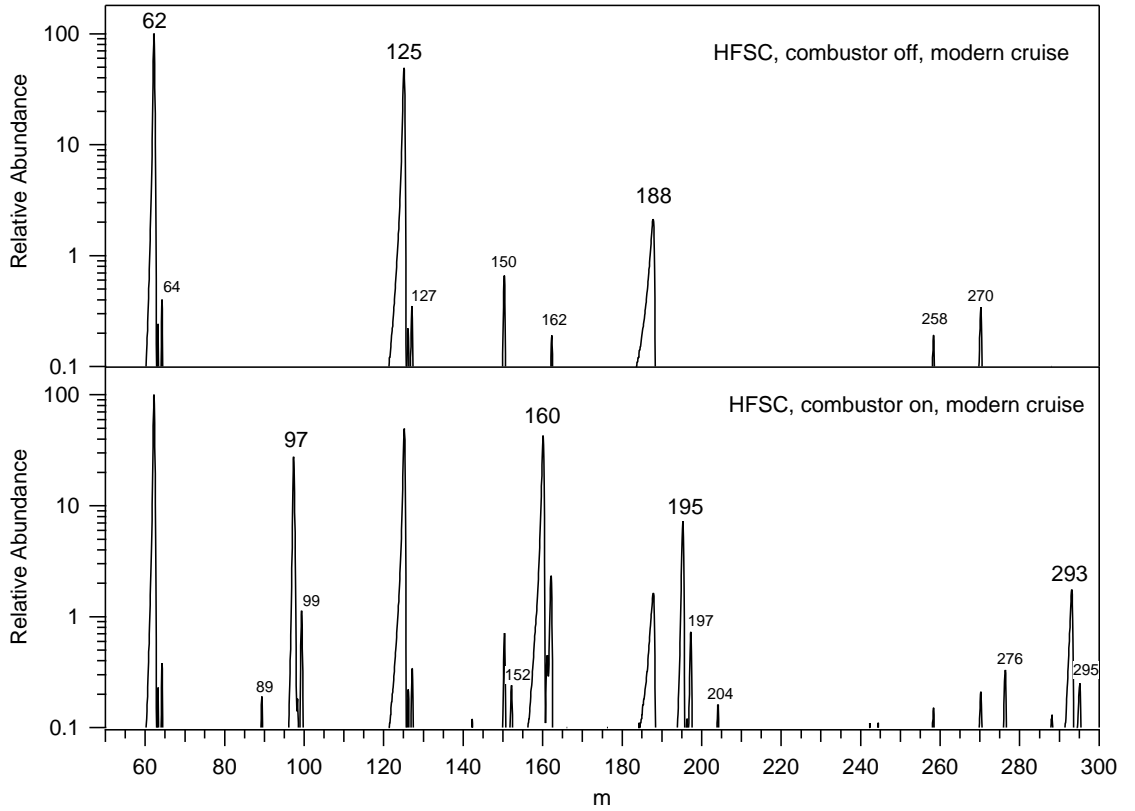

Figure 6.5: Mass spectra of negative ions for combustor off (top panel) and combustor on (bottom panel) for the LP stage, modern cruise condition and FSC=1270 ppm.

to H_2SO_4 via reaction with water vapor molecules. Therefore S(VI) leaving the rear-end of the SL is all in the form of gaseous H_2SO_4 which is subsequently measured by the CIMS instrument.

However, a substantial fraction of the S(VI) gases leaving an aircraft gas turbine engine should be present as SO_3, according to speciated SO_3 and H_2SO_4 measurements recently accomplished by the MPIK-Heidelberg group in the framework of the SULFUR campaign [Sor03]. The measurements were made again in the exhaust of a jet aircraft engine (Type RR M45H) at the ground. For the detection of sulfur trioxide and sulfuric acid was used a linear quadrupole mass spectrometer with an external ion source producing $NO_3^-(HNO3)_n$ ions. Exhaust gas was sampled by an orifice probe (OP; diameter 0.3 cm) located at the front end of the FT and directly at the plume axis at a distance of d=100 cm downstream of the exit plane of the jet engine (Type RR M45H). After entering the FT, exhaust gas was sampled through the FT (inner diameter: 4 cm; length 430 cm) by a mechanical pump which was attached to the rear end of the FT. The total gas pressure in the FT was P_{FT}=30 mbar and the time span for gas passage through the FT was t_{FT}=150 ms. The point of reagent-ion introduction into the FT was located at a distance of 300 cm downstream of the OP and the time for ions to react with trace gases was 45-50 ms. The exhaust gas in this experiment was diluted immediately after the sampling in order to reduce SO_3 conversion to H_2SO_4 in the SL. Indeed, the presence of lines 142, 177 and 205 in the spectra indicated the presence of gaseous SO_3 in the FT, suggesting that a major fraction of SO_3 did not experience conversion to GSA in the post combustor flow.

The data obtained from this experiment, which was similar to the PartEmis experiment (compare the experimental set up), were interpreted with the help of some model calculations which included, among other processes, conversion of SO_3 to H_2SO_4 in the SL. The model calculations showed that at least 50 % of the S(VI) gases at combustor exit should be represented as SO_3 and that an essential conversion of SO_3 to H_2SO_4 conversion takes place in the SL. Even an assumed zero concentration of sulfuric acid at the combustor exit (i.e. $S(VI)_{CE}$=SO_3) in the model, would be sufficient to explain the H_2SO_4 measured by CIMS. Thus, for the PartEmis experiment, what is measured as gaseous sulfuric acid in the FR, is in fact the sum of S(VI) gases i.e. SO_3 and H_2SO_4 at the exit of the HES; information of partitioning between SO_3
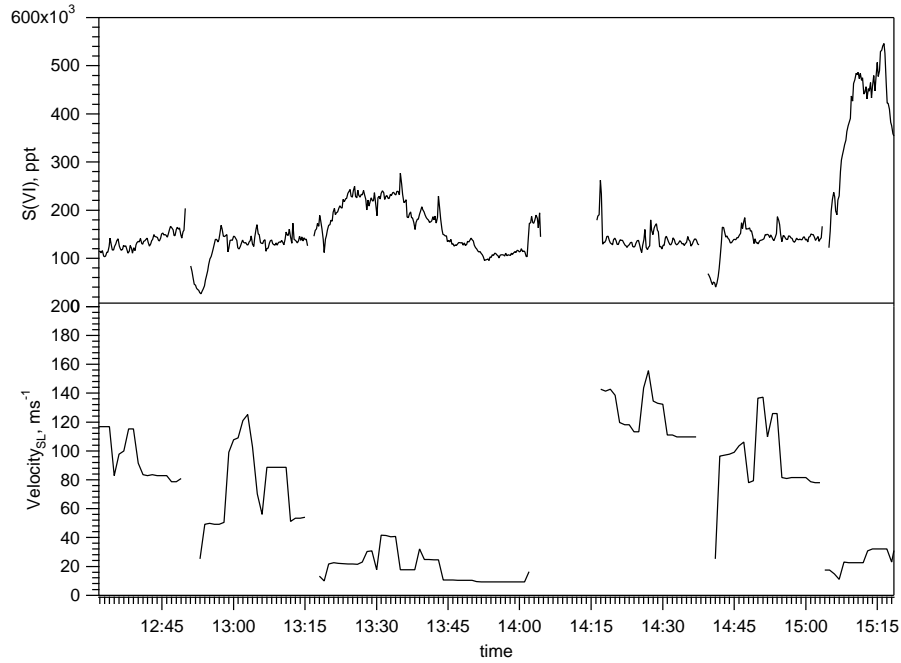
Figure 6.6: Measured S(VI) and gas flow velocities in the sampling lines for FSC=1270 ppm for the old (test points 1-3) and modern cruise conditions (test points 4-6)

and H_2SO_4 species is lost.

6.3.3   S(VI) and Sulfur Conversion efficiency

The measured mixing ratios of S(VI) before being diluted in the FR are given in the top panel of Figure 6.6. There is a total of six test points, three for each cruise condition, starting with the old cruise. For both cruise conditions the S(VI) concentration is increasing from the HP to LP stage, though not monotonously as expected. This behaviour, neglecting for the moment the IP-stage data, is in good agreement with the model results of Starik et al, 2002 [Sta02] which, as well, predict a gradual increase of S(VI) gases in the internal gas flow of an aircraft engine. A malfunction of the HES at the IP stage was proposed but not yet clarified by the HES crew. An interesting feature is the steep increase of S(VI) followed by a plateau at the beginning of some test points (2nd and 5th: for the rest test points, data was not saved at the very beginning of the run) (Figure 6.6). That observed behavior suggests that S(VI) wall losses in the SL were initially very large, then decreased very markedly and became ultimately negligible. This decrease of S(VI) wall losses may reflect deactivation of

the inner SL-surface. It is suspected that re-activation of the surface before each run may have been caused by back-purging of the SL applied by QinetiQ mainly in order to reduce clogging at the sampling holes at the front-end of the SL. For a purge gas compressed laboratory air was used. It is conceivable that trace substances like gaseous ammonia or ammonium nitrate containing aerosols contained in the purge air may become deposited at the inner wall of the SL. If so S(VI) gases may have experienced wall reaction with these substances.

At the LP stage for both cruise conditions there is a significant S(VI) variation observed: the S(VI) mixing ratios for the 3rd test point increase from 100 ppb to around 300 ppb and then fall down to the initial values. The same seems to happen for the 6th test point, although only the first 10 min of this run were saved. Within this time span the S(VI) mixing ratios increased form 100 to 500 ppb. Due to some software complications data for the rest 30 min were lost. It was checked whether the variation of residence times in the SL affects the S(VI) concentrations but there was no correlation observed (see Figure 6.6). We can deduce, therefore, that it is caused by the combustor-HES system. Comparison with the hygroscopic growth factors of combustion particles measured on line by PSI revealed similar time evolution at every test point (M. Gysel, personal communication). This hygroscopic behaviour may be attributed to sulfuric acid adsorbed on black carbon particles. The good correlation of the hygroscopic growth factors with our H_2SO_4 is a confirmation that the observed variations are real and not an artifact.

Building on the $S(VI)_{SL}$ and the total sulfur S_T measured by QinetiQ the conversion factor ϵ can be determined $\epsilon = SO_2/S_T$. Since there is no S_T time series available the S(VI) should be averaged for each test point so that a representative S(VI) value id delivered. For the test points that the S(VI) concentration reaches a plateau and remains constant the average value will be the arithmetic mean of the plateau values. In case that the values increasing without reaching a plateau the last highest S(VI) values will be used. The averaged S_T and $S(VI)_{SL}$ and the calculated epsilon values are given in Table 6.3.3. The error of S(VI) is ±43% determined mostly by the error of k (±30%) and the error of t_R (±30%). Taking a ±30% error for the S_T and a ±43% for the S(VI) the error of ϵ is ±52%.

Figure 6.7 shows ϵ values obtained during the two PartEmis campaigns for the

tp	Description	$S_T\,ppm$	$S(VI)_{SL}\,ppb$	$\epsilon\,\%$
1	HP; OC	18.1 ± 5.4	165 ± 71	0.9 ± 0.5
2	IP; OC	18.5 ± 5.6	143 ± 62	0.8 ± 0.4
3	LP; OC	17.8 ± 5.3	240 ± 103	1.4 ± 0.7
4	HP; MC	20.7 ± 6.2	225 ± 97	1.1 ± 0.6
5	IP; MC	20.7 ± 6.2	180 ± 77	0.9 ± 0.5
6	LP; MC	20.1 ± 6.2	450 ± 194	2.2 ± 1.1

Table 6.3: S_T measured by QinetiQ, S(VI) and derived epsilon values for FSC=1270 ppm

high FSC test. Data is given for three sampling positions CE (Combustor Exit), HP and LP (High and Low Pressure stage) for both old and modern cruise condition. The CE data were obtained during the PartEmis I campaign. There is one trend noticable and namely the increase of ϵ with increasing exhaust age, predicted as well by the models of Tremmel and Schumann 1999 [Tre99] and Starik et al., 2002 [Sta02]. The rate of conversion between combustor exit and engine exit is different for the two models and for the PartEmis measurements. In the Tremmel and Schumann model - assuming no conversion in the combustor - the oxidation of SO_3 to H_2SO_4 is essentially occurring at the HP stage and the equilibrium value of $\epsilon = 3.81\%$ is reached only after a few milliseconds after the combustor exit. The model of Starik calculates a conversion of around 1% at the combustor exit and a more gradual conversion between the different pressure turbines reaching a value of around 8% at the engine exit. The PartEmis measurements suggest that the conversion factor at the combustor exit (CE) is around 1%, it slightly increases from CE to HP stage and and it takes it's final and highest value at the HP stage. Although the trend of increasing ϵ with exhaust age observed in the PartEmis tests is reproducible by the models there is a difference between different models and experiments in the way ϵ evolves in the internal engine flow and in the final absolute numbers of the ϵ.

This difference in the model results can be attributed to the sensitivity of ϵ on the reaction of SO_2 with OH. The sensitivity analysis of Tremmel and Schumman showed
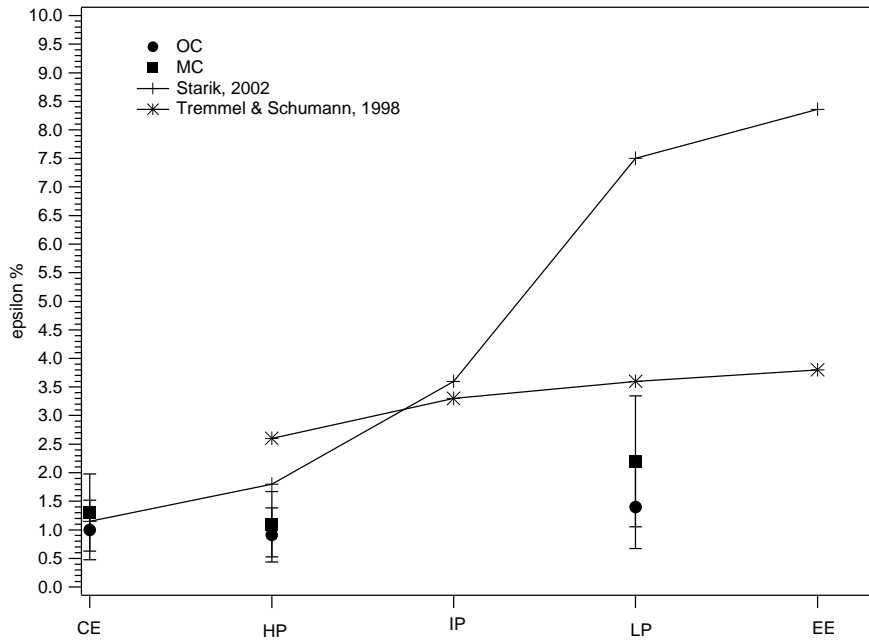
Figure 6.7: ϵ obtained during the PartEmis 2002 campaign at the high and low pressure stages and LP for FSC=1270ppm, old and modern cruise conditions (OC; MC). Comparison is made with the theoretical model conversion efficiencies reported by Tremmel and Schumann, 1999 and Starik at al., 2002 [Kat03].

that this reaction has the greatest effect on ϵ [Tre99]. As this reaction is termolecular, its low effective bimolecular rate constant is calculated from a termolecular low pressure value k_o and a bimolecular high pressure value k_∞ via the expression [Tr083]

$$k = \frac{k_o k_\infty \cdot [M]}{k_\infty + k_o \cdot [M]} \cdot F_c^{(1+(log_{10}(k_o \cdot [M]/k_\infty))^2)^{-1}} \qquad (6.5)$$

where k_o is the low pressure limiting rate constant, k_∞ the high pressure limiting rate constant and F_c the broadening factor of the fall off curve, the actual value of which depends on the particular reaction and can be calculated theoretically. For the reaction of SO_2 with OH, F_c is taken to be 0.6. The rate constants and its uncertainty range can be extracted from the NIST data base which comprises a large body of published data. Since these data are only available for a temperature range up to 450 K, the temperature dependencies of k_o and k_∞ should be extrapolated to higher temperatures. In the Tremmel and Schumann model the higher and lower pressure limit rate constants that have been used were k_o=1.97(-32) and k_∞=2.00(-12) $cm^3 \, molecule^{-1} \, s^{-1}$, leading to a reference value for their baseline scenario $k_{eff} =$

5.83(-13) $cm^3\,molecule^{-1}\,s^{-1}$ for p=7700 hPa and T=1200 K, assuming a normal Arrhenius behaviour for k_o. The uncertainty range at this pressures and temperatures is 9.23(-14)<k<9.27(-13)$cm^3\,molecule^{-1}\,s^{-1}$ and leads to simulated sulfur conversion efficiencies varying between 1.07 % and 6.17 %, provided that there is no deviation from the assumed Arrhenious temperature dependence of the rate constant. The Starik model which uses a high pressure limit rate constant k=9.03(11) $cm^3\,molecule^{-1}\,s^{-1}$ instead of an effective one, predicts significantly higher conversion efficiencies than the Tremmel and Schumann model.

Model calculations have also shown that the sulfur conversion efficiency is sensitively dependent on different parameters including combustor operating conditions. It is, therefore, understandable to get different results from experiment and models, as many of the parameters have not been identical. Important is that the same trends are followed in both cases. The PartEmis measurements suggest additionally a dependence of ϵ on operation parameters. Modern cruise operating conditions resulted in higher conversion efficiencies (ϵ=1.4±0.7 % and 2.2±1.1 % for old and modern cruise condition respectively, see Table 6.3.3). An increase of ϵ with combustor exit pressure and temperature is also confirmed by modeling work [Schu02].

6.4 Medium Fuel Sulfur Content

The measurements in the exhaust of the HES burning fuel with the medium sulfur content FSC=410 ppm took place on 20th March 2002. The measuring parameters were not kept constant in the two cruise conditions. In the modern cruise were applied higher temperatures and a lower pressure in the flow reactor resulting in a lower reaction time.

6.4.1 Old Cruise condition

The pressure in the flow reactor for the old cruise condition measurements was kept constant at 60 mbar and the temperature at 21 ^oC (flow reactor unheated). The flow velocity was 10 ms^{-1} resulting in a reaction time of 130 ms. In Figure 6.8 are shown the combustor off and on average spectra for the LP stage. In the bottom panel are given the additional lines that appear in the combustor on spectrum.
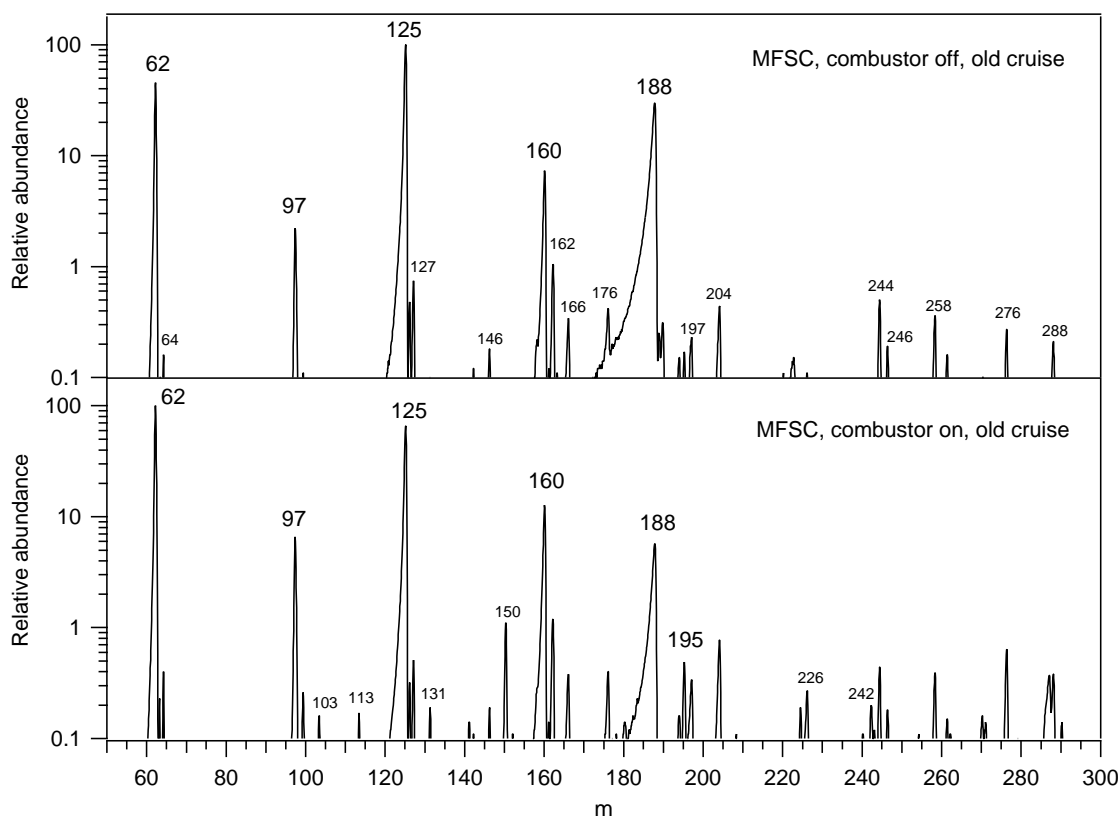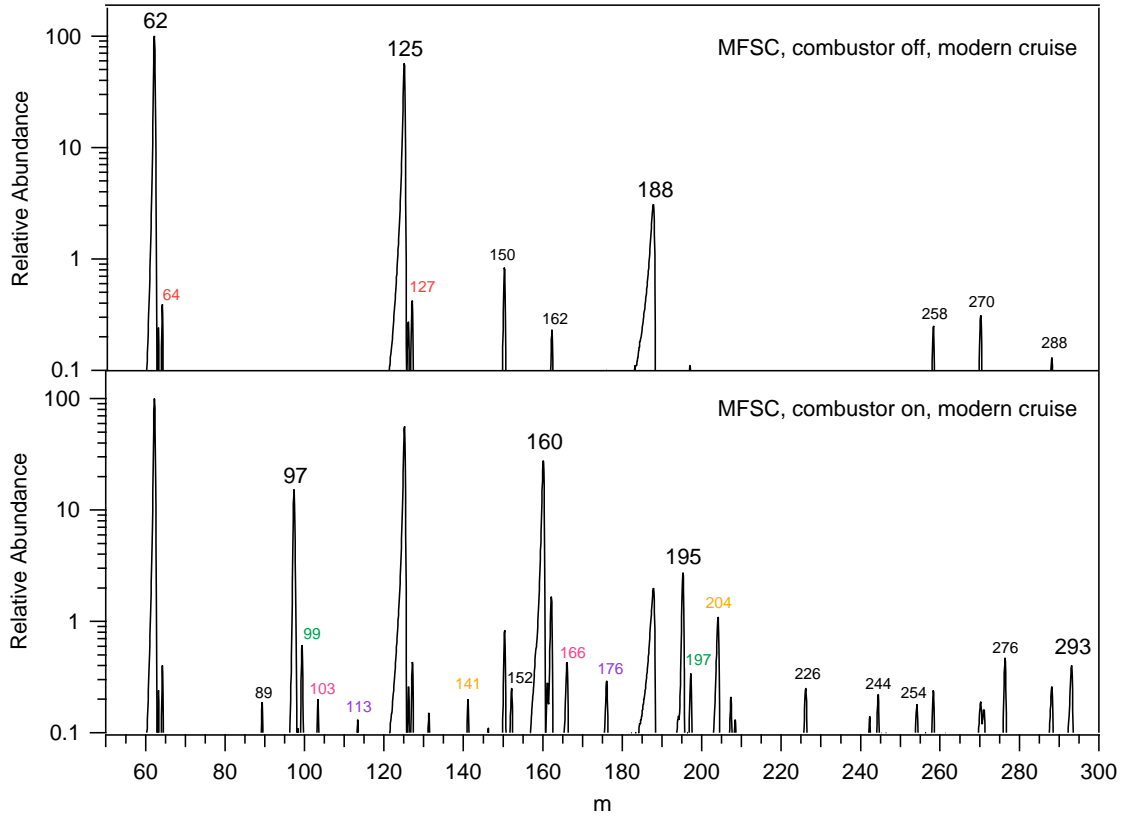
Figure 6.8: Mass spectra of negative ions for combustor off (top panel) and combustor on (bottom panel)for LP stage and FSC=410 ppm.

Compared with the background spectrum of the high FSC case, line 150 is absent while some more unidentified lines appear in addition to the ones already mentioned. These lines are: 146 and 244=146+98; line 197 which was present only in the 'combustor on' spectrum for the high FSC case; lines 244 and 288. In the combustor on spectrum the dominant lines are 97 and 160 and 195, identified as the product ions, and with lower intensities lines 166, 176, 193, 204, 222, 246, 261 and 276 which were not present during the background measurements. The reason for having more unidentified lines in the combustor on spectrum in comparison with the old cruise condition of the high FSC is not clear.

6.4.2   Modern Cruise condition

During the measurements with the combustor running in modern cruise the flow reactor was heated and the temperature was kept constant at $71\,^oC$. The pressure was

Figure 6.9: Mass spectra of negative ions for combustor off (top panel) and combustor on (bottom panel)for LP stage and FSC=410 ppm.

40 mbar and the gas flow velocity 14ms^{-1} resulting in reaction time of 93 ms. The combustor on and off spectra for this run are given in Figure 6.9. When compared with the background spectrum of the old cruise condition, the combustor off spectrum appears somewhat different as far as the equilibrium of reagent ions and the presence of certain lines are concerned. When the flow reactor is not heated the dominant reagent ion is 125 and when is heated, ion 62. The relative abundances of the three reagent ions 62-125-188 are 41-100-33 % and 100-57-3 % in the unheated and heated flow reactor, respectively. It is apparent that higher temperatures favor reagent ions with less HNO_3 molecules attached to the core ion NO_3^-. In this context, the background spectrum of the modern cruise operating condition for which the flow reactor was heated, is almost identical to the background spectrum obtained during the high FSC test and bears no similarities with the background obtained during the old cruise, medium FSC test: line 150 is present, while lines 146, 197 and
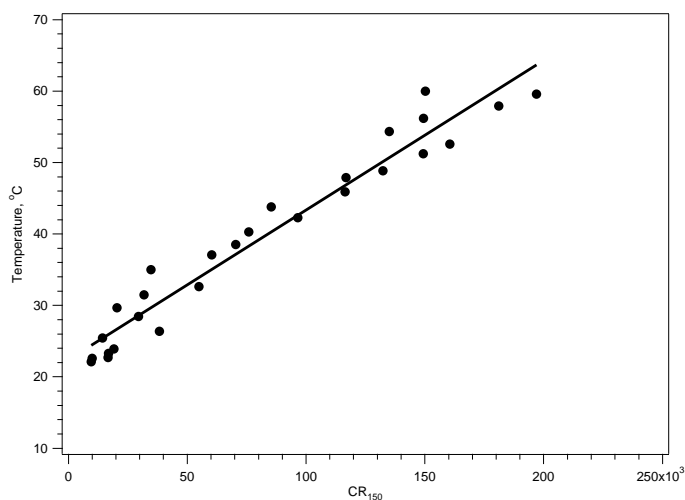
Figure 6.10: Correlation of mass 150 with temperature in the flow reactor
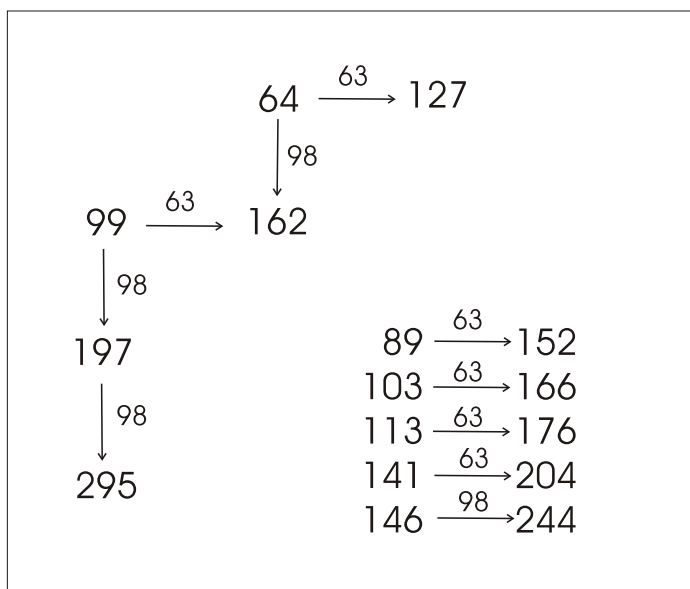
Figure 6.11: Possible fragment ions of some unknown ions present in the mass spectra.

244 disappear. It seems that line 150 is strongly related to temperature as its CR follow the increase/decrease of temperature (see Figure 6.10).

The new lines appearing when the combustor is running are noted in the bottom panel of Figure 6.9. With same colors are presented lines that seem to share the same core ion and have an additional HNO_3 or H_2SO_4 molecule attached. In Figure 6.11 are given some of the unknown peaks present in the mass spectra and the potential dissociated fragments.
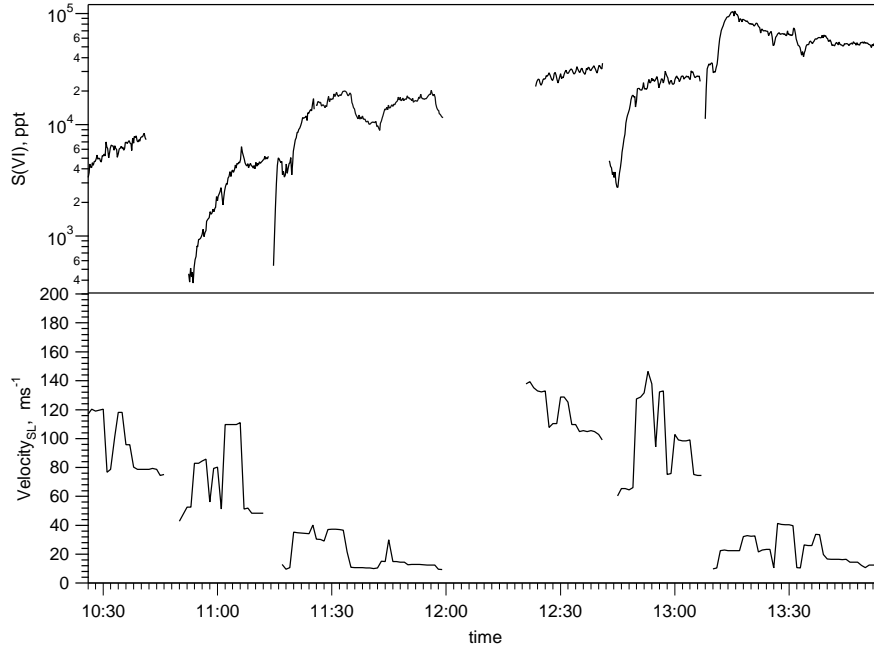
Figure 6.12: Measured S(VI) and gas flow velocities in the sampling lines for FSC=410 ppm and the two cruise conditions.

6.4.3 S(VI) and Sulfur conversion efficiency

Measured S(VI) mole fractions and gas flow velocities in the sampling lines are given in Figure 6.12. The velocities in the sampling lines are ranging between 15 and $140\,ms^{-1}$ resulting in residence times variating between 130 and 15 ms. As in the high FSC test, there is no correlation between the flow velocities and the S(VI) concentrations in the sampling lines. This is an indication that no wall losses occur in the sampling lines: if this was not the case then the S(VI) concentrations should be associated with the residence times in the sampling lines i.e. longer residence times would result in higher wall losses and lower S(VI).

In the beginning of each test point S(VI) is markedly increased, probably, as already mentioned, due to reactive wall losses with an unknown substance (potentially NH_3) that is present in the sampling lines. Interestingly, this 'deactivation' time is variating and namely decreases with increasing S(VI) mixing ratios. For the 2nd test point the highest S(VI) concentration is reached in 12 min, for the 5th test point in 3 min and for the 6th test point in 2 min. The same trend in the surface deactivation times is followed in the high FSC test: it seems that when the sulfuric acid mixing

| tp	Description	$S_T\,ppm$	$S(VI)_{SL}\,ppb$	$\epsilon\,\%$
1	HP; OC	5.6 ± 1.1	9 ± 3.9	0.16 ± 0.08
2	IP; OC	5.7 ± 1.1	5 ± 2.2	0.09 ± 0.05
3	LP; OC	5.6 ± 1.1	20 ± 8.6	0.36 ± 0.2
4	HP; MC	6.4 ± 1.2	35 ± 15	0.56 ± 0.3
5	IP; MC	6.3 ± 1.3	26 ± 11	0.41 ± 0.2
6	LP; MC	6.3 ± 1.3	105 ± 44	1.58 ± 0.8
6	mean	6.3 ± 1.3	60 ± 26	0.95 ± 0.5

Table 6.4: S_T measured by QinetiQ, S(VI) and derived epsilon values for FSC=410 ppm

ratios are higher the deactivation reaction occurs faster.

In Table 6.4.3 are presented the calculated total sulfur mixing ratios for every test point together with the S(VI) and the inferred epsilon values. For the 6th test point the maximum and a mean value is given: the sulfuric acid concentration reaches a maximum (105 ppb) and then decreases without remaining constant but variating between 50 and 70 ppb. Since the nature of these variation is unclear, it is not easy to decide for the most characteristic value of this test point, therefore both maximum and mean values are given.

In Figure 6.13 are shown the calculated epsilon values for the three pressure stages for medium FSC. In comparison with the epsilon values obtained in the high FSC test (also presented in the same Figure) they are lower for both old and modern cruise. This result contradicts the majority of model calculations which report a decrease of epsilon with FSC due to limitations of oxidants. This behaviour can not be explained by a known combustion mechanism. It is conceivable, that it is an artifact due to insufficient precision of the S(VI) and total sulfur calculations. An increase of epsilon in the modern cruise condition, on the other hand, seems to be reproducible by model calculations, which report an increase in conversion efficiency at higher combustor temperatures and pressures.
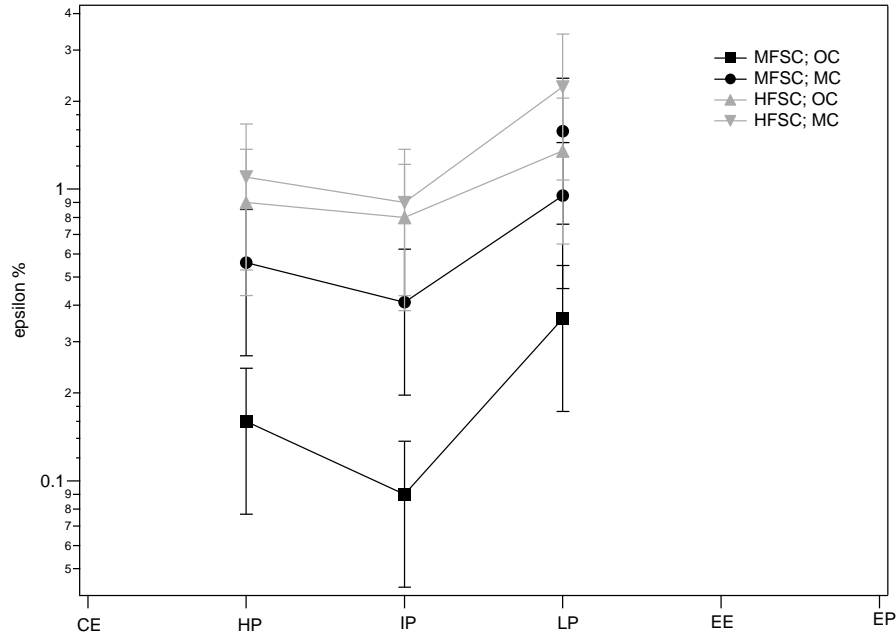
Figure 6.13: Measured ϵ for MFSC=410 ppm compared with the ϵ obtained for HFSC=1270 ppm at the three pressure stages (HP;IP;LP) for old and modern cruise conditions (OC;MC).

6.5 Low Fuel Sulfur Content

On the 18th of March 2002 were made measurements for the lowest FSC=50 ppm and for the two operating conditions of the combustor in the exhaust of the HES. During this run the FR was not heated and the temperatures of the gas were ranging between 20-23 °C. The pressure in the FR was kept constant at 60 mbar and the total flow was ranging between 21-22 slm.

In Figures 6.14-6.15 are presented the spectra obtained in this run. Test points (tp) 1-3 correspond to high and low pressure stage of the old cruise respectively. Apart from the educt ions which can be easily distinguished, appear unknown peaks with relative abundances which remain almost unchanged between combustor off and on spectra (142, 146, 162, 176, 197, 204, 208, 225, 244, 246, 258, 288). The product ion peaks 97 and 160 are very low almost reaching the detection limit (mixing ratios in the range of some ppt).

For the modern cruise run (tp4 and tp6 corresponding to the high and low pressure stages of the modern cruise) the spectra look similar, lines 97 and 160 are noticeably
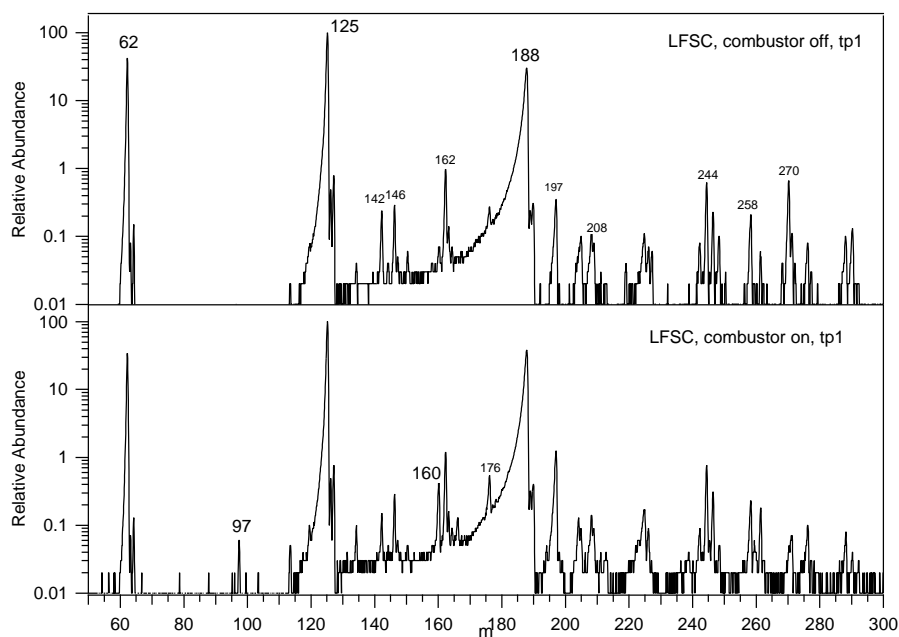
Figure 6.14: Mass spectra of negative ions for combustor off (top panel) and combustor on (bottom panel) for the HP stage, old cruise condition and FSC=50 ppm.
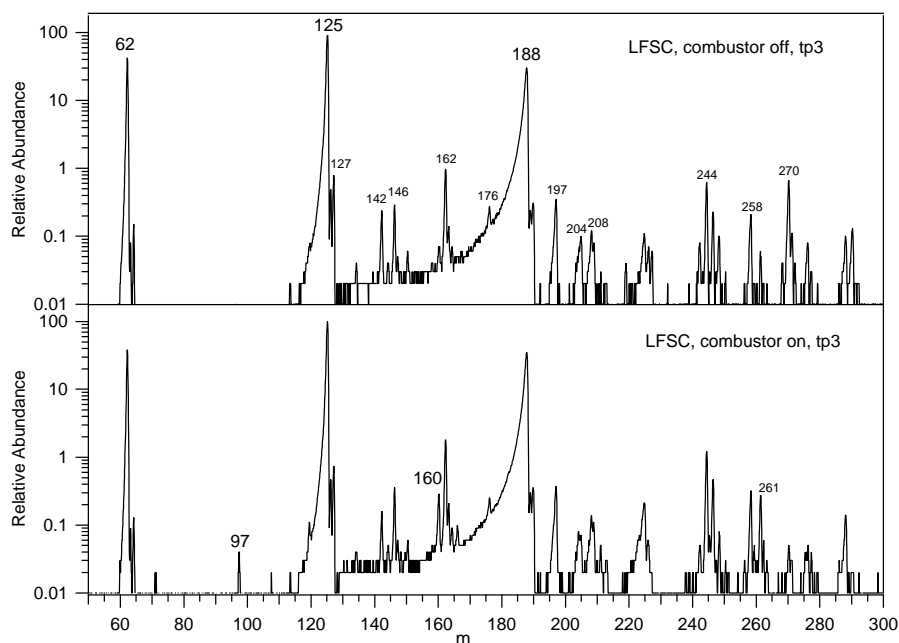
Figure 6.15: Mass spectra of negative ions for combustor off (top panel) and combustor on (bottom panel) for the LP stage, old cruise condition and FSC=50 ppm.
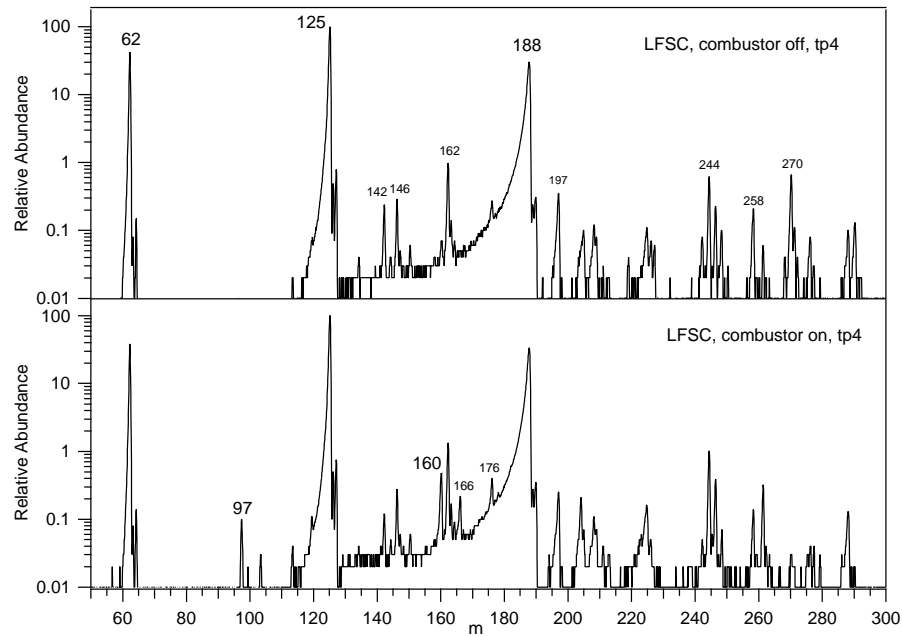
Figure 6.16: Mass spectra of negative ions for combustor off (top panel) and combustor on (bottom panel) for the HP stage, modern cruise condition and FSC=50 ppm

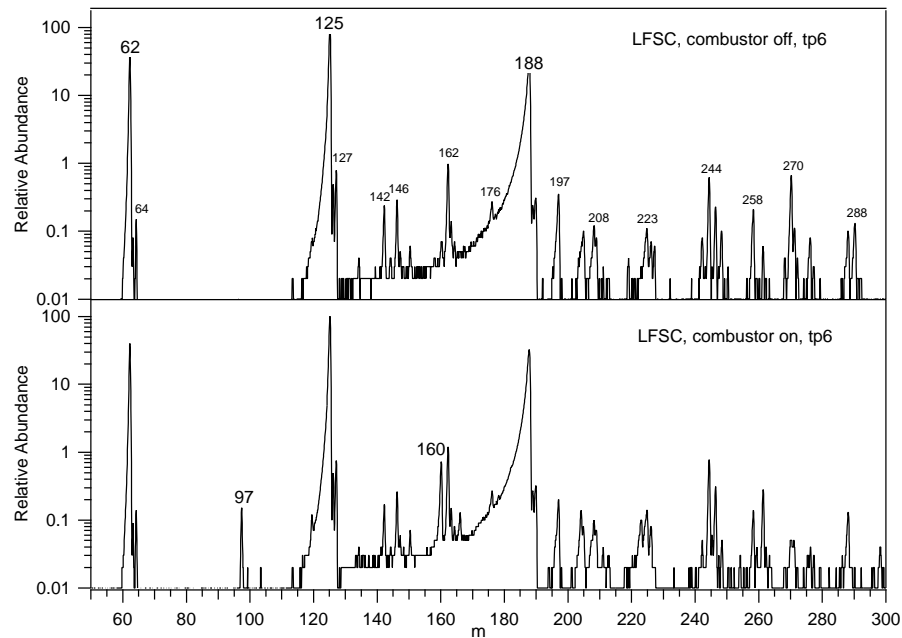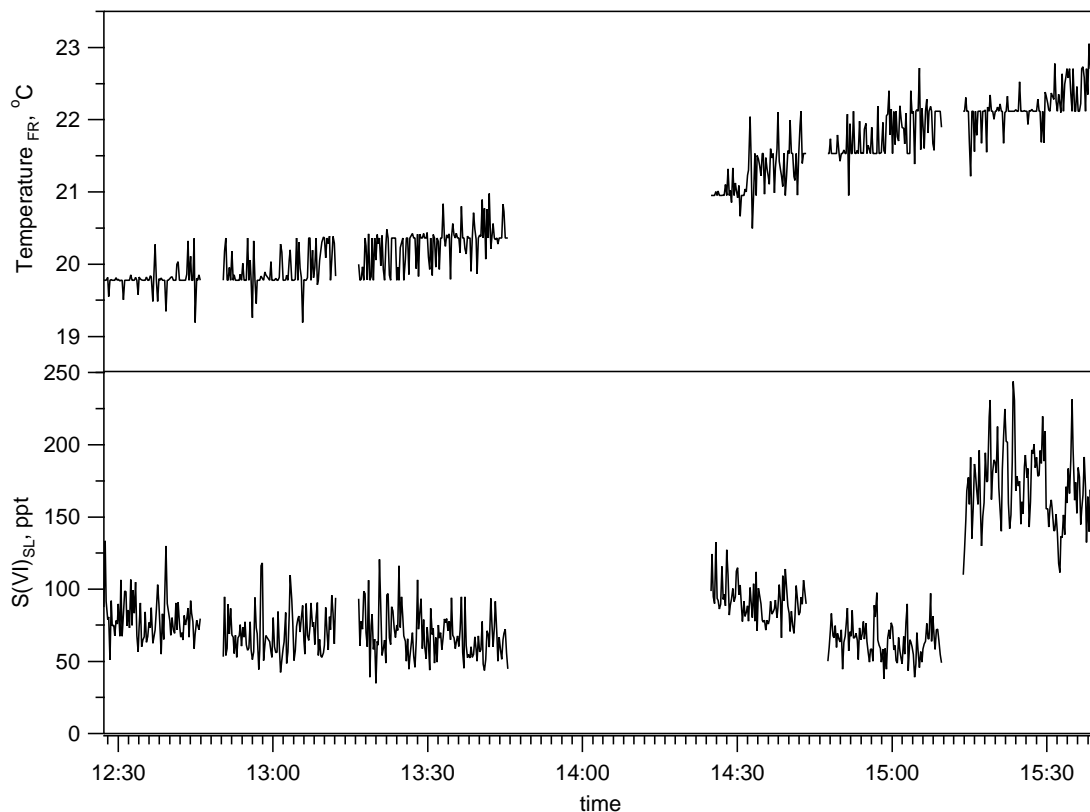**Figure 6.17:** Mass spectra of negative ions for combustor off (top panel) and combustor on (bottom panel) for the LP stage, modern cruise condition and FSC=50 ppm

Figure 6.18: Flow reactor temperature and measured S(VI) in the sampling lines for FSC=50 ppm

higher in comparison to the old cruise condition, a trend already observed in the previous measurements.

The measured mixing ratios of sulfuric acid in the SL before being diluted in the FR are given in the bottom panel of Figure 6.18. The first run (12:30-14:00) includes measurements in the three pressure stages for the old cruise combustor operating conditions. Although it would have been expected to see a monotonous increase of S(VI) in the three successive pressure stages due to ongoing oxidation of SO_2 by OH radicals in the HES, there is hardly any variation observed. This may mean that additional SO_2 oxidation by OH radicals occurred in the SL. Since we can measure $S(VI)_{SL}$ at the end of the SL and not $S(VI)_{HES}$ at the HES exit, we can not see the increase of S(VI) in the internal flow of the HES.

For the modern cruise condition run (14:20-15:30) gaseous S(VI) appears to be somewhat higher at the HP stage in comparison to the concentration measured in the

old cruise and increases noticeably at the LP stage. It seems that for higher SO_2 concentrations in the SL the perturbation of additional oxidation is not so pronounced. For the low FSC data set there will not be an attempt to calculate conversion efficiencies since i) there is a possibility of such perturbations in the S(VI) data and ii) the S_T data delivered by Qinetiq cannot approximate real values (2.8 and 3.2 ppm for old and modern cruise respectively are unrealistic for FSC=50 ppm).

6.6   Low Fuel Sulfur Content and Phosphor-bearing fuel additive

On March 17th 2002 there were conducted measurements with low FSC=50 ppm doped with a fuel additive provided by the Shell company. Shell Aviation's Aeroshell Performance Additive 101 (APA) is a patented jet fuel additive designed to improve thermal stability of the fuel and to prevent soot build up (coking) along the walls of the fuel manifold systems and nozzle. It has been field tested at Air Force and Air National Guard locations and is also available to non-US customers. Kerosene has been doped with 1250 mg ASA /lt fuel. The exact composition of the additive is not known, the only information confirmed is its sulfur and phosphor content both 0.2 % by mass. If we assume an average density for kerosene of 0.8 kg/lt then the content of P in the fuel would be 0.625 ppm while the contribution in the S content would be insignificant.

The background spectra for old and modern cruise show no significant differences and they are similar to the background spectra of the low FSC run without additive, confirming a stable response of the instrument. Besides the reagent ions, $NO_3^-(HNO_3)_n$ (n=0,1,2) (m=62,125,188) some additional ions are noticeable both in combustor off and on spectra, of which 142, 146, 162 and 197 are most abundant. These remain unchanged so it will be assumed that the do not affect the detection of sulfuric acid. In all the combustor on spectra for old and modern cruise condition there are some similarities: the product lines 97, 160 and 223 are somewhat higher than in the low FSC spectra without additive. This may mean either that higher sulfuric acid is produced when the fuel is doped with ASA or that another molecule is present in the flow reactor which reacts with the ion family 62 $NO_3^-(HNO_3)_n$
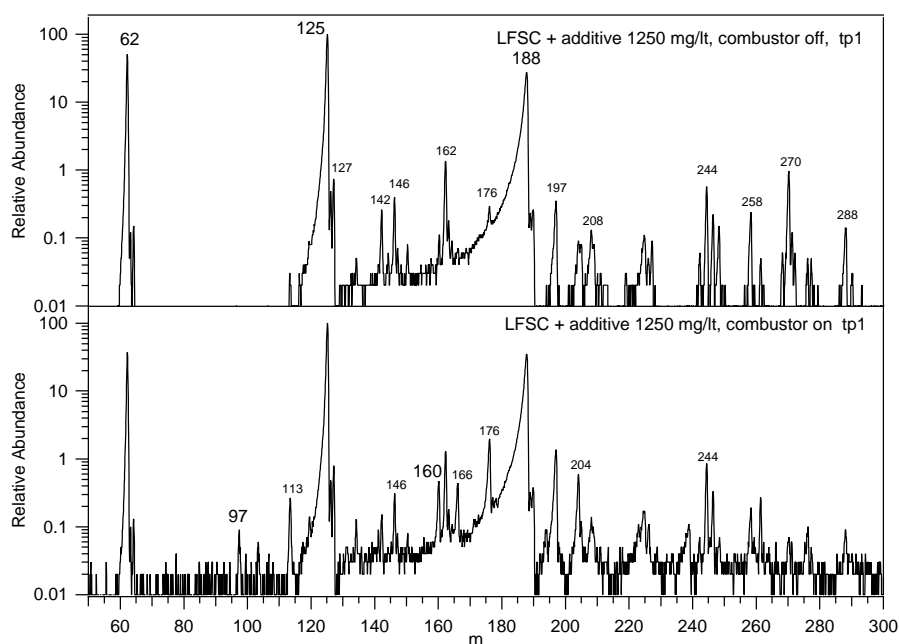
Figure 6.19: Mass spectra of negative ions for combustor off and on, tp1, FSC=50 ppm and additive
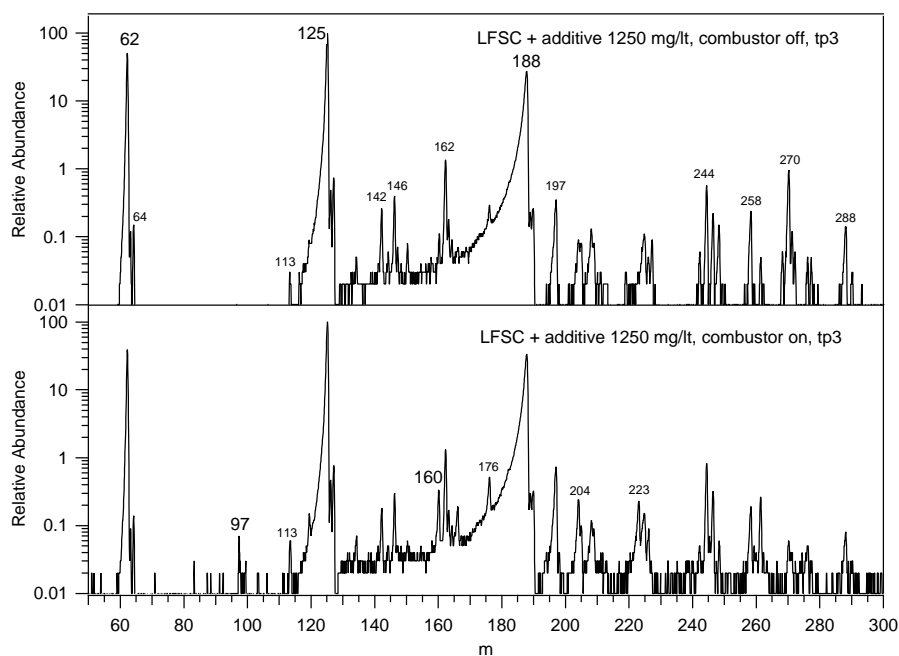
Figure 6.20: Mass spectra of negative ions for combustor off and on, tp3, FSC=50 ppm and additive
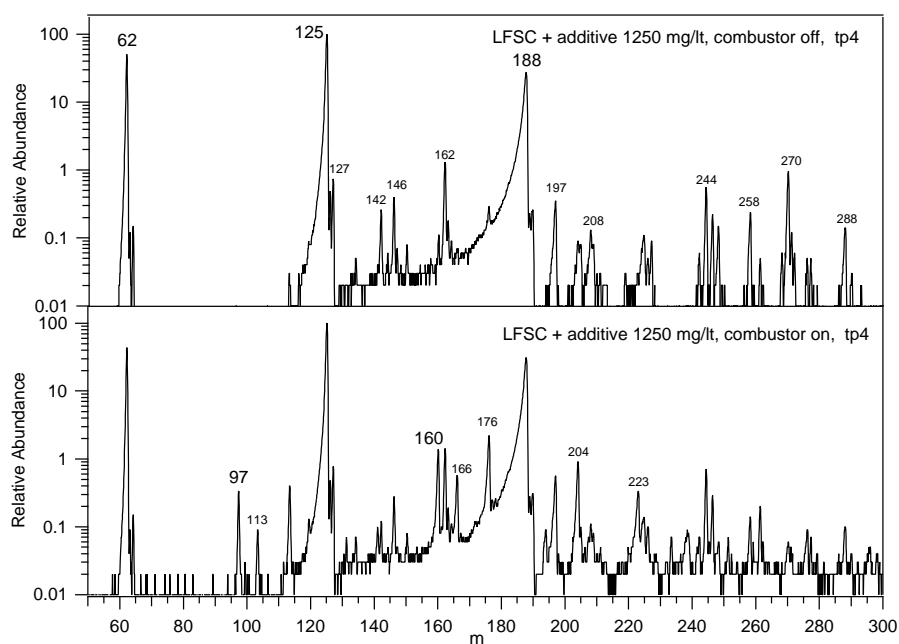
Figure 6.21: Mass spectra of negative ions for combustor off and on, tp4, FSC=50 ppm and additive

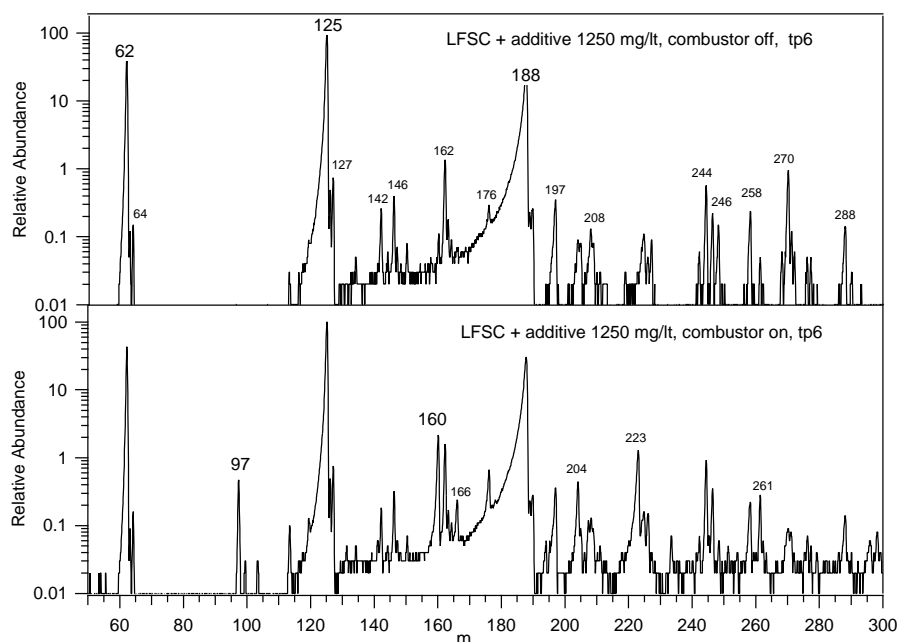**Figure 6.22:** Mass spectra of negative ions for combustor off and on, tp6, FSC=50 ppm and additive

(n=0,1,2) producing ions with masses 97 and 160 and 223, like H_2SO_4. Since the contribution of ASA in the FSC is negligible and would be impossible to be detected by the CIMS instrument, there should be suggested another potential candidate ion having the above mentioned characteristics. It seems that phosphoric acid (H_3PO_4) is a very good candidate with the required profile. The reaction scheme of phosphoric acid with the educt ions injected in the flow reactor would be:

$$NO_3^-(HNO_3)_n + H_3PO_4 \quad \rightarrow \quad H_2PO_4^-(HNO_3)_n + HNO_3 \tag{6.6}$$

The rate coefficient for this reaction is not known.

Apart from the ion family 97 (f97) (97+160+223) which appears with enhanced relative abundance when the ASA is present, there are three other families which also make a systematic appearance when the fuel is doped with the additive. These families are: f103, f113 and f141 where 103, 113 and 141 are the unknown core ions with one or two (n=1, 2) accompanying HNO_3 molecules. As already mentioned a tentative identification of the 97 ion can be phosphoric acid. The acidic trace gas 113 observed in our experiment may be peroxyphosphoric acid (H_3PO_5), while the acidic trace gas 103 may be tentatively identified as $HOP(CO)_2$. However, this identification is quite uncertain. In Table 1.5 are given the masses of the ions that seem to be related to ASA. For a more quantitative view of the contribution of the additive to each of these families the relative abundances of f97, f103, f113 and f141 for low FSC with additive are plotted in a semi-log graph together with f97, f103, f113 and f141 for low FSC without additive (see Figures 6.23-6.24). Although the enhancement of the relative abundances in the four families is not the same for every test point, the trend is clear in all cases.

In the following the relative abundances are translated into concentrations in the sampling lines and for reasons of simplicity presented only for the 6th test point i.e. for the low pressure stage of the modern cruise condition (Figure 6.25). For this calculation it was assumed that these acidic trace gases react like H_2SO_4 with NO_3^- reagent core ions on every collision (reaction rate coefficient: k=$2 \cdot 10^{-9} cm^3 s^{-1}$). As it can be seen the f103, f113 and f141 ion family concentrations are approximately twice as high when the fuel is doped with additive. Ion family f97 seems to be more affected as it is almost five times higher when the additive was added in the fuel.
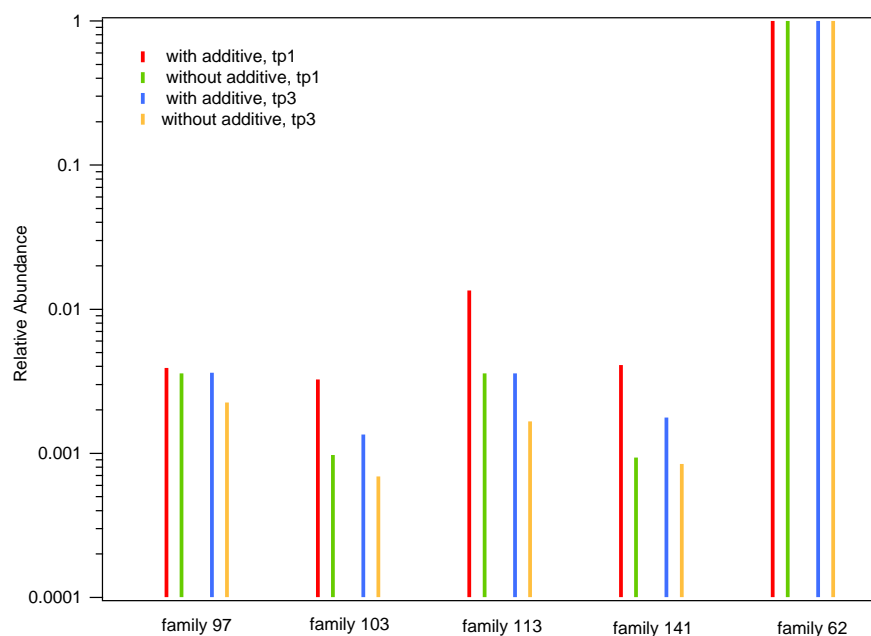
Figure 6.23: Relative abundances for P relates ion families with and without the Shell additive for old cruise condition.
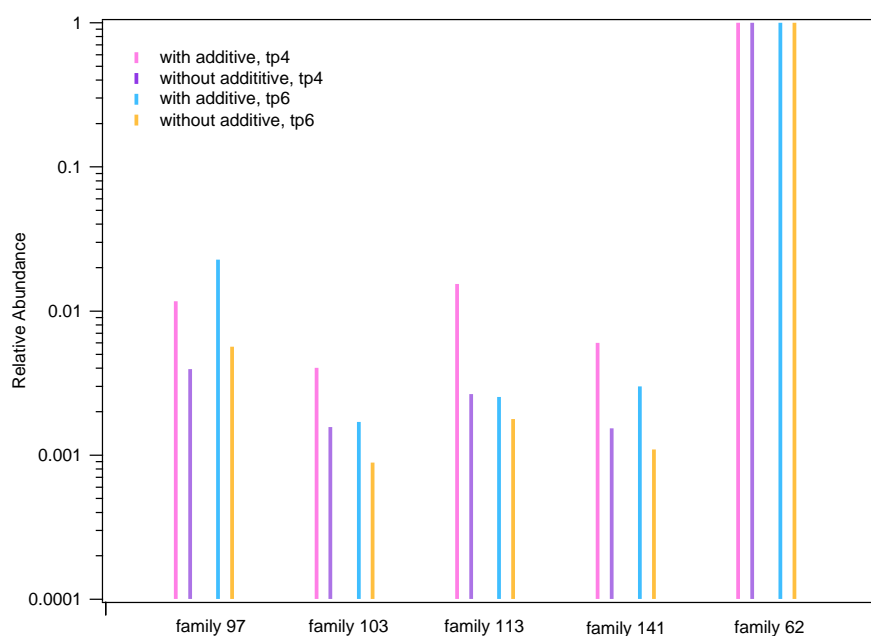
Figure 6.24: Relative abundances for P relates ion families with and without the Shell additive for modern cruise condition.

n	f97	f103	f113	f141
0	97	103	113	141
1	160	166	176	204
2	223	229	239	267

Table 6.5: Masses of ion families possibly related to the ASA
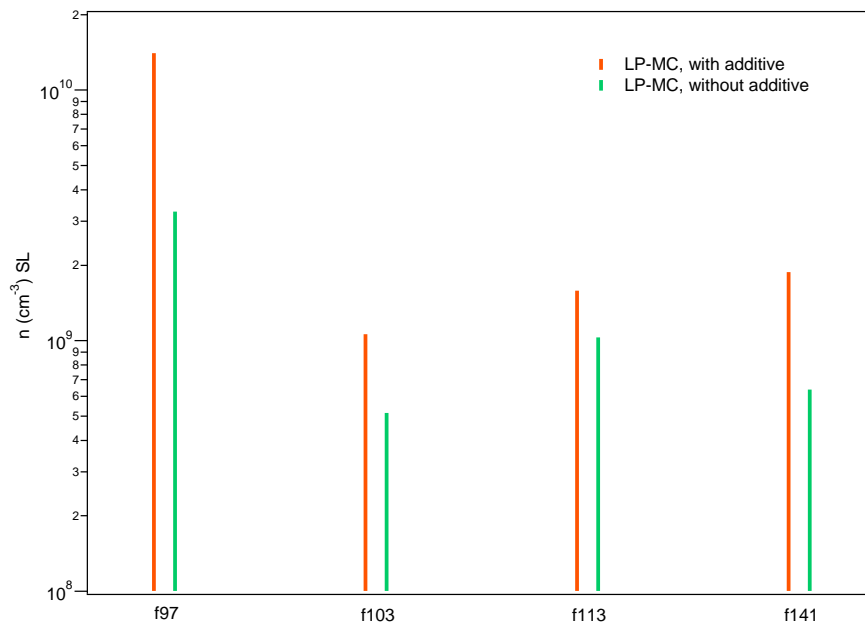
Figure 6.25: Concentrations in the sampling lines of the four ion families related to the presence of the Shell additive in the fuel.

Figure 6.26 shows the hygroscopic volume growth dV_c of the soot particles emitted from the engine versus the concentration n_{HYG} of ion families 97, 103, 113 and 141 which is thought to be the hygroscopic material adsorbed on the particles and causing its growth. Note that particle hygroscopicity was measured $20\,\mathrm{m}$ downstream of the sampling point while n_{HYG} only $2\,\mathrm{m}$ downstream of the sampling point. The volume growth of particles with initial diameter D_o=30 nm was calculated as dV_c=$4/3\pi(r^3 - r_o^3)$, where $r_o = 15\,nm$ the initial radius of the soot particles and r the radius of the particle after the hygroscopic growth [1] [Gys03]. The circles represent
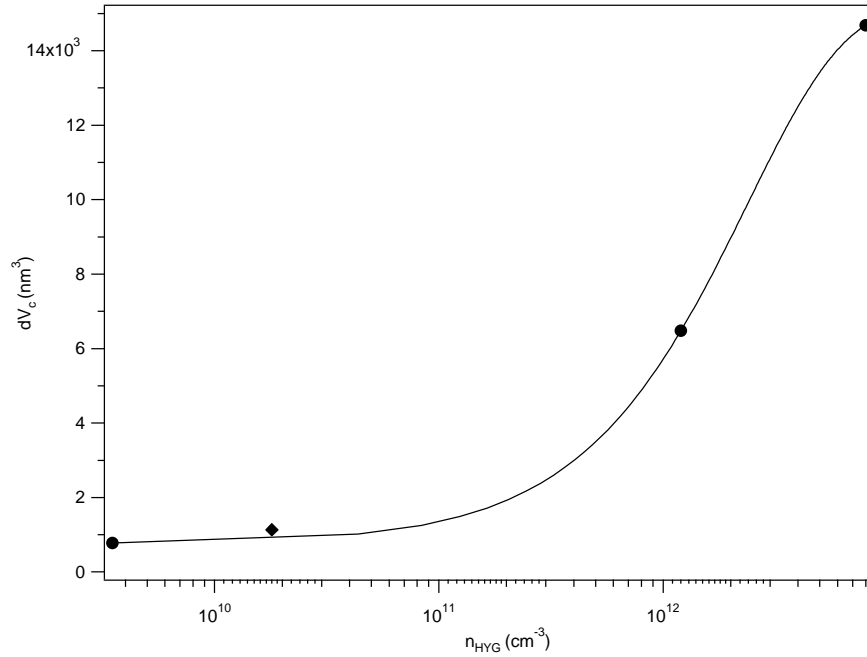
Figure 6.26: Hygroscopic particle volume growth dV_c versus n_{HYG} for the LP-stage and modern cruise condition and the three different FSC (circles). Also added the measurement with the low FSC doped with the ASA additive (diamond) under the same operating conditions. The line is an exponential fit.

the measurements for the three different FSC=50, 410 and 1270 ppm and the diamont the measurement for the low FSC with additive.

Evidently, V_c increases with n_{HYG} but not linearly: dV_c reaches a plateau when $n_{HYG} > 6 \cdot 10^6 cm^{-3}$. If this behaviour is not an artifact, it implies that there is a limit in the FSC above which aircraft emitted particles do not practically grow hygroscopically anymore. On the other hand, it is quite probable that there have been significant wall losses of sulfuric acid in the 20 m long unheated sampling line so that the growth factors are underestimated, it is impossible therefore to draw safely any conclusions about the behaviour of dV_c with FSC. The diamond that has been added in Figure 6.26 is the dV_c observed for the low FSC test with additive. Quite surprisingly this point lies above the fitted curve, implying that the unknown trace substances related to the ASA could be even more hygroscopic than sulfuric acid. Of course this scenario is only speculative and no safe conclusions can be drawn. It is though, an interesting observation that use of fuel additives may produce trace gases,

---

[1]Hygroscopic growth factors were measured by PSI

still unknown, which affect the particle properties. For further support of this idea new experiments should be designed in order to examine whether phosphor bearing compounds indeed react with NO_3^- ions and if yes, which product ions would be.

## 6.7 Complications in measurements - Discussion

As already mentioned a fraction of the non depleted OH in the post combustor-HES gas flow may cause additional SO_2 oxidation leading to additional formation of S(VI) in the SL. If this is the case, the S(VI) values measured by CIMS at the end of the 2 m long SL may be overestimated. The overestimation would be expected to be severe for lower FSCs but not that crucial at least for the high FSC=1250 ppm for which S(VI) exceeds 150 ppb in the SL. The potential overestimation should be also different for the three pressure stages: since OH is expected to deplete rapidly in the internal walls of the HES, less OH radicals would be available for additional oxidation in the SL for the LP stage the overestimation, therefore, would be negligible.

According to results of model calculations OH is rapidly depleted in the internal flow of an aircraft engine, leaving only a small amount of radicals available for further oxidation in the exhaust plume [Han97]. The uncertainty in the amount of OH concentrations at the engine exit is high. Measurements contacted during the PartEmis II campaign at engine exit indicated mixing ratios <1 ppb. Unfortunately, there was no OH measured either at every pressure stage or at the SL, thus it is difficult to quantify the potential perturbation of additional post SO_2 oxidation. It is nevertheless conceivable that the losses of OH radicals are so rapid in the SL due to collisions on the walls, that no additional S(VI) is formed in the post-HES flow. Even if some OH radicals are available, due to the lower rate coefficient of the $(SO_2 + OH)$ reaction at the lower temperatures and pressures prevailing in the SL, S(VI) formation could not be efficient. The PartEmis data support the view of negligible post-HES oxidation, since fluctuations in S(VI) and increase of S(VI) with pressure stages can be clearly seen. A significant disturbance of further OH-imposed SO_2 oxidation would have resulted in a 'flat' profile of S(VI) with no variation at the three pressure stages. An inefficient post-combustor oxidation is also observed in similar measurements in

the exhaust of an aircraft engine at ground level [Sor03]. Comparison of the measured conversion efficiencies with previous measurements in the exhaust plume of an aircraft in flight which yielded $\epsilon = 3.3 \pm 1.8\%$ [Cur02] shows that the results are in good agreement.

Another complication may be the losses of sulfuric acid on the walls and on soot particles. Concerning the wall losses there are two different potential sink sources: the sampling lines and the flow reactor. Due to its sufficient heating (150 °C) no wall losses on the sampling lines are expected. In case there are some significant wall losses, the presented epsilon values could be considered as lower limits. In the FR the wall losses are also not expected to be significant at the higher temperatures (>80 °C) applied partly at the medium FSC and at the high FSC tests. In the old cruise of the medium FSC test though, it is probable that wall losses occurred in the FR. Assuming sulfuric acid-water mole fractions <0.1 and temperatures around 20 °C, the H_2SO_4 equilibrium vapor pressure would be $\sim 10^{-14}$ mmHg. In the FR for the old cruise condition the H_2SO_4 vapor pressure is far above this limit. This implies that H_2SO_4 is super-saturated and therefore removed from the gaseous phase. Thus the marked increase in the S(VI) concentrations observed between old and modern cruise condition in the medium FSC case should be carefully interpreted: it must be an effect of reduced wall losses rather than an effect of the difference in combustor operating conditions, or better to say the combination of the two effect which act in the same direction (i.e. increase of S(VI))

Soot particles also emitted from the combustor is a potential sink for sulfuric acid. As already described in chapter 2.4.1 soot may be activated in a H_2SO_4/H_2O environment. Measurements of chemical properties of combustion aerosol performed by the technical university of Vienna (TUV) showed that the amount of SO_4^{2-} related to aerosol particles increased with FSC (see Figure 6.27). It should be pointed out that these measurements were conducted at the end of a 20 m long SL, while S(VI) was measured at the end of a 2 m long SL. Whether the taking up of S(VI) by soot occurred already in the short SL (residence time of the exhaust gas around 100 ms) is not clear. In case S(VI) is lost on soot surface then there is an underestimation of S(VI) of about 5 ppb, 7.5 ppb and 20 ppb for the low, medium and high FSC tests respectively. Clearly this perturbation is more acute for lower FSC and not really
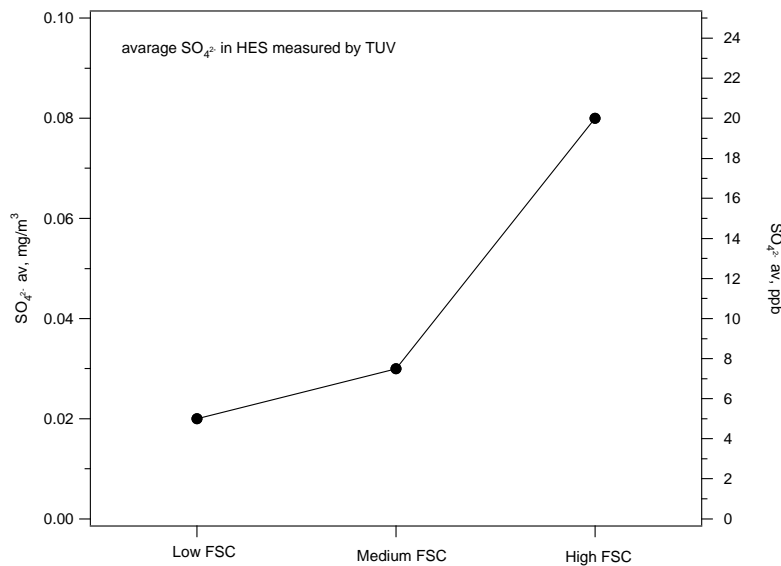
Figure 6.27: Concentration of SO_4^{-2} measured in the exhaust of HES by Technical University of Vienna. Data presented in the 30M PartEmis meeting in Strasbourg, 6th November, 2002.

significant for the high FSC run.

A not clarified issue remains the non-monotonous increase of S(VI) in the internal pressure stages. It is doubtful that this feature is reproduced in real turbines: all model calculations predict gradual increase of S(VI) and thus ϵ. Interestingly, measurements of other parameters by other groups revealed same trends. Shown in Figure 6.28 is the measured S(VI) in the three pressure stages of the high FSC and the modern cruise condition and the SO_4^{-2} measured by TUV under same conditions. The relative decrease/increase is the same for the two data sets, quite unexpected taking into account the different measuring techniques and the differences in sampling lines (length, temperature, pressure).

Relatively good compare, as well, the results of MPI-K with these of PSI. These measurements involved growth of aerosol particles with initial diameters D_o=30, 50, 100 nm. Making the assumption that the hygroscopic materials are exclusively the S(VI) gases, one can translate the hygroscopic growth factors to S(VI) volume fractions responsible for the observed particle growth. Comparison of the derived S(VI) volume fraction and the measured S(VI) shows a fairly good agreement as it can be seen in Figures 6.29-6.30. Attention should be drawn to the fact that the growth factors and thus the derived S(VI) fractions are decreasing with increasing initial particle
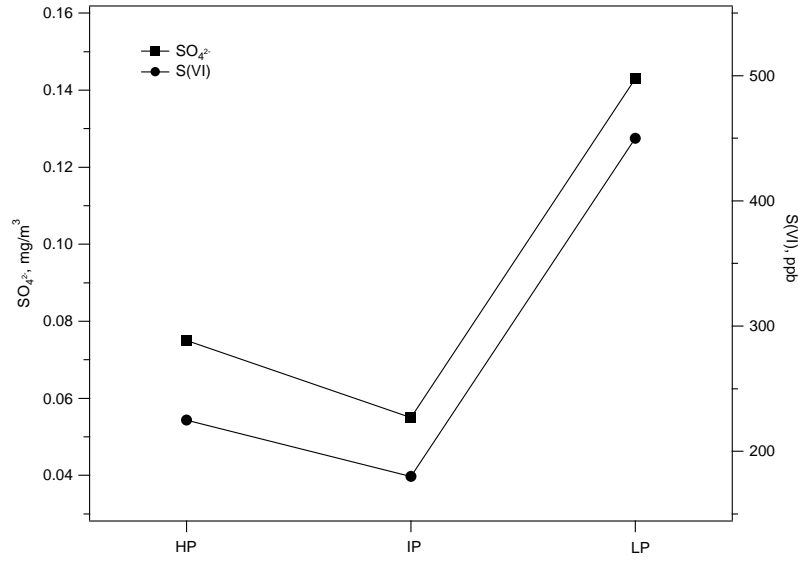
Figure 6.28: Similar trends observed in the S(VI) measurements of MPI-K and the aerosol sulfate SO_4^- measurements of TU Vienna in the internal pressure stages of the HES for high FSC and modern cruise condition. Data presented by TUV in the 30M PartEmis meeting in Strasbourg, on 6th November, 2002.

diameter (in other words, smaller particles are more hygroscopic). In the figures the data corresponding to different initial diameters D_o are scaled with different factors to make the diagrams more demonstrative.

Summarizing, one could highlight the importance of the S(VI) measurements which are the first to be performed in the internal flow of an aircraft engine. Therefore, they can be used for validation of models predicting internal sulfur conversion efficiencies, the results of which currently disperse in a relatively wide range (ϵ from a few up to 10%) ([Bro96b]; [Luk98]; [Tre99]; [Sta02]). The trends predicted by the models (increase of ϵ with the plume age in the aircraft engine and with higher combustor temperatures and pressures) are also observed in the reported measurements. The present results support the view of ϵ in the range of a few percent, suggest higher conversion efficiencies for the modern engines and encourage further investigation of the role of phosphor bearing additives used in aviation fuels.
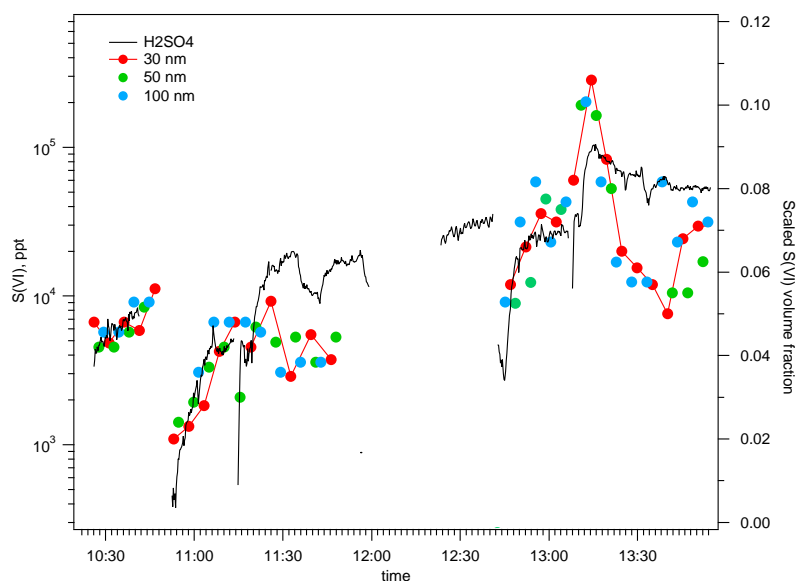
Figure 6.29: Scaled S(VI) volume fractions measured by PSI and comparison with S(VI) for medium FSC=410 ppm. Data presented by PSI in the 30M PartEmis meeting in Strasbourg, on 6th November, 2002.
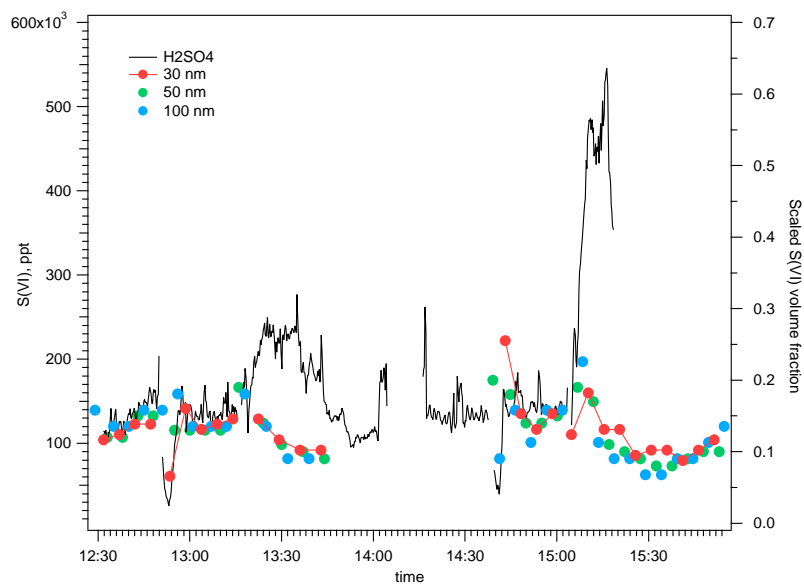
Figure 6.30: Scaled S(VI) volume fractions measured by PSI and comparison with S(VI) for high FSC=1270 ppm. Data presented by PSI in the 30M PartEmis meeting in Strasbourg, on 6th November, 2002.

Chapter 7

Conclusions

In the first part of this work were presented results of the first sulfur dioxide (SO_2) measurements conducted onboard of the research aircraft Falcon with an Ion Trap Mass Spectrometer. The high resolution of the Ion Trap and its compact set up proved to be ideal for aircraft measurements. Several altitude profiles of sulfur dioxide were obtained, giving information on mixing ratios over continental Europe. The highest atmospheric SO_2 mole fraction ($\sim$4 nmol mol^{-1}) were measured over the industrial area of Linz (Austria) at 1 Km altitude. Also, relative high SO_2 concentrations (2.5 nmol mol^{-1}) were observed over Hamburg at 5 Km altitude. Air mass back trajectory analysis indicated that these air masses encountered large-scale upward transport from the 2 km level approximately 36 h prior to the measurements, thus suggesting that polluted air masses may survive a fast vertical transport from the planetary boundary layer up to the middle troposphere without being removed by cloud processes. Under favorable conditions sulfur dioxide may lead to formation of gaseous sulfuric acid, which promotes aerosol formation and growth. Simultaneous atmospheric aerosol particle measurements showed that the sulfur dioxide peak coincides with a peak in the number density of particles with diameters d >4 nm. These may have been either preexisting particles which grew in the presence of abundant gaseous sulfuric acid or freshly nucleated particles. Calculations based on the measured SO2 concentrations and particle number densities, can not exclude a new particle formation event.

In the second part of this work were presented the results of ground measurements of gaseous S(VI) ($SO_3+H_2SO_4$) in the internal flow of a jet aircraft engine. Gaseous

S(VI) and sulfur conversion efficiencies were reported for three different fuel sulfur contents FSC=30, 300 and 1270 mg kg^{-1} and two combustor operating conditions in the three successive pressure stages of the simulated gas turbine engine. Gaseous S(VI) and ϵ increased gradually in the three pressure stages as a result of the ongoing oxidation of sulfur dioxide by OH radicals. Higher combustor temperatures and pressures, which correspond to modern aircraft cruise, resulted in higher S(VI) and ϵ values. Engines of modern aircrafts, therefore, should be more efficient in sulfate aerosol particle formation. These results, so far, agree with previous reported modeling work [Luk98]; [Tre99]; [Sta02]. There is, though, no known mechanism explaining the increase of ϵ with increasing fuel sulfur content. Most theoretical calculations predict a decrease of sulfur conversion efficiency with fuel sulfur content, as a result of the limitation in oxidants available in the aircraft turbine engine [Bro96b]. The results presented in this work suggest the opposite trend, which could be an artifact due to the combination of uncertainties in the S(VI) measurements ($\pm 52\%$) and the uncertainty in the calculation of total sulfur especially for the lower fuel sulfur contents. If not, there should be proposed another mechanism to explain the observed trend. The highest ϵ=2.24$\pm$1.2% was observed for the high fuel sulfur content (1270 mg kg^{-1}), the modern cruise condition and the last pressure stage, suggesting that internal sulfur conversion efficiencies are in the range of a few percent. This result is in good agreement with previous measurements of total sulfuric acid (gaseous and particle phase) in the exhaust plume of an aircraft in flight. Finally, measurements with a fuel doped with a phosphor bearing additive indicated the presence of four yet unidentified compounds, one of them having the same mass as sulfuric acid: this was tentatively identified as phosphoric acid (H_3PO_4). Further measurements would be still needed to explore the potential role of additives as potential aerosol precursors.

Summarizing, in this dissertations were reported for the first time measurements of gaseous S(VI) in the internal flow of a jet aircraft engine. The results have important implications on volatile aerosol particle formation and growth and on soot hygroscopicity and activation. The aircraft measurements of atmospheric sulfur dioxide have been performed for the first time with the Ion Trap Mass Spectrometer. The measurements indicated a potential new particle formation event. Further modeling work would be necessary to explore the atmospheric conditions under which

nucleation of gaseous sulfuric acid may occur.

Acknowledgments

Bibliography

[Arn80]   Arnold, F., and R. Fabian: First measurements of gas phase sulfuric acid in the stratosphere, *Nature* **283** (1980), 289–292.

[Arn95]   Arnold, S. T., R. A. Morris, A. A. Viggiano: Ion chemistry relevant for chemical ionization detection of SO3, *J. Geophys. Res.* **100** (1995), 14,141–14,146.

[Arn95a] Arnold, S., R. A. Morris, A. A. Viggiano: Temperature dependancies of tHe reactions of $CO_3^-(H_2O)$ and O_3 with NO and NO_2, *J. Chem. Phys.* **103** (1995), 2454–2458.

[Arn97]   Arnold, F., J. Schneider, K. Gollinger, H. Schlager, P. Schulte, D. E. Hagen, P. D. Whitefield, P. van Velthoven: Observation of upper tropospheric sulfur dioxide and acetone pollution: Potential implications for hydroxyl radical and aerosol formation *Geophys. Res. Lett.* **24** (1997), 57–60.

[Arn98]   Arnold, F., Th. Stilp, R. Busen, U. Schumann: Jet engine exhaust chemi-ion measurements: Implications for gaseous SO_3 and H_2SO_4, *Atm. Env.* **32** (1998), 3073–3077.

[Arn03]   Arnold, F., H. Haverkamp, A. Sorokin, S. Wilhelm : Electrically charged small positive and negative soot particles in jet aircraft combustor exhaust: first measurements of concen-trations and sizes, *submitted in Atm. Env.*

[Bou99]   Boucher O.: Influence of ar trafic on cirrus occurrence, *Nature* **397** (1999), 30–31.

[Bra98]   Brasseur G.P., R.A. Cox, D. Hauglustaine, I. Isaksen, J. Lelieveld, D.H. Lister, R. Sausen, U. Schumann, A. wahner, P. Wiesen: European scientific

assessment of the atmospheric effects of aircraft emissions, *Atm. Env.* **32** (1998), 2329–2418.

[Bra99]   Brasseur, G., J. Orlando und G. Tyndall: *Atmospheric chemistry and global change*, Oxford University press, 1999.

[Brock00] Brock, C.A., F. Scröder, B. Kärcher, A. Petzold, R. Busen, M. Fiebig: Ultrafine particle size distributions measured in aircraft exhasut plume, *J. Geophys. Res.* **105** (2000), 26555–26567.

[Bro96a]   Brown, R. C., R. C. Miake-Lye, M. R. Anderson, , C. E. Kolb, and T. J. Resch: Aerosol dynamics in near field aircraft plumes, *J. Geophys. Res.* **101** (1996), 22939–22953.

[Bro96b]   Brown, R. C., R. C. Anderson, R. C. Miake-Lye, C. E. Kolb, A. A. Sorokin und Y. I. Buriko: Aircraft exhaust sulfur emissions, *Geophys. Res. Lett.* **23** (1996), 3603–3606.

[Bro02]   Brown, R. C., R. C. Miake-Lye, S. P. Lukachko,I. A Waitz: Hetergenous reactions in aircraft gas turbine engines, *Geophys. Res. Lett.* **29** (2002), 10.1029/2000GL011447

[Cul80]   Cullis C.F., Hirschler M.M., Atmospheric Sulfur: Natural and man made sources, *Atm. Env.* **14** (1980), 1263–1278.

[Cur98]   Curtius, J., B. Sierau, F. Arnold, J. Baumann, P. Schulte und U. Schumann: First direct sulfuric acid detection in the exhaust of a jet aircraft in flight, *Geophys. Res. Lett.* **25** (1998), 923–926.

[Cur99a]   Curtius, J.: *Aerosol Schwefelsäure in der Atmosphäre und im Nachlauf von Düsenflugzeugen: Entwicklung und Einsatz einer neuartigen, flugzeugge-tragenen Massenspektrometersonde*, Dissertation, Universität Heidelberg, 1999.

[Cur02]   Curtius., J., F. Arnold and P. Schulte: Measurements of sulfuric acid concentrations in the exhaust of a jet aircraft in flight: Implications

for the sulfuric acid formation efficiency, *Geophys. Res. Lett.* **96** (2002), 10.1029/2001GL023813, 17-1–17-4.

[Eic01]   Eichkorn,   S.:   *Entwicklung   eines   flugzeuggetragenes   Ionen-Massenspektrometers mit grossem Massenbereich: Messungen im Labor, im Abgasstrahl von Duesenflugzeugen und in der oberen Troposphaere,* Dissertation, Universität Heidelberg, 2001.

[Exn92]   Exner M., H. Herrmann, R. Zellner: Laser based studies of reactions of the nitrate radical in aqueous solution, *Ber. Bunsens. Phys. Chem.* **96** (1992), 470–477.

[Fah95]   Fahey, D. W. *et al.*: Emission measurements of the Concorde supersonic aircraft in the lower stratosphere, *Science* **270** (1995), 70–74.

[Fin96]   Finnigan, LCQ; MS detector hardware manual, Revision B , July 1996.

[Fin00]   Finlayson Pits B. and Pits J., *Chemistry of the upper and lower atmosphere* Academic Press, 2000.

[Fla91]   Flagan R., S. C. Wang, F. Yin, J. Seinfeld, G. Reischi, W. Winklmayr, R. Karch: Electrical Mobility measurements of particle formation during chamber studies of atmospheric photochemical reactions, *Env. sci. Techn.* **25** (1991), 883–890.

[For95]   Fortuin J.P.F., R. van Dorland, W.M.F. wauben, H. Kelder: Greenhouse effects of aircraft emissions by a radiative transfer model, *Annales Geophysicae* **13** (1995), 413–418.

[Fre94]   Frenzel, A. und F. Arnold: Sulfuric acid cluster ion formation by jet engines: implications for sulfuric acid formation and nucleation, *Proc. Intern. Scientific Coll on impact of emissions from aircraft and spacecraft upon the atmosphere*, Bd. 94-06 von *DLR-Mitt.*, S. 106–112, 1994.

[Ger03]   Gerlinger, K.: *Atmosphaerische Spurengasmessungen mit einem flugzeug-getragenen Ionenfallenmassenspektrometer: SO_2 und andere Spurengase*

sowie Erprobung einer In-Flug Eichung von SO_2, Diplomarbeit, Universität Heidelberg, 2003.

[Gri00]   Grimm, F.: *Flugzeug-gestuetzte messungen atmosphaerischer spurengase in der troposphaere und untere stratosphere: Weiterentwicklung und einsatz einer hochempfindlichen CIMS sonde.*, Dissertation, Universität Heidelberg, 2000.

[Gys03]   Gysel M., U. Baltensperger, S. Nyeki, E. Weingartner, H. Giebl,, R. Hitzenberger, A. Petzold and C. W. Wilson, Properties of jet engine combustor particles during the PartEmis experiment. Part II: Hygroscopic properties at subsaturated conditions *submitted in Geophys. Res. Lett.*

[Ham82]   Hamill, P., R. Turco, C. Kiang, O. Toon und R. B. Whitten: An analysis of varoius nucleation mechanism for sulfate particles in the stratosphere, *J. Aerosol Sci.* **13** (1982), 561–585.

[Han97]   Hanisco, T. F., P. Wennberg, R. C. Cohen, J. G. Anderson, D. W. Fahey, E. R. Keim, R. S. Gao, R. C. Wamsley, S. G. Donnelly, L. A. DelNegro, R. J. Salawitch, K. Kelly und M. Profitt: The role of HO_x in super- and subsonic aircraft exhaust plumes, *Geophys. Res. Lett.* **24** (1997), 65–68.

[Han99]   Hanke, M.: *Develpoment of a novel method for measuring atmospheric peroxy radicals: calibration, aircraft-borne measurements and selective measurements of HO_2 and RO_2*, Dissertation, Universität Heidelberg, 1999.

[Hav03]   Haverkamp, H.: *Ionen aus Flugzeug-Strahltriebwerken: Messungen von Konzentrationenund Grössenverteilungen*, Diplomarbeit, Universität Heidelberg, 2003.

[Hof86]   Hoffmann, M.R., P.Schleyer: On the kinetics and mechanism of oxidation aquated sulfur dioxide by ozone, *Atm. Environ.* **20** (1986),1145–1154.

[Hun82]   Hunter, S.C.: Formation of SO_3 in gas turbines, *J. Eng. Power* **104** (1982),44–51.

[Hun00]   Hunton, D.E., J.O. Ballenthin, J.F. Borghetti, G.S. Federico, T.M. Miller, W.F. Thorn, A.A. Viggiano, B.E. Anderson, W.R. Cofer, D.S. McDougal, C.C. Wey: Chemical ionization mass spectrometric measurements of SO_2 emmissions from jet engines in flight and test chamber operations, *J. Geophys. Res.* **105** (2000),26.841–26.855.

[Jay97]   Jayne J.T., U.Poeschl, Y. Chen, D. Dai, L.T. Molina, D.R. Worsnop, C.E. Kolb, M.J. Molina: Pressure and temperature dependence of the gas phase reaction of SO_3 with H_2O and the heterogeneous reaction of SO_3 with H_2O/H_2SO_4 surfaces, *J. Phys. Chem.* **101** (1997),10000–10011.

[Kae95]   Kärcher, B.: A trajectory box model for aircraft exhaust plumes, *J. Geophys. Res.* **100** (1995), 18835–18844.

[Kae96]   Kärcher, B., M. M. Hirschberger und P. Fabian: Small scale evolution of aircraft exhaust species at cruising altitudes, *J. Geophys. Res.* **101** (1996), 15169–15190.

[Kae97]   Kärcher, B. und D. W. Fahey: The role of sulfur emissions in volatile particle formation in jet aircraft exhaust plumes, *Geophys. Res. Lett.* **24** (1997), 389–392.

[Kae98]   Kärcher, B., F. Yu, F. Schröder und R. Turco: Ultrafine aerosol particles in aircraft plumes: Analysis of growth mechanisms, *Geophys. Res. Lett.* **25** (1998), 2793–2796.

[Kae99]   Kaercher B., R. P. Turco, F. Yu, M. Y. Danilin, D. K. Weisenstein, R. C. Miake-Lye and R. Busen, A unified model for ultrafine aircraft particle emissions,*J. Geoph. Res.,* **105** (2000), 29,379-29,386

[Kae00]   Kärcher, B.: Aviation produced aerosols and contrails, *Surveys in Geophysics.* **20** (1999), 113–167.

[Kat03]   Katragkou E., S. Wilhelm, A. Kiendler and F. Arnold and C. Wilson: First gaseous Sulfur (VI) measurements in the simulated internal flow of an aircraft gas turbine engine during project PartEmis, *accepted in Geoph. Res. Lett.* (2003)

[Ker00] Kerminen V.M., Pirjola L., Boy M., Eskola A., Teinila K., Laakso L., Asmi
         A., Hienola J., Lauri A., vainio V., Lehtinen K., Kulmala M.: Interaction
         between SO_2 and submicron atmospheric particles, *Atm. Res.* **54** (200),
         41–57.

[Kie00] Kiendler, A.: *Aufbau und Einsatz einer neuartigen flugzeuggetragenen
         Ionenfallen-Massenspektrometersonde zur Analyse von Spurengasen und Io-
         nen: Messungen im Labor, im Abgas von Düsentriebwerken und atmo-
         sphärische Spurengasmessungen mit Flugzeugen*, Dissertation, Universität
         Heidelberg, 1999.

[Kje99] Kjellstroem E., J. Feichter, R. Sausen, R. Hein: The contribution of aircraft
         emissions to the atmospheric sulfur budget, *Atm. Env.* **33** (1999), 3455–
         3465.

[Kno89] Knop, G.: *Messungen der stratosphärischen Salpetersäure mittlels einer
         neuartigen ballongetragenen Massenspektrometersonde*, Dissertation, Uni-
         versität Heidelberg, 1989.

[Kol94] Kolb C.E., J.T. Jayne, D.R. Worsnop, M.J. Molina, R.F. Meads and A.A.
         Viggiano: Gas phase rection of sulfur trioxide with water vapor, *J. Am. Soc.*
         116 (1994), 10314–10315.

[Kon97] Konopka P., U. Schumann, H. Schlager, D.E. Hagen, P.D. Whitefield and
         J. Ovarlez: Particulate emissions of commercial jet aircraft ubder cruise
         conditions, *Rep. 93, Ins. für Phys. der Atmos. Dtsch. Zentrum für Luft-
         und Raumfahrt, OP, Germany* (1997).

[Kul98] Kulmala M., A. Laaksonen, L. Pirjola: Parametrizations for sulfuric
         acid/water nucleation rates, *J. Geoph. Res.* **103** (1998), 8301–8307.

[Laa00] Laaksonen A., L. Pirjola, M. Kulmala, K-H. Wohlfrom, F. Arnold, F. Raes:
         Upper tropspheric SO_2 conversion into sulfuric acid aerosols and cloud con-
         densation nuclei, *J. Geophys. Res.* **105** (2000), 1459–1469.

[Lam87]   Lamb D., D.F. Miller, N.F. Robinson, A.W. Gertler: The importance of liquid water concentration in the atmospheric oxidation of SO_2, *Atm. Env.* **21** (1987), 2333–2344.

[Lov96]   Lovejoy E.R., D.R. Hanson, L.G. Huey :KInetics and products of gas phase rection of SO_3 with water, *J. Phys. Chem.* **100** (1996), 19911–19916.

[Luk98]   Lukacko, S. P., I. A. Waitz, R. C. Miake-Lye, R. C. Brown und M. R. Anderson: Production of sulfate aerosol precursors in the turbine and exhaust nozzle of an aircraft engine, *J. Geophys. Res.* **103** (1998), 16159–16174.

[Mar97]   March R.: An introduction to Quadropole Ion Trap Mass Spectrometry, *Journal of Mass Spectrometry* **32** (1997), 351–369.

[Mar97]   Marti J.J., R.J. Weber and P.H. McMurry: New particle formation at a remote contintental site: assesing the contributions of SO_2 and organic procursors, *J. Geoph. Res.* **102** (1997), 6331–6339.

[Mia93]   Miake-Lye, R.,C., M. Martinez Sanchez, R. C Brown, and C. E Kolb: Plume and wake dynamics, mixing and chemistry behind a high speed civil transport aircraft, *J. Aircr.* **30** (1993), 467–479.

[Mia98]   Miake-Lye, R. C., B. E. Anderson, W. R. Cofer, H. A. Wallio, G. D. Nowicki, J. O. Ballenthin, D. E. Hunton, W. B. Knighton, T. M. Miller, J. V. Seeley und A. A. Viggiano: SO_x oxidation and volatile aerosol in aircraft plumes depend on fuel sulfur content, *Geophys. Res. Lett.* **25** (1998), 1677–1680.

[Min97]   Minnis, P., J.K. Ayers, S.P. Waever,: Surface based observations of contrail occurece frequency over the US, April 1993-April 1994, *NASA reference publication 1404, National aeronautics and Space administration, Hampton, VA, USA* (1997).

[Min98]   Minnis P., Young D.F., Nguyen L., Garber D.P., Smith Jr. W.L., Palikonda R.,: Tranforamtions of contrails into cirrus during SUCCESS, *Geophys. Res. Lett.* **25** (1998), 1157–1160.

[Moe92] Möhler, O., T. Reiner und F. Arnold: The formation of SO_5^- by gas phase ion-molecule reactions, *J. Chem. Phys.* **97** (1992), 8233–8239.

[Pet03] Petzold A., C. Stein, S. Nyeki, M. Gysel, E. Weingartner, U. Baltensperger, H. Giebl, R. Hitzenberger, A. Döpelheuer, S. Vrchoticky, H. Puxbaum, M. Johnson, C.D. Hurley, R. Marsh, and C.W. Wilson: Properties of jet engine combustor particles during the PartEmis experiment. Part I: Microphysical and chemical properties, *submittes in Geophys. Res. Lett.*

[Pen99] Penner, J. E., D. H. Lister, D. J. Griggs, D. Dokken und M. McFarland: *Aviation and the Global Atmosphere, special report to the IPCC*, Cambridge University Press, 1999.

[Pru98] Pruppacher H.P. and J.D. Klett: Micriphysics of clouds and precipitation, *Kluwer, Dordrecht* (1998).

[Rei93] Reiner T. and F. Arnold: Laboratoratory flow reactor measurements of the reaction SO_3+H_2O+M->H_2SO_4+M: Implications for gaseous H_2SO_4 and aerosol formation in the plumes of jet aricraft, *Geophys. Res. Lett.* **20(23)** (1993), 2659–2662.

[Rei94] Reiner T. and F. Arnold: Laboratoratory investigations of gaseous sulfuric acid formation via SO_3+H_2O+M->H_2SO_4+M: Measurements of the rate constant and product identification, *J. Chem. Phys.* **101(9)** (1999), 7399–7407.

[Rei97] Reiner T. and F. Arnold: Stratspheric SO_3: Upper limits inferred form io composition measurements: Implications for H_2SO_4 and aerosol formation, *J. Res. Lett.* **24** (1997), 1751–1754.

[Sav02] Savel'ev A.s., A.M. Starik and N.S. Titova: Formatin kinetics of Sulfur-Bearing Compounds in Combustion of Hydrocarbon Fuels in Air, *Combustion, Explosion and Schock Waves* **38(6)** (2002), 609–621.

[Schr00] Schroder F. Karcher B. Duroure C. Strom J. Petzold A. Gayet JF. Strauss B. Wendling P. Borrmann S.: On the transition of contrails into cirrus clouds, *J. Atmos. Sc.* **57(4)** (2000), 464–480.

[Schu98a] Schumann, U., H. Schlager, F. Arnold, R. Baumann, P. Haschberger and
           O. Klemm: Dilution of aircraft exhaust plumes at cruise altitudes, *Atmos.
           Environ.* **32** (1998), 3097–3103.

[Schu98b] Schumann, U., editor: Pollution From Aircraft Emissions in the North
           Atlantic Flight Coirridor (POLINAT-2), Air pollution research report 68
           Contract No. ENV4-CT95-043, Techn. Ber., European Comission, 1998.

[Schu01]   Schumann U., J. Strom, F. Arnold, T.K. Berntsen, P.M. de F. Forster,
           J.-F. Gayet and D. Hauglustaine: Aviation impact on atmospheric compo-
           sition and climate, *European Research in the Stratosphere 1996-2000, Eur.
           Comm., Brussels* , 2001

[Schu02]   Schumann, F. Arnold, R. Busen, J. Curtius, B. Kärcher, A. Kiendler, A. Pet-
           zold und H.Schlager, F. Schröder and K-H. Wohlfrom: Influence of fuel sul-
           fur on the composition of aircraft exhaust plumes: The experiments SUL-
           FUR 1-7, *J. Geophys. Res.* **107** (2002),10.1029/2001JD00813.

[See97]   Seeley J.,. R. Morris, A. Viggiano: Rate constants of $CO_3^-(H_2O)_n + SO_2$:
           implications for CIMS detection of SO_2, *Geoph. Res. Let.* **24** (1997), 1379–
           1382.

[Sei98]   Seinfeld, J. und S. N. Pandis: *Atmospheric Chemistry and Physics*, John
           Wiley + Sons, 1998.

[Sor03]   Sorokin A., E. Katragkou, F. Arnold, R. Busen and U. Schumann: Gaseous
           SO_3 and H_2SO_4 in the exhaust of an aircraft gas turbine engine: Measure-
           ments by CIMS and implications for fuel sulfur conversion to S(VI) and
           SO_3-conversion to H_2SO_4, *accepted in Atm. Environ.*

[Sta02]   Starik, A. M., A. M Savelev, N. S. Titova und U. Schumman: Modeling
           of sulfur gases and chemiions in aircraft plumes, *Aerospace Science and
           Technology.* **6** (2002), 63–81.

[Sto83]   Stockwell W.R., J. G. Calvert: The mechanism of the HO-SO_2 reaction,
           Atm. Env. **17(11)** (1983), 2231–22351.

[Tre98]   Tremmel, H. G., H. Schlager, P. Konopka, P. Schulte, F. Arnold, M. Klemm und B.Droste-Franke: Observations and model calculations of B747 engine exhaust products at cruise altitude and inferred initial OH emissions, *J. Geophys. Res.* **103** (1998), 10803–10816.

[Tre99]   Tremmel, H. G. and U. Schumann: Model simulations of fuel sulfur conversion efficiencies in an aircraft engine. Dependence on rate constants and initial species mixing ratios, *Aerospace Sci. Tech.* **3** (1999), 417–430

[Tro83]   Troe, J.: Theory of thermal unimolecular reactions in the fall off range. Strong collision rate constnants, *Ber. Bunsenges. Phys. Chem.* **87** (1983), 161–169

[Tur98]   Turco, R. P., J. X. Zhao und F. Yu: A new source of tropospheric aerosols: Ion-ion recombination, *Geophys. Res. Lett.* **25** (1998), 635–638.

[Twa93]   Twarowsky Allen: The influence of Phosphorus Oxides and Acids on the rate of H+OH recombination, *Comb. and Flame* **94** (1993), 91–107.

[Twa96]   Twarowsky Allen: The temperature dependence of H+OH recpmbnation in phosphorus oxide containing post combustion gases *Comb. and Flame* **105** (1996), 407–413.

[Tyn91]   Tyndall, S. C. und A. R. Ravishankara: Atmospheric oxidation of reduced sulfur species, *Int. J. Chem. Kinet.* **23** (1991).

[Uma01]   Uman, B.: *Erste atmosphaerische Untersuchungen der wechselwirkung von Mineralstaub mit den Spurengasen HNO_3 und SO_2: Einsatz einer hochempfindlichen CIMS-Sonde*, Diplomarbeit, Universität Heidelberg, 2001.

[Vig80]   Viggiano, A., R.A. Perry, D.L. Albritton, E.E. Ferguson, F.C. Fehsenfeld: The role of H_2SO_4 in stratospheric negative ion chemistry, *J. Geoph. Res.* **85** (1980), 4551–4555.

[Vig82]   Viggiano A., R.A. Perry, D.L. Albritton, E.E. Ferguson, F.C. Fehsenfeld: Stratospheric negative ion reaction rates with H_2SO_4, *J. Geoph. Res.*, **87** (1982), 7340–7342.

[Vig92]   Viggiano A., M.J. Henchman, F. Dale, C.A. Deakyne, J.F. Paulson: Gas
          phase reactions of weak Bronsted bases I-, PO_3^-, HSO_4^-, FSO_3^- and
          $CF_3SO_3^-$ with strong Bronsted acids H_2SO_4, FSO_3H, and CF_3SO_3H. A
          quantitative intrinsic Superacidity scale for sulfonic acids XSO_3H (X=HO,
          F, CF_3). *J. Am. Chem. Soc.*, **114** (1992), 4299–4306.

[Vig97]   Viggiano, A., J. Seeley, P. Mundis, J. Williamson und R. Morrison:
          Rate constants for the reaction of $XHO_3^-(H_2O)_n$ (X=C, HC, and N)
          and $NO_3^-(HNO_3)_n$ with H_2SO_4: Implications for atmospheric detection of
          H_2SO_4, *J. Phys. Chem. A* **101** (1997), 8275–8278.

[Whi68]   White, F. A.: *Mass spectrometry in science and technology*, John Wiley
          +Sons, 1968.

[Woh99]   Wohlofrom, K-H.: *Messungen atmosphaerischer Spurengase und Ionen mit
          flugzeuggetragenen Massenspektrometern: Neue Erkenntnisse fuer Ozon,
          Aerosole und den Einfluss des Luftverkehrs auf die Atmosphaere.*, Disserta-
          tion, Universität Heidelberg, 1999.

[Wil03]   Wilson C. W, A. Petzold, Nyeki S., Schuman U., Zellner R.: Measurement
          and Prediction of Emissions of Aerosols and Gaseous Precursors from Gas
          Turbine Engines (PartEmis): An Experimental Overview, *to be submitted
          to: Aerospace Science and Technology*

[Win95]   Winkel H., E. Mereand, A. Castleman: Gas phase reactions fo $HO_2CO_2^-$
          with molecular species of possible atmospheric interest, *J. Phys. Chem.* **99**
          (1995), 6601–6607.

[Yu97]   Yu, F. and R. Turco: The role of ions in the formation and evolution of
          particles in aircraft plumes, *Geophys. Res. Lett.* **24** (1997), 1927–1930.

[Yu98a]   Yu, F. and R. Turco : The formation and evolution of aerosols in strato-
          spherc aircraft plumes: Numerical simulations and comparisons with obser-
          vations, *J. Geophys. Res.* **25** (1998) 313–316.

[Yu98b]   Yu, F. and R. Turco : Contrail formation and impacts on aerosol properties
          in aircraft plumes: Effects on fuel slfur content, *Geophys. Res. Lett.* **103**
          (1998) 25915–25934.

[Yu99]   Yu, F., R. Turco und B. Kärcher: The possible role of organics in the
          formation and evolution of ultrafine aerosol particles, *J. Geophys. Res.* **104**
          (1999) 4079–4087.

[Zha95]   Zhao J. and R.P. Turco: Nucleation simulations in the wake of a jet aircraft
          in stratospheric flight, *J. Aeros. Sci.* **26** (1995) 779–795.